Cell Reports

Article

Chromatin-associated YTHDC1 coordinates heat-induced reprogramming of gene expression

Graphical abstract

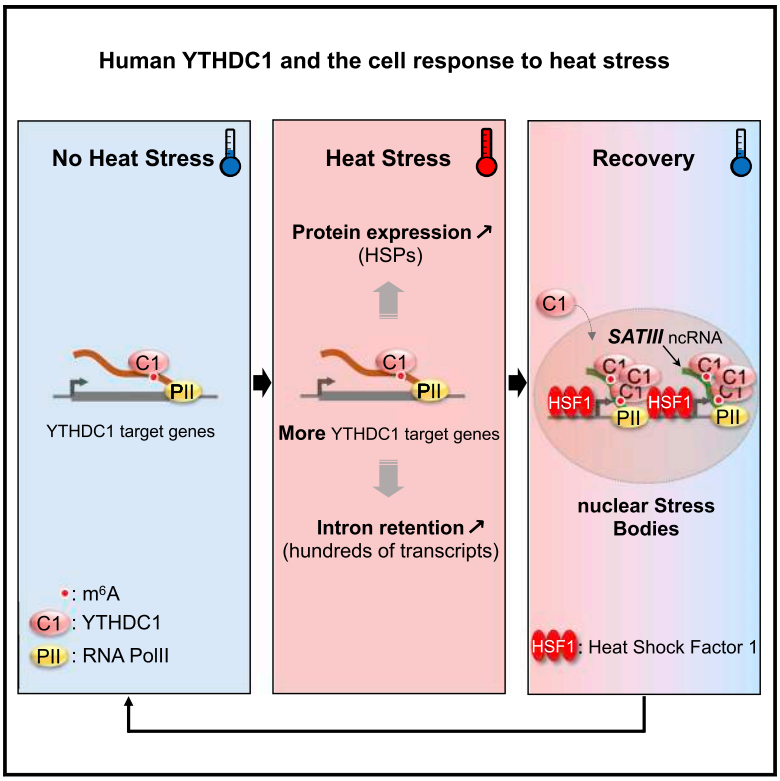

Highlights

- YTHDC1 predominantly localizes to chromatin, and heat stress reshapes its genomic location
- Upon heat stress, YTHDC1 binds to m^{6}A-modified HSP RNAs and promotes expression of HSPs
- Upon heat stress, YTHDC1 also mediates a broad m^{6}A-dependent intron retention regulation
- Later, YTHDC1 relocates to nuclear stress bodies by binding to m^{6}A-modified *SATIII* ncRNAs

Authors

Kalina Timcheva, Solenne Dufour, Leila Touat-Todeschini, ..., Rosemary Kiernan, Daphné Seigneurin-Berny, André Verdel

Correspondence

daphne.berny@univ-grenoble-alpes.fr (D.S.-B.), andre.verdel@univ-grenoble-alpes.fr (A.V.)

In brief

Timcheva et al. show that human m^{6}A reader YTHDC1 is a key player in heat-induced gene expression reprogramming. Upon heat stress, YTHDC1 co-transcriptionally promotes expression of HSPs and regulates intron retention of hundreds of transcripts. Later, as these two YTHDC1-dependent activities diminish, YTHDC1 relocates to nuclear stress bodies.

Timcheva et al., 2022, Cell Reports *41*, 111784
December 13, 2022 © 2022 The Authors.
https://doi.org/10.1016/j.celrep.2022.111784

CellPress

Cell Reports

CellPress
OPEN ACCESS

Article

Chromatin-associated YTHDC1 coordinates heat-induced reprogramming of gene expression

Kalina Timcheva,[1] Solenne Dufour,[1] Leila Touat-Todeschini,[1] Callum Burnard,[2] Marie-Christine Carpentier,[3,4] Florent Chuffart,[5] Rémy Merret,[3,4] Marion Helsmoortel,[2] Sabrina Ferré,[6] Aude Grézy,[1] Yohann Couté,[6] Sophie Rousseaux,[5] Saadi Khochbin,[5] Claire Vourc'h,[1] Cécile Bousquet-Antonelli,[3,4] Rosemary Kiernan,[2] Daphné Seigneurin-Berny,[1,*] and André Verdel[1,7,*]

[1]RNA, Epigenetics and Stress, Institut pour l'Avancée des Biosciences, CR UGA/Inserm U1209/CNRS UMR5309, Site Santé - Allée des Alpes, 38700 La Tronche, France

[2]Gene Regulation Laboratory, Institut de Génétique Humaine, UMR9002, 141 rue de la Cardonille, 34396 Montpellier, France

[3]University Perpignan Via Domitia, LGDP-UMR5096, 58 Av. Paul Alduy, 66860 Perpignan, France

[4]CNRS LGDP-UMR5096, UPVD, 58 Av. Paul Alduy, 66860 Perpignan, France

[5]Epigenetic Regulations, Institut pour l'Avancée des Biosciences, CR UGA/Inserm U1209/CNRS UMR5309, Site Santé - Allée des Alpes, 38700 La Tronche, France

[6]University Grenoble Alpes, Inserm, CEA, UMR BioSanté U1292, CNRS, CEA, FR2048, 38000 Grenoble, France

[7]Lead contact

*Correspondence: daphne.berny@univ-grenoble-alpes.fr (D.S.-B.), andre.verdel@univ-grenoble-alpes.fr (A.V.)

https://doi.org/10.1016/j.celrep.2022.111784

SUMMARY

Heat stress (HS) induces a cellular response leading to profound changes in gene expression. Here, we show that human YTHDC1, a reader of N^6-methyladenosine (m^6A) RNA modification, mostly associates to the chromatin fraction and that HS induces a redistribution of YTHDC1 across the genome, including to heat-induced heat shock protein (HSP) genes. YTHDC1 binding to m^6A-modified HSP transcripts co-transcriptionally promotes expression of HSPs. In parallel, hundreds of the genes enriched in YTHDC1 during HS have their transcripts undergoing YTHDC1- and m^6A-dependent intron retention. Later, YTHDC1 concentrates within nuclear stress bodies (nSBs) where it binds to m^6A-modified *SATIII* non-coding RNAs, produced in an HSF1-dependent manner upon HS. These findings reveal that YTHDC1 plays a central role in a chromatin-associated m^6A-based reprogramming of gene expression during HS. Furthermore, they support the model where the subsequent and temporary sequestration of YTHDC1 within nSBs calibrates the timing of this YTHDC1-dependent gene expression reprogramming.

INTRODUCTION

The highly conserved heat stress (HS) response can be triggered by multiple external stresses that include heat, hypoxia, protein aggregation, and heavy metals, as well as in physiopathological states.[1–5] HS induces profound changes at key stages of the gene expression process, from the stage of transcription,[6–8] to RNA processing,[9–11] mRNA export,[12,13] and translation.[14,15] Genome-wide studies have shown that, upon HS, transcription of thousands of genes is rapidly downregulated while transcription of hundreds of others is activated.[6–8,16,17] Heat shock protein (HSP) encoding genes are among the most upregulated stress-responsive genes upon HS. HSPs, which are highly conserved across evolution, are molecular chaperones whose primary function is to protect cells, notably by preventing misfolded protein aggregation.[18,19] Heat-induced expression of HSPs is mainly driven by heat shock transcription factor 1 (HSF1).[20,21] Beyond HSP genes, HSF1 directly activates transcription of more than 200 stress-responsive genes in response to HS.[6,7] In parallel, HSF1 directly activates the transcription of non-coding regions of the genome[22] encompassing pericentromeric[23] and subtelomeric[24] DNA repeats, unique interspersed regions, such as enhancers,[7,8] and the non-coding *NEAT1* gene.[25]

Following HS, cells enter a recovery period during which the heat-induced adaptive changes continue to take place. In humans, a remarkable cytological feature of the recovery period is the HSF1-dependent formation of subnuclear structures, known as nuclear stress bodies (nSBs), at pericentric regions highly enriched in satellite III (*SATIII*) DNA repeats.[23,26] Upon HS, HSF1 binds *SATIII*-rich regions[23,26] and triggers the recruitment of histone acetyltransferases and readers of acetylated histones leading to their transcription by RNA polymerase II (RNAPII).[9,24,27] The produced *SATIII* non-coding RNAs (ncRNAs) act in *cis* as they remain bound to their site of transcription and are essential to the formation of nSBs.[27,28] nSBs have long been proposed to contribute to the heat-induced reprogramming of gene expression by trapping factors regulating transcription and RNA processing, especially splicing factors.[29] Recently, *SATIII* ncRNAs were found to promote intron retention in more

This is an open access article under the CC BY license (http://creativecommons.org/licenses/by/4.0/).

than 400 pre-mRNAs, during the recovery period from heat stress.[30] This heat-induced intron retention regulation during the recovery period has been proposed to rely on serine- and arginine-rich pre-mRNA splicing factors (SRSFs) that concentrate on *SATIII* ncRNAs, where they may be efficiently phosphorylated by the heat-induced kinase CLK1.[30] Importantly, during the HS period an even larger number of RNAs undergo intron retention regulation and their export from the nucleus to the cytoplasm is blocked.[10] However, what controls this earlier and broader heat-induced intron retention and whether it is linked to the HSF1-mediated gene expression control remains unclear.

N^6-Methyladenosine (m^6A) RNA modification is a critical element of regulation of the heat stress response.[31–33] The m^6A modification is widely conserved and is the most prevalent internal RNA modification among living species.[34,35] In eukaryotes, m^6A contributes to RNA stability, splicing, export, and translation, as well as RNA-protein interactions.[34–37] METTL3 is the main cellular methyltransferase and deposits m^6A co-transcriptionally.[38,39] The level of m^6A in specific RNAs changes upon cell stress exposure, such as heat,[31,33,40] UV,[41] oxidative stress,[42] and chemical drugs.[43] Under heat stress, m^6A levels can increase at the 5′ or 3′ UTRs of mRNAs. Deposition of m^6A at the 5′ UTR of HSP mRNAs promotes their cap-independent translation,[32,33] while m^6A at the 3′ UTR has been linked to degradation of the modified mRNAs.[31] Recently, the *SATIII* ncRNAs were reported to be also m^6A methylated by METTL3 in response to heat stress.[44]

Most of the functions of m^6A rely on reader proteins that specifically bind to this mark. The best characterized m^6A readers are members of the YTH domain-containing protein family, which are expressed from yeast to humans.[34,35,37] Mice and humans express five members of the YTH protein family, known as YTHDC1-2 and YTHDF1-3. In the context of heat stress, the cytoplasmic m^6A reader YTHDF2 has been implicated in cap-independent translation of m^6A-modified HSP mRNAs during heat stress,[32,33] while the nuclear m^6A reader YTHDC1 has been implicated in splicing control during the recovery period from heat stress.[44]

Here, we show that the human m^6A reader YTHDC1 is a chromatin-bound protein and a key player in the coordination of the heat-induced reprogramming of gene expression triggered by the HS. Upon HS, YTHDC1 distribution across the genome changes leading to a marked enrichment at heat stress-responsive genes, in particular HSP genes. Upregulation of HSP expression induced by HS requires YTHDC1 binding to their m^6A-modified transcripts and YTHDC1 co-transcriptionally promotes their m^6A-dependent expression. In parallel, we show that YTHDC1 controls heat-induced retention of thousands of introns during HS in addition to the recovery period, including introns in HSP pre-mRNAs and *CLK1* pre-mRNA. YTHDC1 localizes to many of their genes and associates to the pre-mRNAs in a m^6A-dependent fashion, indicating that at least part of YTHDC1-dependent regulation of intron retention takes place in *cis*. Furthermore, we show for several transcripts that they remain bound to chromatin when subjected to heat-induced intron retention. Finally, we show that, subsequent to the YTHDC1-dependent upregulation of HSP transcripts and intron retention regulation, which both take place rapidly in response to HS, YTHDC1 relocates to nSBs. This intranuclear redistribution of YTHDC1 comes with a marked decrease in YTHDC1 binding to HSP mRNAs and a strong increase in its binding to m^6A-modified *SATIII* ncRNAs. Altogether, these results uncover that, in response to heat stress, YTHDC1 chromatin-associated functions coordinate an m^6A-dependent reprogramming of gene expression. In addition, they highlight that the ncRNA-dependent sequestration of YTHDC1 within the nSBs constitutes an efficient way to calibrate the amplitude and timing of the reprogramming of gene expression that takes place mostly during HS.

RESULTS

YTHDC1 associates with chromatin and co-transcriptionally acting RNA processing complexes

To investigate the function of the nuclear m^6A reader YTHDC1, we first purified YTHDC1 to identify its protein interactome by using mass spectrometry-based quantitative proteomic analysis (Figures 1A and 1B). Protein extracts were subjected to DNase and RNase digestions prior to the immunoprecipitation step. We identified 86 putative partners of YTHDC1 (Table S1). Gene ontology (GO) revealed that proteins co-purifying with YTHDC1 are mostly involved in the process of splicing and particularly in alternative splicing, with the presence of 10 out of the 14 known SR/SRSF proteins (Figures 1B, S1A, and S1B). The interaction between endogenous YTHDC1 and SRSF1 or SRSF6 was confirmed by using co-immunoprecipitation experiments (Figure S1C). Proteins previously identified as partners of YTHDC1, such as SRSF3, SRSF10, CPSF6, and DDX39B, were also identified.[45–47] Among the remaining YTHDC1 interactants, proteins involved in other co-transcriptional RNA processing steps or RNA export were also highly represented, such as subunits of the alternative polyadenylation complex (CPSF5 and 6) and of the THO/TREX complex with its associated proteins (THOC 1, 2, 6, and 7, CHTOP, DDX39B, ERH, POLDIP3, and SRRT) (Figures 1B and S1A). Because the YTHDC1 interactome showed a strong enrichment in proteins acting in co-transcriptional processes we also examined whether YTHDC1 associates with chromatin using subcellular fractionation. Remarkably, YTHDC1 preferentially associated with the chromatin fraction (Figure 1C). From these results, we conclude that YTHDC1 mainly acts on, or in close proximity to, transcriptionally active chromatin where it may contribute to RNA processing.

Heat stress reshapes genomic localization of YTHDC1

In mouse, co-transcriptionally deposited m^6A participates in the heat stress response.[31] To assess whether human YTHDC1 could participate in a chromatin-associated response to heat stress, we further characterized YTHDC1 localization to chromatin in unstressed cells (non-heat-stressed, [NHS]) or heat-stressed (HS) cells. Cell fractionation experiments showed that HS has no major impact on the overall association of YTHDC1 with chromatin (Figures 2A and S2A). To study YTHDC1 distribution along the genome we then performed chromatin immunoprecipitation experiments coupled to massively parallel sequencing (ChIP-seq) from unstressed and

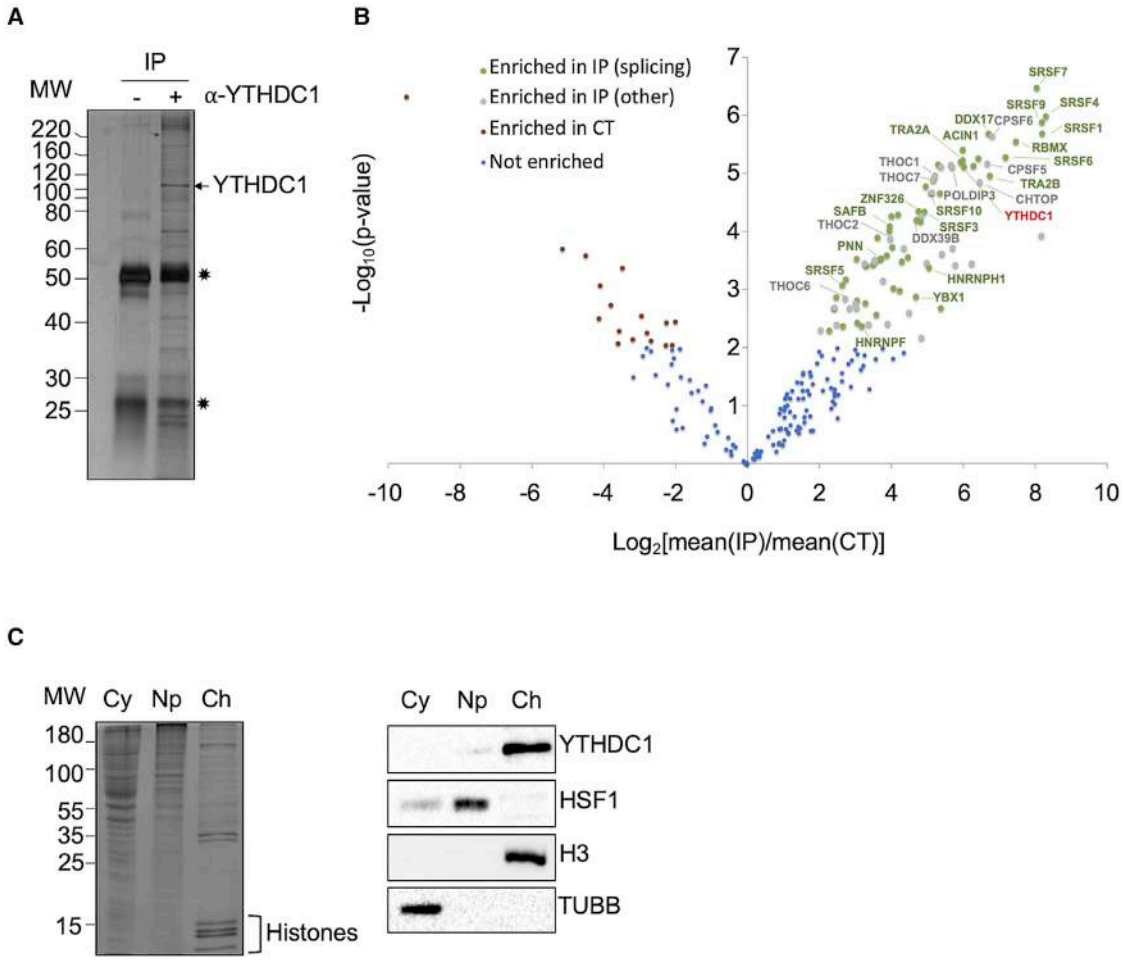

Figure 1. YTHDC1 is physically connected to chromatin and co-transcriptional processes

(A) Silver-stained gel of YTHDC1 immunoprecipitation eluates obtained using an irrelevant antibody (–) or a specific antibody against YTHDC1 (+). Asterisks, heavy and low chains of IgG used for the immunoprecipitation.

(B) Volcano plot of the proteins identified in YTHDC1 purification. Each protein identified by mass spectrometry analysis is represented as a single dot. Average enrichment (Log_2[mean(IP)/mean(CT)]) was plotted along the x axis and p values [–Log_{10}(p value)], obtained for each protein from three independent experiments, along the y axis (ProStaR software tool). Proteins enriched in YTHDC1 IP and implicated in alternative splicing are in green. Enriched proteins with other functions are in gray. CT, control immunoprecipitation done with irrelevant antibody.

(C) Cell fractionation experiments showing YTHDC1 association with the chromatin fraction. Left panel: Coomassie stained-gel of the cytosolic (Cy), nucleoplasmic (Np), and chromatin-associated (Ch) fractions. Right panel: western blots from the indicated fractions, using antibodies against YTHDC1, HSF1, H3, and Tubulin-β.

heat-stressed cells. YTHDC1 ChIP-seq peaks predominantly matched with genomic regions annotated as protein-coding or non-coding genes, under both NHS and HS conditions (Figure S2B). The genomic association of YTHDC1 was, however, subjected to a significant redistribution between the NHS and HS conditions, with 2,368 genes enriched in YTHDC1 in NHS which increased to include 6,923 genes under HS (Figure 2B), and 1,648 genes that were targeted by YTHDC1 under both conditions (Figure S2C). Under both NHS and HS conditions, approximately 75% of YTHDC1 target genes were protein-coding genes (Figure 2B).

Further analysis of the localization of YTHDC1 on chromatin was performed by ranking protein-coding genes according to the extent of binding of YTHDC1 over the gene body (normalized ChIP-seq reads over the gene body + 500 bp on both ends) under both HS and NHS conditions. Based on these criteria, genes strongly associated with YTHDC1 in NHS, HS, or both conditions were identified (Figure 2C, red, black, and yellow dots, respectively). Genes displaying the highest normalized YTHDC1 ChIP-seq signal (top 30% of genes) in each condition were selected for further analysis. GO analysis showed that protein-coding genes enriched in YTHDC1 in unstressed cell were associated with translation and cell-cycle regulation (Figure S2D, top panel). Upon HS, YTHDC1 associated with genes involved in stress responses, translation, apoptosis, cell cycle, and RNA processing (Figure S2D, lower panel). These different categories of genes correspond to those whose expression is the most affected upon heat stress in mouse and human cell lines.[6,7]

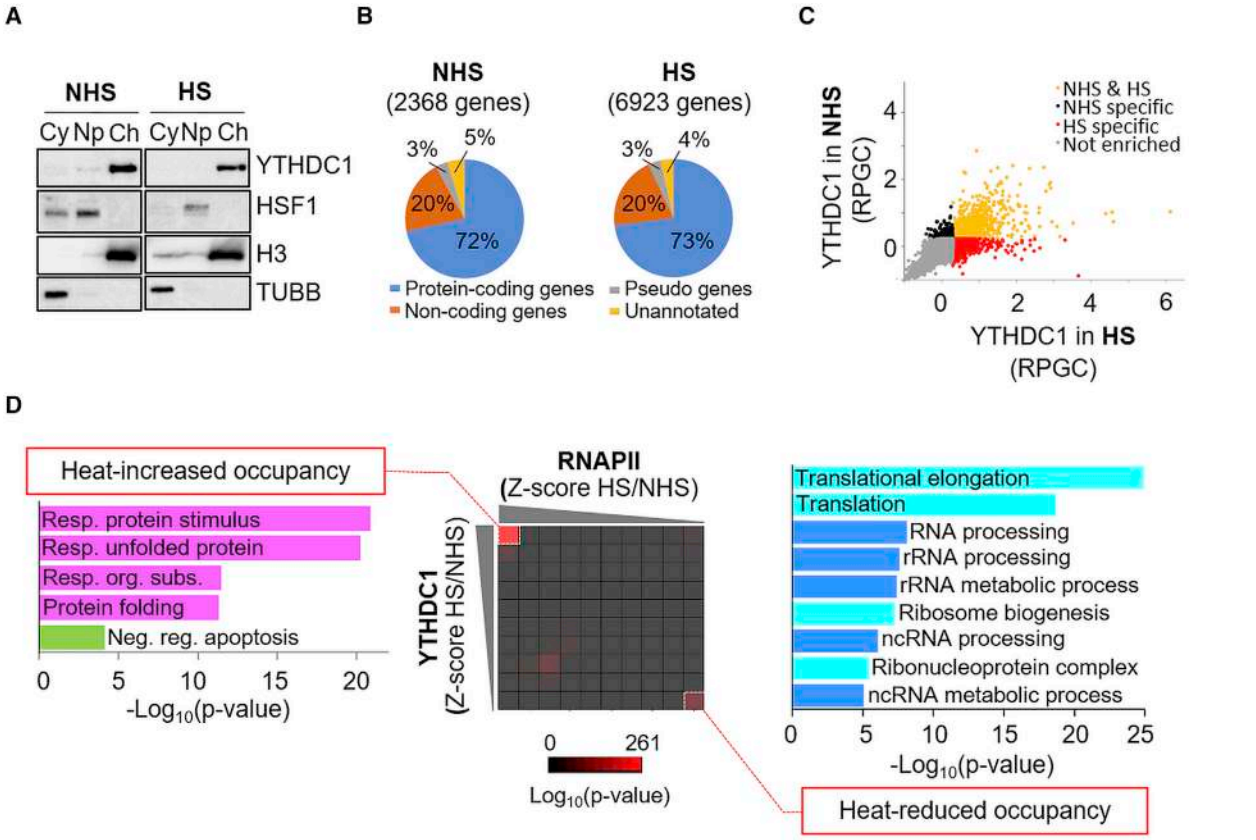

(legend on next page)

We then determined the transcriptional status of the genes bound by YTHDC1, by considering their association with RNAPII, in both NHS and HS conditions.[48] Among YTHDC1 genomic targets, approximately 75% were also associated with RNAPII, under both NHS and HS conditions (Figure S2E). Conversely, less than 25% of the RNAPII-associated genes were enriched in YTHDC1 under NHS and HS conditions (Figure S2F). Thus, the presence of RNAPII is not sufficient to recruit YTHDC1 to transcriptionally active regions of the genome since most RNAPII-occupied genes do not show an enrichment for YTHDC1.

We next analyzed co-variations of RNAPII and YTHDC1 occupancy on protein-coding genes upon HS. Genes were ranked following the change in normalized ChIP-seq reads of RNAPII or YTHDC1 upon HS. Remarkably, among the genes showing the greatest increase in RNAPII occupancy during HS a significant portion of them also exhibited the greatest increase in YTHDC1 occupancy (Figure 2D, middle panel, top deciles, top left square, and S2G). Similarly, genes with the most important reduction in RNAPII occupancy during HS also showed the greatest reduction in YTHDC1 association (Figure 2D, middle panel, bottom deciles, bottom right square). Interestingly, stress-responsive genes, in particular HSP genes, were highly enriched in the upregulated category (Figure 2D, left panel), while genes implicated in translation, and to a lesser extent in RNA processing, were enriched in the downregulated category (Figure 2D, right panel). Averaged profiles of YTHDC1 occupancy across target genes further showed that YTHDC1 localization within genes also strongly diverged depending on whether the genes were up- or downregulated upon HS. For the 500 genes that had the most upregulated RNAPII signal upon HS, YTHDC1 and RNAPII average occupancies were high across the gene and at both their 5′ and 3′ ends (Figure 2E, left panel). Noticeably, in the case of HSP upregulated genes, they tended to accumulate at their 3′ end upon HS, as shown, for example, at the *DNAJB1* gene (Figure 2F, left panel). In contrast, for the 500 genes with the most downregulated RNAPII signal, YTHDC1 and RNAPII accumulate at the 5′ end, near the transcription start site (Figure 2E, right panel), as shown for the downregulated *RPL13* gene (Figure 2F, right panel). Overall, these results show that YTHDC1 localizes to a subset of RNAPII-occupied genes and that HS induces a genome-wide redistribution of YTHDC1, as well as a relocation within the gene body itself depending on whether the gene is upregulated or downregulated in response to HS.

YTHDC1 binding to m^{6}A co-transcriptionally controls heat-induced expression of HSPs

Given the pronounced heat-induced enrichment of YTHDC1 at HSP genes and their importance in the heat stress response, we wished to determine the role of YTHDC1 in controlling HSP expression. We first focused on *DNAJB1* and *HSPA1A* genes, which showed strong enrichment of YTHDC1 in response to HS (Figures 2F, left panel, and S3A). While DNAJB1 and HSP70 proteins accumulate upon HS in different cell lines this accumulation was strongly reduced in cells knocked down for YTHDC1 (Figures 3A, WT and C1 KD, and S3B and S3C). To directly test whether YTHDC1 binding to m^{6}A plays a role in the accumulation of HSPs, we established a cellular system that allows the KD of the endogenous YTHDC1 and its replacement with an ectopic wild-type (C1 WT) or mutated (C1-*W428A*) version of YTHDC1. Ectopic YTHDC1 is resistant to RNA interference (RNAi) KD due to silent nucleotide mutations introduced in the coding sequence. Structural studies have demonstrated that YTHDC1 *W428A* mutation, which is located within the hydrophobic cage of the YTH domain, disrupts YTHDC1 binding to m^{6}A without significantly changing the structure of the domain.[49] Importantly, while the ectopic expression of WT YTHDC1 rescued the heat-induced accumulation of DNAJB1 and HSP70 proteins, expression of the YTHDC1-*W428A* mutant did not (Figure 3A, compare C1 KD + C1 WT and C1 KD + C1-*W428A*), indicating that YTHDC1 m^{6}A recognition is critical for the proper accumulation of DNAJB1 and HSP70 proteins in response to HS. In agreement with YTHDC1 and m^{6}A acting directly on *DNAJB1* and *HSP70* (*HSPA1A*) mRNAs, the abundance of these transcripts decreased in YTHDC1 KD cells (Figure 3B). Moreover, YTHDC1 interacted with both transcripts in a METTL3-dependent manner (Figure 3C) and the m^{6}A level on *DNAJB1* and *HSPA1A* mRNAs increased upon HS (Figure 3D).

Figure 2. Heat stress reshapes YTHDC1 genomic localization with a marked enrichment to HSP genes

(A) Extracts of unstressed (NHS, no heat stress) and heat-stressed (HS) cells after separation into cytosolic (Cy), nucleoplasmic (Np), and chromatin (Ch) fractions, were analyzed by immunoblotting using the indicated antibodies.

(B) Pie charts showing the distribution of YTHDC1 peaks under NHS and HS conditions into protein-coding, pseudo, non-coding, and uncategorized genomic regions. Total numbers of genes associated with YTHDC1 in unstressed and heat-stressed cells are indicated in parentheses.

(C) Scatterplot showing normalized YTHDC1 ChIP-seq reads of YTHDC1 targeted over gene bodies +/− 500 bps in unstressed (NHS), heat stressed (HS) or both conditions. The top 30% of genes exclusively enriched in unstressed condition are in black, in heat stressed in red, and both in unstressed and heat stressed in yellow. RPGC, read per genomic content.

(D) Analysis of the co-variation of RNAPII and YTHDC1 gene occupancy in heat-stressed cells relative to unstressed cells. Middle panel: matrix showing changes (*Z* score) in RNAPII or YTHDC1 binding across genes in the HS compared with the NHS conditions, and ranked by deciles from the most upregulated to the most downregulated. The scale represents p values for the intersection of the number of genes determined for each decile, as shown in Figure S2G, compared with expected. The lowest intersection is black while the highest is red (10^{-0} to 10^{-261}, hypergeometric test). Left panel: GO enrichments for the 382 genes that have their highest enrichments both for RNAPII and YTHDC1 (first decile, left upper corner of the matrix). Right panel: GO enrichments for the 262 genes that have their largest reduction of enrichments for both RNAPII and YTHDC1 occupancy. GO enrichments are ranked according to the $-\text{Log}_{10}$ of their p value.

(E) Average profiles of RNAPII and YTHDC1 over the 500 protein-coding genes with the largest increase (left panel) or the largest decrease (right panel) of RNAPII occupancy at their transcript end site, in HS (red) compared with NHS (black) cells. Transcription start site (TSS) and transcript end site (TES) are marked by the vertical gray lines.

(F) Browser shots of YTHDC1 and RNAPII ChIP-seq reads at upregulated HSP gene *DNAJB1* (left panel) and downregulated *RPL13* gene (right panel) from unstressed (NHS) and heat-stressed samples (HS). A scheme of *DNAJB1* and *RPL13* gene organization is shown above the browser shots.

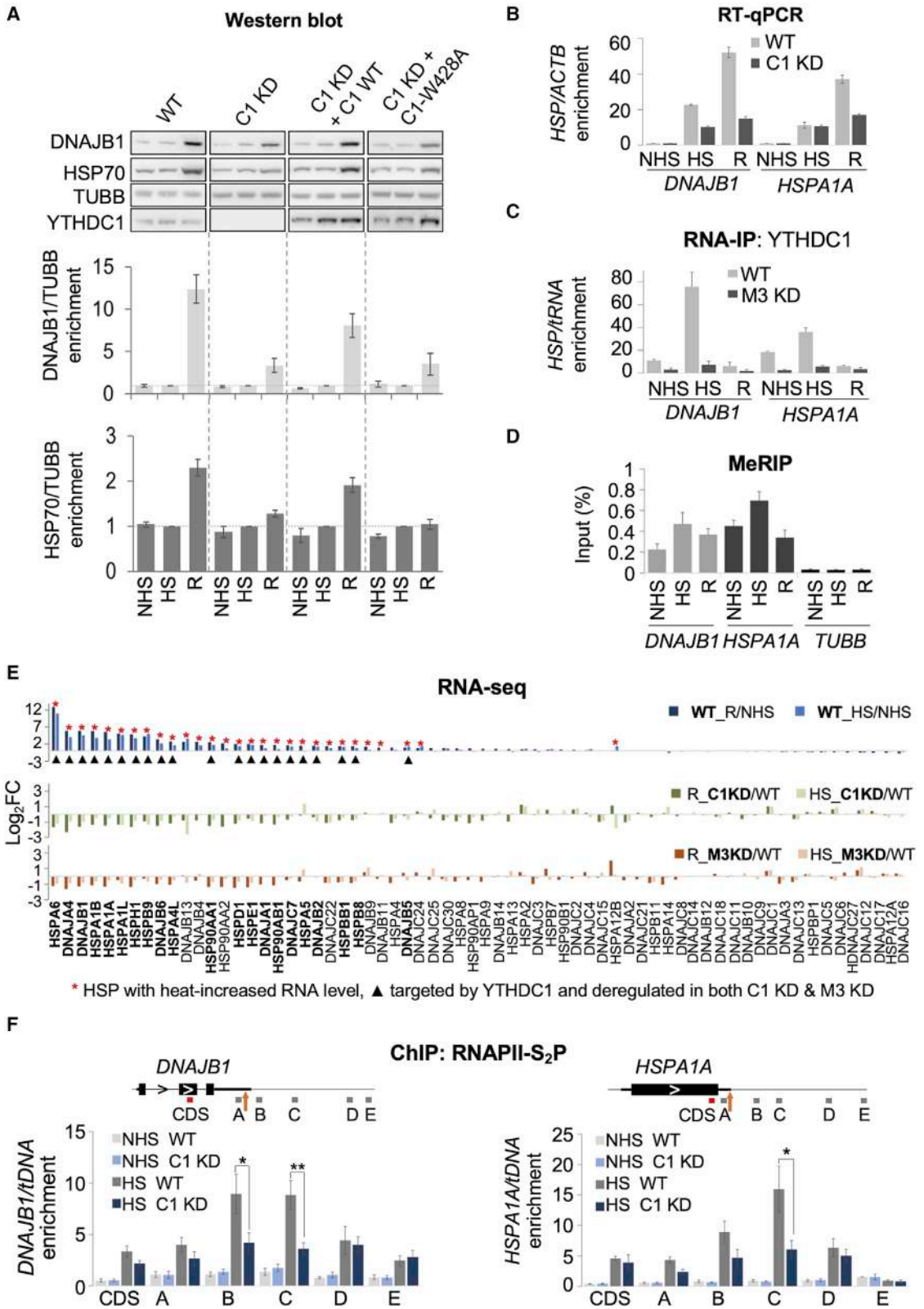

(legend on next page)

We then broadened this study by conducting RNA-seq analysis on WT, YTHDC1 KD, and METTL3 KD in unstressed and heat-stressed cells (Figures S3D–S3F). Importantly, among the 29 HSP transcripts found to accumulate in response to HS, 25 required both YTHDC1 and METTL3 for their heat-induced accumulation (Figure 3E), showing that YTHDC1 together with METTL3 are required for the upregulation of the vast majority, if not all, of the heat-induced HSP genes.

Interestingly, we found that YTHDC1 was enriched at 21 of the 25 HSP genes upregulated in a YTHDC1- and METTL3-dependent fashion upon HS (Figure 3E), indicating that YTHDC1 may upregulate expression of HSP proteins by acting on their genes. In support of this possibility, the levels of chromatin-associated *DNAJB1* and *HSPA1A* transcripts decreased in YTHDC1 KD cells (Figure S3G). ChIP-qPCR experiments that detected RNAPII phosphorylated on serine 2 of its C-terminal repeat (RNAPII-S2P), the elongating form of RNAPII, showed that RNAPII-S2P occupancy was significantly reduced at the 3′ end of *DNAJB1* and *HSPA1A* genes relative to the rest of the gene and the downstream region, in YTHDC1 KD stressed cells (Figure 3F). In addition, RNA-seq experiments showed that the number of reads within the gene body region of heat-induced HSP genes was more reduced than within the adjacent downstream region in YTHDC1 KD and METTL3 KD cells (Figure S3H), further suggesting that most of the heat-induced HSP genes were experiencing a transcription or co-transcriptional defect at their 3′ end, in the absence of YTHDC1 or METTL3. Altogether, these results indicate that, during HS, YTHDC1 co-transcriptionally promotes the m^{6}A-dependent production of HSP transcripts.

We note that the RNA-seq analysis showed that the KD of YTHDC1 or METTL3 prevented or reduced the accumulation of approximately one-third of the transcripts accumulating during HS (37%, corresponding to 963 transcripts) or recovery (31%, corresponding to 881 transcripts) in WT cells (Figures S3D and S3F; Table S2), suggesting that, beyond HSP genes, hundreds of other genes may also rely on YTHDC1 and m^{6}A for their proper regulation of expression in response to HS.

HSF1, *SATIII* ncRNAs, and METTL3 promote YTHDC1 relocation to nSBs

To allow cells to properly recover, the cellular response continues several hours after the HS. Interestingly, while YTHDC1 mostly displays an even distribution in the nucleus (with the exception of the nucleoli) in unstressed and heat-stressed cells, we found that YTHDC1 concentrates in nuclear foci in cells undergoing the recovery phase after heat stress (Figure 4A). This striking subcellular relocation of YTHDC1 is not accompanied by a significant change in YTHDC1 protein level (Figure 4B). In human cells, a hallmark of the recovery period is the appearance of nSBs in which pre-mRNA processing factors accumulate, especially regulators of alternative splicing.[29,30] We thus tested whether YTHDC1 localize to nSBs.

Formation of nSBs takes place predominantly on the juxtacentromeric heterochromatin of chromosome 9 where HSF1 is massively recruited and activates transcription of the non-coding *SATIII* DNA repeats.[29] After 3 h of recovery, 85% of the nuclei displayed HSF1 foci, and all of HSF1 foci co-localized with YTHDC1, suggesting that YTHDC1 is recruited to the nSBs (Figure 4A). A similar relocation of YTHDC1 into foci co-localizing with HSF1 foci was observed in several cell lines (Figure S4A). *SATIII* DNA and RNA FISH experiments confirmed YTHDC1 relocation to nSBs during recovery (Figures 4C and 4D). In agreement with the reversibility of the nSBs formation, YTHDC1 localization to nSBs was lost 24 h after HS, with YTHDC1 nuclear distribution resembling that of unstressed cells (Figure 4A). In addition, we examined the subcellular distribution of the other four human YTH domain containing proteins, YTHDF1-3 and YTHDC2, fused to GFP, using fluorescence microscopy.

Figure 3. YTHDC1 binding to m^{6}A promotes heat-induced expression of HSPs in *cis*

(A) Top panel: western blots showing the levels of DNAJB1, HSP70, and YTHDC1 proteins in wild-type (WT) cells, YTHDC1 knockdown cells (C1 KD), YTHDC1 KD cells expressing an ectopic copy of WT YTHDC1 (C1 KD + C1 WT; Table S3), or expressing an ectopic mutant YTHDC1-*W428A* (C1 KD + C1-*W428A*; Table S3), in unstressed (NHS, no heat stress) cells, heat-stressed (HS) cells, or heat-stressed cells subjected to 6 h of recovery (R). Tubulin-β (TUBB) was used as loading control. Bottom panels: quantification of the western blot signals. Graphs show the mean and standard error of the mean (SEM) of three independent experiments.

(B) qRT-PCR showing the level of *DNAJB1* and *HSP70* (*HSPA1A*) mRNAs in WT or YTHDC1 KD cells, under NHS, HS, or R3 conditions. Variation of RNA levels is expressed in fold-change relative to the NHS condition and normalized to *ActinB* (*ACTB*). Graphs show the mean and SEM of three independent experiments.

(C) RNA-IP qPCR showing the interaction of YTHDC1 with *DNAJB1* and *HSP70* (*HSPA1A*) RNAs in WT or METTL3 KD cells, under NHS, HS, or R3 conditions. Variation of RNA levels is expressed in fold-change relative to control IP (with irrelevant IgG) and normalized to tRNA (*TRS-CGA1-1* RNA). Graphs show the mean and SEM of three independent experiments.

(D) M^{6}A-RIP(MeRIP)-qPCR showing the enrichment of m^{6}A at *DNAJB1*, *HSP70* (*HSPA1A*), and *TUBB* RNAs in WT cells under NHS, HS, or R3 conditions. Variation of m^{6}A RNA levels is expressed as a percentage of enrichment compared to the input. Graphs show the mean and SEM of three independent experiments.

(E) RNA levels of 65 of the 79 HSP RNAs from cells subjected to HS or to HS and 3 h of recovery (R) versus NHS conditions in WT cells (upper graph), in YTHDC1 KD (C1 KD) versus WT cells (middle graph), and in METTL3 KD (M3 KD) versus WT cells (lower graph). RNAs were ordered according to the variation of their levels during the recovery compared with the NHS condition in WT cells. HSP RNAs accumulating in HS or R conditions and accumulating less in both YTHDC1 KD cells and METTL3 KD cells are highlighted by red stars. HSP RNAs with their genes targeted by YTHDC1 (ChIP-seq data) are highlighted by black triangles. Note the strong overlap between the RNAs with a red star and RNAs with black triangle. These RNAs are highlighted in bold.

(F) ChIP-qPCR showing the occupancy of the elongating form of RNAPII (RNAPII-S2P) at *DNAJB1* and *HSP* (*HSPA1A*) genes, in WT or YTHDC1 KD (C1 KD) cells, under NHS and HS conditions. The enrichment of elongating RNAPII was determined by qPCR amplification of genomic DNA from their coding sequence (CDS, red segment), 3′ UTR or beyond (schematized by the A to E gray segments). Data show the fold enrichment normalized to control IP (conducted with irrelevant IP) and to tDNA (*TRS-CGA1-1* gene). Brown arrows indicate the position of the putative cleavage/polyadenylation site. Values are mean ± SEM from three independent biological replicates. p values were calculated using a two-tailed Student's t test. Only significant p values are indicated. Left panel: *p = 0.042; **p = 0.006. Right panel: *p = 0.041.

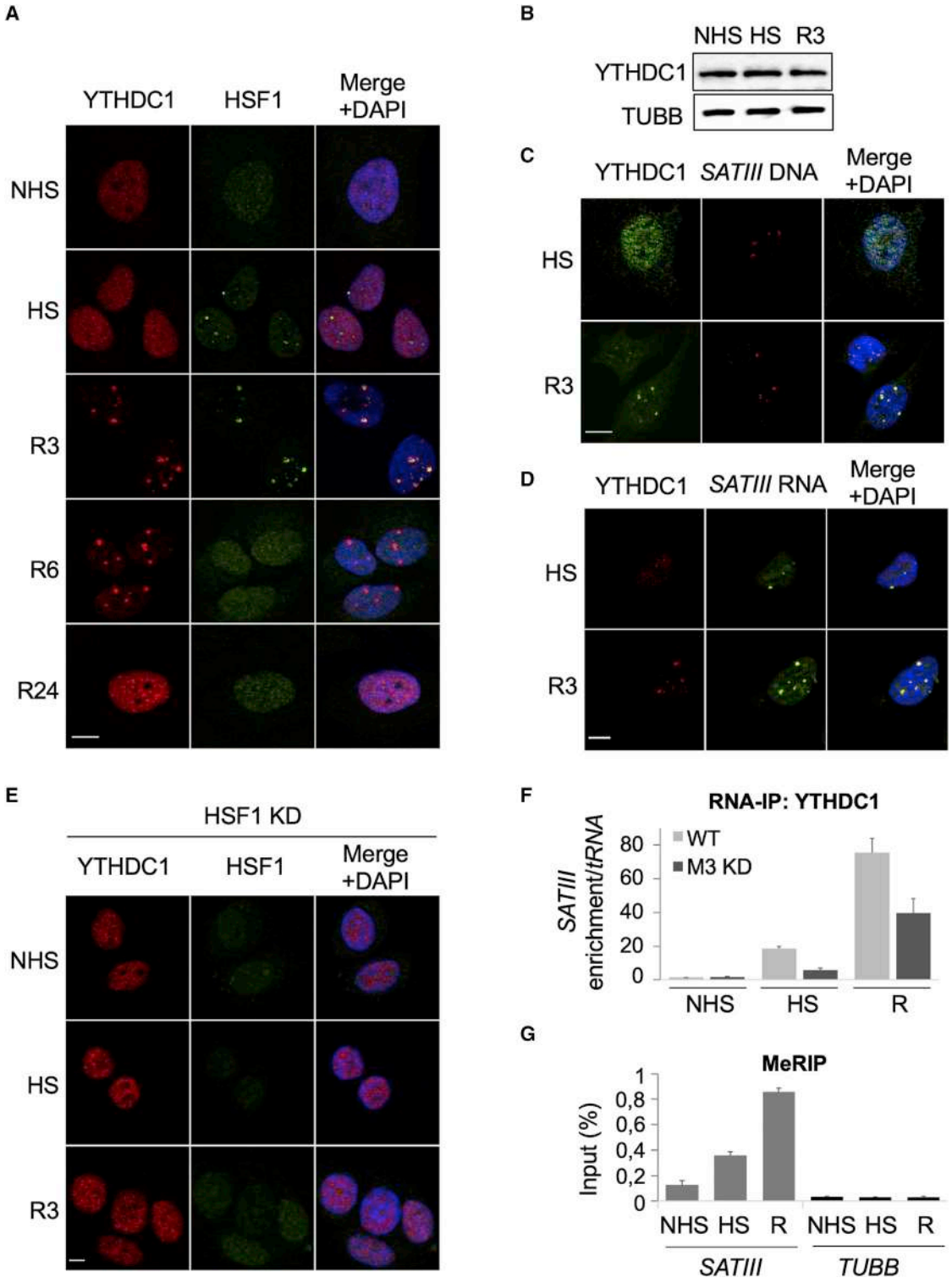

Figure 4. YTHDC1 relocates to nSBs in a HSF1-dependent manner and associates with *SATIII* ncRNAs

(A) Microscopy images of YTHDC1 (red) and HSF1 (green) fluorescent immunostainings showing their subcellular localization in cells not heat stressed (NHS), in cells subjected to a heat stress (HS), or in cells subjected to a heat stress followed by 3, 6, or 24 h of recovery (R3, R6, or R24). Nuclear DNA was stained with DAPI (blue). Data shown are representative of three independent experiments. Scale bar, 10 μm.

(B) Western blot showing YTHDC1 protein level in NHS, HS, or R3 cells. Tubulin-β (TUBB) was used as a loading control.

(legend continued on next page)

YTHDF2 cellular localization had been reported to change upon heat stress.[33] Under HS, YTHDF2 indeed showed a change of its location but only within the cytoplasm, while the other YTH proteins did not undergo major subcellular relocation (Figure S4B). Thus, YTHDC1 is the only member of the YTH protein family that displays a stress-dependent relocation to nSBs in response to an HS.

We next explored the mechanisms responsible for YTHDC1 relocation to nSBs. We found that YTHDC1 co-localization with nSBs was lost when cells were subjected to RNAse digestion, suggesting that YTHDC1 localization to nSBs is RNA dependent (Figures S5A and S5B). HSF1-dependent activation of transcription of the 9q12 *SATIII* DNA repeats is essential to the formation of nSBs.[23] Importantly, YTHDC1 did not form nuclear foci in heat-stressed HSF1 KD cells (Figure 4E). Moreover, in cells expressing a dominant-negative mutant form of HSF1 (HSF1-*DBDtrim*-GFP), no redistribution of YTHDC1 to the 9q12 locus was observed in response to HS (Figure S5C). This dominant-negative mutant was previously reported to still bind *SATIII* DNA repeats and to prevent WT HSF1 from activating transcription of the *SATIIII* DNA repeats.[23,27] Together with the fact that, when HSF1 no longer associated with nSBs, YTHDC1 still concentrated into nuclear foci (Figure 4A, compare 6 h of recovery with earlier time points), these results indicate that the heat-induced RNA-based relocation of YTHDC1 to nSBs depends on HSF1-activated transcription of *SATIII* DNA repeats, and that YTHDC1 does not require HSF1 to stay within the nSBs.

Interestingly, we found also that METTL3 co-localized with YTHDC1 during the recovery period and that the YTHDC1 signal at nSBs was reduced in METTL3 KD cells (Figure S5D), suggesting that m^{6}A-methylated *SATIII* ncRNAs is involved in YTHDC1 recruitment to nSBs. Accordingly, RNA-IP-qPCR experiments showed that YTHDC1 associated with *SATIII* ncRNAs (Figure 4F). The enrichment of YTHDC1 on *SATIII* ncRNAs mirrored the enrichment of m^{6}A on *SATIII* ncRNAs (Figures 4F and 4G) and YTHDC1 association with *SATIII* ncRNAs was impaired in METTL3 KD cells (Figure 4F). Noticeably, the ectopic YTHDC1-*W428A* mutant protein, expressed in place of the endogenous YTHDC1, still relocated to nSBs (Figures S5E and S5F). Thus, YTHDC1 association with m^{6}A may facilitate YTHDC1 relocation to nSBs rather than being a prerequisite. In support of this possibility, RNA-IP-qPCR experiments showed that METTL3 KD had a lesser effect on YTHDC1 association with *SATIII* ncRNAs than on HSP transcripts (compare Figures 4F and 3C). Finally, RNA-IP-qPCR experiments also showed that YTHDC1 enrichment on *SATIII* ncRNAs gradually increased upon HS to the recovery period, while its enrichment on HSP transcripts was restricted to the HS period (compare Figures 4F and 3C). These later findings show that YTHDC1 concentration within nSBs coincides with its dissociation from HSP transcripts.

YTHDC1 controls heat-induced intron retention

The *SATIII* ncRNAs have been proposed to concentrate splicing regulators within nSBs to facilitate their efficient and timely phosphorylation by the CLK1 kinase during the recovery period.[30] Our finding that YTHDC1 massively relocates to nSBs led us to investigate whether YTHDC1 functions as a regulator of splicing in response to HS, and whether this function might contribute to the global reprogramming of the genome expression induced by HS. Remarkably, among the proteins found to be associated with *SATIII* ncRNAs during recovery,[30] were YTHDC1 and 31 of its interacting proteins (Figure 5A). Furthermore, 25 of these proteins were involved in splicing, with 16 specifically implicated in alternative splicing.

We examined *TAF1D* and *DNAJB9* pre-mRNAs, which were previously identified by RNA-seq analysis and validated by qRT-PCR experiments, as pre-mRNAs subjected to heat induced *SATIII*-dependent intron retention during recovery.[30] Splicing efficiency of *TAF1D* and *DNAJB9* pre-mRNAs was monitored before, during, and after HS, in WT and YTHDC1 KD cells. In NHS and HS cells, no noticeable difference was observed between WT and YTHDC1 KD cells when analyzing the monitored splicing events (Figures S6A and S6B). In contrast, during recovery, YTHDC1 KD cells experienced a delay in restoring the normal level of intron retention compared with WT cells. This defect was intron specific since it was not observed with constitutively spliced introns of the same pre-mRNAs, indicating that YTHDC1 is required for the selective heat-induced retention of introns of *TAF1D* and *DNAJB9* transcripts during recovery. Analysis of the subcellular localization of *TAF1D* and *DNAJB9* transcripts showed that, while 18%–20% of the spliced *TAF1D* and 35%–50% of the spliced *DNAJB9* transcripts accumulated in the nucleoplasm or cytoplasm, less than 5% of the retained intron-containing *TAF1D* and *DNAJB9* transcripts were present in the nucleoplasm or cytoplasm (Figure 5B), indicating that *TAF1D* and *DNAJB9* transcripts experiencing heat-induced intron retention mostly remained associated with chromatin.

To identify transcriptome-wide the differentially retained introns in response to HS we analyzed our RNA-seq data from WT, YTHDC1 KD, and METTL3 KD cells (Figure 5C). Like *TAF1D* and *DNAJB9* transcripts, a total of 272 transcripts were found to require YTHDC1 for their intron retention regulation during the recovery period (Figures 5C and 5D). Strikingly, during the HS period, when most of the heat-induced intron retention regulation takes place (Figure S6C), 412 transcripts, representing 63% of the transcripts experiencing intron retention, also

(C and D) DNA- and RNA-FISH images showing YTHDC1 co-localization with, respectively, *SATIII* DNA repeat pericentromeric region or *SATIII* ncRNAs, during the recovery period 3 h (R3) after a heat stress. Nuclear DNA was stained with DAPI (blue). Scale bar, 10 μm.

(E) Microscopy images showing YTHDC1 (red) and HSF1 (green) fluorescent immunostainings in HSF1 KD cells under NHS, HS, and R3 conditions. Nuclear DNA was stained with DAPI (blue). Scale bar, 10 μm.

(F) YTHDC1 RNA-IP-qPCR showing the enrichment of *SATIII* ncRNA in WT or METTL3 KD cells, under NHS, HS, or R3 conditions. The enrichment is expressed in fold-change relative to IP control (done with irrelevant IgG) and normalized to tRNA (*TRS-CGA1-1* RNA). Graphs show the mean and standard error of the mean (SEM) of three independent experiments.

(G) MeRIP-qPCR showing the enrichment of m^{6}A on *SATIII* ncRNA and *TUBB* RNA in WT cells under NHS, HS, or R3 conditions. The enrichment of m^{6}A is expressed as a percentage of the input. Graphs show the mean and SEM of three independent experiments.

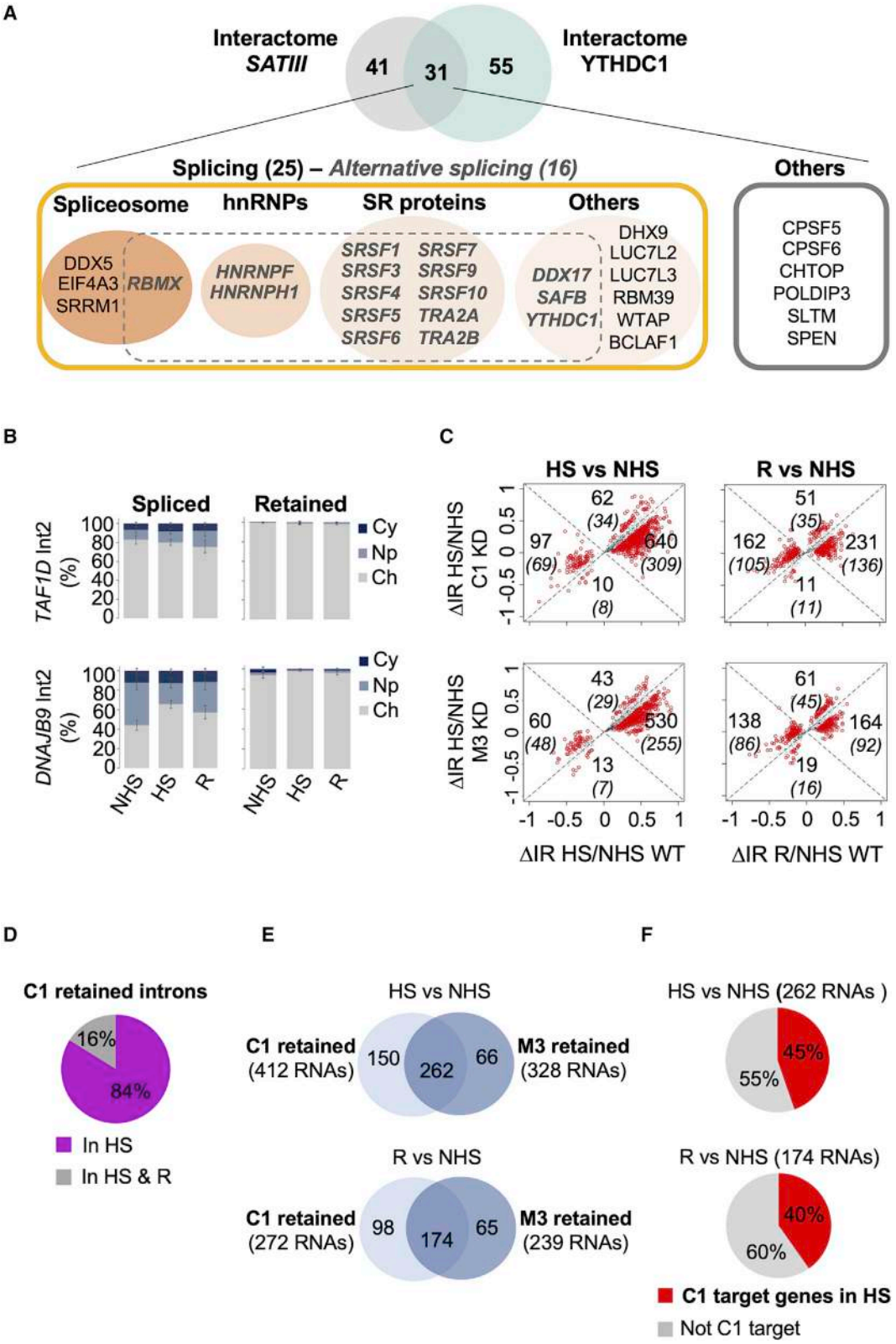

(legend on next page)

required YTHDC1 for their retention (see Figures 5C and S6D, for an example of intron retention). During this period, YTHDC1 predominantly promoted intron retention (Figure 5C, upper left plot, compare the size of the four populations of differentially retained introns). More than 80% of the introns experiencing YTHDC1-dependent retention during the HS period were then properly spliced out during recovery (Figure 5D). Furthermore, most intron retention events regulated by YTHDC1 were coregulated by METTL3 (Figure 5E). Importantly, in agreement with YTHDC1-regulated intron retention taking place at the site of transcription, at least 45% of the respective genes were enriched in YTHDC1 (Figure 5F). Thus, YTHDC1 controls a majority of the intron retention events taking place in response to HS. Moreover, during HS, these YTHDC1-dependent events may occur at the site of transcription for a sizable portion of them.

YTHDC1 indirect regulation of intron retention during recovery

Our ChIP-seq experiments showed enrichment of YTHDC1 at the *CLK1* gene during HS (Figure 6A). Moreover, the level of CLK1 protein increased early in the recovery period in a YTHDC1-dependent manner (Figure 6B). Interestingly, these results, together with the fact that *CLK1* kinase regulates heat-induced intron retention during recovery,[50,51] suggested that during recovery YTHDC1 might control heat-induced intron retention in an indirect manner by controlling expression of CLK1.

To explore how YTHDC1 regulates heat-induced expression of CLK1, we first determined if YTHDC1 binds *CLK1* transcripts in response to HS. Indeed, YTHDC1 associated with *CLK1* transcripts during HS and this association required METTL3 (Figure 6C). The level of m^{6}A enrichment on *CLK1* transcripts also significantly increased during HS (Figure 6D). Since the intron retention status of *CLK1* introns 3 and 4 was previously reported to change between NHS and HS, as part of an autoregulatory loop that controls the production of the catalytically active form of CLK1 kinase,[50,51] we then checked their retention status in YTHDC1 KD cells. Our RNA-seq and RT-PCR analyses showed that retention of these introns was independent of YTHDC1, except for the latest time point during recovery (Figure S7A). Quite unexpectedly, our RNA-seq analysis revealed that introns 5, 7, and 8 of *CLK1* experienced a heat-induced retention in WT cells, but this time specifically during HS (Figures 6E and S7B). In YTHDC1 KD and METTL3 KD cells, the retention of introns 5, 7, and 8 was now also observed in the recovery period (Figure 6F). Moreover, in a similar fashion, *CLK1* intron-3-spliced transcripts associated with chromatin specifically during HS, in WT cells, while they also stayed associated with chromatin during recovery in YTHDC1 KD cells (Figure 6G). Collectively, these results strongly suggest that heat-induced upregulation of CLK1 protein level is controlled by YTHDC1-dependent splicing and release of *CLK1* transcripts from chromatin.

We noted that both YTHDC1-dependent splicing and release of *CLK1* transcripts from chromatin (Figures 6F and 6G) were observed during recovery when YTHDC1 had lost its binding to *CLK1* transcripts (Figure 6C). This result suggested the intriguing possibility that these two YTHDC1 regulations might be "primed" during HS when YTHDC1 binds to *CLK1* transcripts. We then investigated whether other transcripts could experience a similar indirect control by YTHDC1. Remarkably, among a total of 102 transcripts that had, like *CLK1* transcripts, at least one intron retained independently of YTHDC1 during HS but spliced in a YTHDC1-dependent manner during recovery (Figure 6H), 68 of them also had YTHDC1 enriched at their gene during HS (Figure 6I). Moreover, HSP heat-induced genes were clearly over-represented among this list of genes (Figure 6J). Thus, during recovery, dozens of pre-mRNAs, including HSP pre-mRNAs, experience a YTHDC1-dependent splicing, which may be primed during HS when they are targeted by YTHDC1 and which may significantly contribute to the indirect YTHDC1-dependent regulation of intron retention taking place during the recovery period.

DISCUSSION

This study provides evidence that YTHDC1 and m^{6}A signaling are key players in the coordination of the heat-induced reprogramming of gene expression, with YTHDC1 and m^{6}A acting on, or in the close environment of, chromatin. Below, we discuss the implication of these findings on our understanding of the rapid and profound readjustment of gene expression taking place in response to HS (Figure S8).

Figure 5. YTHDC1 controls heat-induced intron retention both during and after HS

(A) Venn diagram of YTHDC1 and *SATIII* protein interactomes. The proteins common to both interactomes are listed below the diagram. For both interactomes only proteins identified by mass spectrometry with at least one peptide in three independent purifications were selected. Proteins involved in alternative splicing are in bold and italic.

(B) Distribution of *TAF1D* and *DNAJB9* RNAs between the cytoplasmic (Cy), nucleoplasmic (Np), and chromatin-associated (Ch) fractions in unstressed cells (no heat stress, NHS), heat stressed (HS), or heat-stressed cells allowed to recover (R) for 3 h, quantified by qRT-PCR after their purification from the different fractions. The RNA distribution is expressed as a percentage of the total RNA population. Graphs show the mean and standard error of the mean (SEM) of three independent experiments.

(C) Scatterplots showing intron retention changes between WT cells (x axis) versus YTHDC1 KD cells or METTL3 KD cells (y axis) in HS (left panel) or R3 (right panel) compared with NHS conditions. Introns with significant retention changes (10%) between cell lines are plotted in red and their number indicated according to their variation between WT and KD cells. The number of corresponding transcripts is shown in brackets and italic. The total number of RNAs with retained introns that are YTHDC1 dependent is of 412 in HS versus NHS conditions and 272 in R versus NHS conditions.

(D) Pie chart showing the percentage of RNAs experiencing YTDHC1-dependent intron retention only during HS or during HS and recovery.

(E) Venn diagram showing the transcripts experiencing both YTHDC1- and METTL3-dependent heat-induced intron retention regulation during HS (HS versus NHS) or during recovery (R versus NHS).

(F) Pie charts showing the percentage of RNAs experiencing both YTHDC1- and METTL3-dependent heat-induced intron retention regulation (in HS versus NHS and R3 versus NHS) and having at their genes enriched in YTHDC1 during HS.

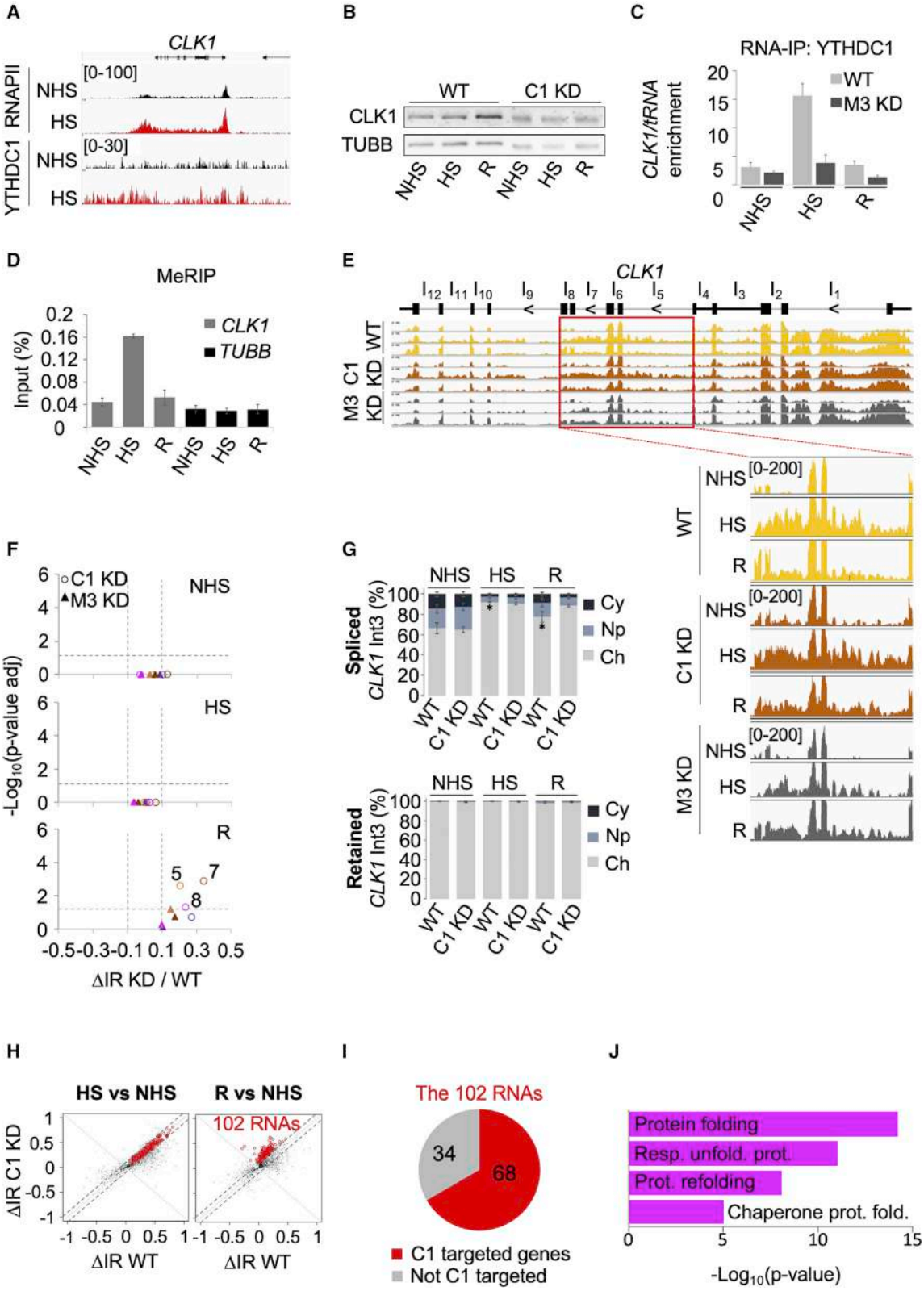

(legend on next page)

Our initial characterization of YTHDC1 showed that YTHDC1 predominantly associates to the chromatin fraction both in unstressed and heat-stressed cells. This finding is in agreement with recent studies showing that m^{6}A is deposited co-transcriptionally on RNAs, in particular during heat stress,[31] and that it mediates co-transcriptional regulations,[38,39] such as RNA processing and degradation[34,35,52] or deposition of repressive histone marks.[53] Our study uncovered that, during HS, YTHDC1 co-transcriptionally promotes expression of HSPs in a METTL3-dependent manner, by facilitating one or more processes occurring at the 3′ end of their genes, such as cleavage/polyadenylation, termination, or transcript release from the site of production. This may be related to what has been recently described for YTHDC1 in the mouse[45] and for other nuclear YTH proteins in plants[54] and in fission yeast,[54,55] indicating that YTHDC1 chromatin-associated regulation of gene expression may be evolutionarily conserved. In addition, YTHDF2 m^{6}A reader and m^{6}A modification of HSP mRNAs were reported to promote translation of HSP mRNAs under HS.[32,33] This indicates that heat-induced expression of HSPs may result from a close functional interplay between two m^{6}A readers acting on the same HSP transcripts. Importantly, regardless of the intimate mechanisms involved in this m^{6}A-based regulation and their potential conservation, which will require further studies to be better understood, our study provides evidence that YTHDC1 plays a key role in co-transcriptionally upregulating the expression of HSPs, and indicates that expression of potentially many other heat-induced genes may be regulated in a similar fashion in response to HS.

In parallel, our study also uncovered a critical and broad function for YTHDC1 in controlling intron retention events triggered by HS. Heat-induced intron retention regulation was reported to take place within hundreds to thousands of transcripts during HS[9,10] and recovery.[30,44] Our findings support a model whereby, during the HS period, YTHDC1 acts at the site of transcription of many of these transcripts to mostly promote m^{6}A-dependent intron retention. In addition, YTHDC1 controls the splicing and expression of the *CLK1* transcript, which encodes a key regulator of intron retention during the recovery period, indicating that YTHDC1 not only acts directly by regulating intron retention of the transcripts it binds to, but also indirectly through a control of CLK1 expression. This indirect regulation of intron retention is particularly relevant with the model where the primary function of YTHDC1's relocation to nSBs is to sequester most of YTHDC1 to stop YTHDC1-dependent intron retention as well as upregulation of HSPs triggered by HS (Figure S8). In support of a role for nSBs in a negative feedback mechanism, more than 80% of the introns that required YTHDC1 for their retention during HS were spliced when YTHDC1 relocated to nSBs. Furthermore, inhibition of the formation of nSBs enhances heat-induced intron retention during HS.[9]

Introns 3 and 4 of *CLK1* were previously defined as retained introns in unstressed cells.[50] Our study identified *CLK1* introns 5, 7, and 8 as introns that are retained only during HS in WT cells. Transcripts experiencing heat-induced intron retention have been reported to accumulate in the nucleus.[10] Our subcellular fractionation experiments showed that *CLK1* transcripts, as well as other transcripts containing one or more retained introns, stay associated to the chromatin fraction, indicating that heat stress may not only block protein expression by inhibiting transcription but also inhibit the release of certain transcripts from chromatin by interfering with their splicing. YTHDC1-dependent splicing of *CLK1* introns 5, 7, and 8 takes place at a time when YTHDC1 no longer associates with *CLK1* transcripts. An intriguing possibility may be that YTHDC1-mediated splicing of introns 5, 7, and 8 is bookmarked during HS when YTHDC1 binds to *CLK1* transcript. Importantly, whatever the exact molecular mechanism is, our data also indicate that this regulation

Figure 6. YTHDC1 promotes the splicing of *CLK1* and *HSP* introns, retained during HS

(A) Browser shot of YTHDC1 and RNAPII ChIP-seq reads at *CLK1* gene from non-heat-stressed (NHS, non-heat stressed) and heat-stressed (HS) cells, with a scheme of *CLK1* gene shown above.

(B) Western blots showing the levels of CLK1 protein in WT or YTHDC1 KD cells from NHS, HS, or heat stressed and then allowed to recover (R) for 3 h conditions. Tubulin-β (TUBB) is shown as loading control.

(C) RNA-IP-qPCR showing YTHDC1 enrichment on *CLK1* RNA in WT or METTL3 KD cells, under NHS, HS, or R conditions. Variation of RNA signal is expressed as fold-change relative to IP control (done with irrelevant IgG) and normalized to tRNA (*TRS-CGA1-1* RNA). Graphs show the mean and standard error of the mean (SEM) of three independent experiments.

(D) MeRIP-qPCR showing m^{6}A enrichment on *CLK1* RNA in WT cells under NHS, HS, or R3 conditions. The enrichment is expressed as a percentage of the input. Graphs show the mean and SEM of three independent experiments.

(E) Browser shot showing RNA-seq reads at *CLK1* locus in WT, YTHDC1 KD, and METTL3 KD cells under NHS, HS, or R conditions. The rectangle and the zoom shown below highlight the pre-mRNA sequence where introns remain in YTHDC1 KD and METTL3 KD cells during the recovery period. A scheme of *CLK1* gene organization is shown above the browser shots, with the positions of the exon and intron sequences that are highlighted and the introns numbered from 1 to 12.

(F) Volcano plots of *CLK1* introns 5–8 retention in YTHDC1 KD versus WT cells (circles) and in METTL3 KD versus WT cells (triangles), under NHS, HS, and R3 conditions. The average intron retention change (ΔIR) from three independent experiments in KD versus WT cells is plotted along the x axis and p values [$-\text{Log}_{10}$(p value adjusted)] along the y axis. Introns with ΔIR > 0.1 or ΔIR < 0.1 and a $-\text{Log}_{10}$(p value adjusted) > 1.3 have their intron number indicated.

(G) qRT-PCR showing the distribution of *CLK1* transcripts, containing or not intron 3, between the chromatin-associated (Ch), nucleoplasmic (Np), and cytoplasmic (Cy) fractions in WT and YTHDC1 KD cells, under NHS, HS, or R3 conditions. The RNA distribution is expressed as a percentage of the total *CLK1* RNA population found in the Ch, Np, and Cy fractions. Graphs show the mean and SEM of three independent experiments. The p value was calculated using a two-tailed Student's t test. *p = 0.04 for the difference in percentages of spliced *CLK1* transcript in WT cells in HS versus recovery. The same percentages in YTHDC1 KD cells shows no significant difference.

(H) Scatterplots showing, for the introns that have their retention regulated in response to HS in WT cells in HS and R conditions (Figure S6C), the changes in intron retention (IR) between WT cells (x axis) and YTHDC1 KD cells (y axis), in HS (left panel) or R3 (right panel) relative to NHS conditions. Plotted in red are the 102 transcripts containing at least one intron retained independently of YTHDC1 during HS and spliced in a YTHDC1-dependent manner during recovery.

(I) Pie charts showing that 68 RNAs among the 102 RNAs identified in (H) have their gene enriched in YTHDC1 during the HS period.

(J) GO enrichments among the 68 genes (identified in [I]) as targeted by YTHDC1 during HS.

potentially takes place on dozens of other transcripts, including HSP transcripts.

This study also sheds light on the mechanism by which YTHDC1 relocates to nSBs and on the function of these membrane-less structures as the cell progresses through the heat stress response. Our study demonstrates that YTHDC1 relocation to nSBs relies on the HSF1-dependent transcription of *SATIII* DNA repeats triggered by HS. The nSBs have long been proposed to regulate the splicing process via the relocation of splicing regulators within the bodies.[29,56,57] Strikingly, by comparing the list of proteins co-purifying with YTHDC1 and with *SATIII* ncRNAs,[30] it appeared that not only YTHDC1 but many of its co-purifying proteins associate with *SATIII* transcripts, in particular, SRSFs proteins. In addition, our study shows *in vivo* that YTHDC1 binds to *SATIII* ncRNAs and that METTL3 also relocates to nSBs. After our study was submitted for publication, Ninomiya and co-workers provided evidence that METTL3 and YTHDC1 localize to nSBs in response to HS, that *SATIII* are m^{6}A-methylated by METTL3, and that m^{6}A-dependent *SATIII* sequestration of YTHDC1 is part of the mechanism controlling splicing during the recovery period.[44] From all these findings, we propose that the primary function of *SATIII* m^{6}A-dependent sequestration of YTHDC1 within nSBs is to inhibit YTHDC1 functions, in promoting intron retention and HSP expression, which are induced during the HS period. Noteworthy, this sequestration mechanism is reminiscent of the rapid and reversible nuclear sequestration of the unique YTH protein in fission yeast that governs entry into meiosis, and which, in this case, is triggered by nutrient starvation stress and occurs on a *cis*-acting ncRNA, but in an m^{6}A-independent fashion.[58,59]

Taken together, our findings identify a regulatory system centered around YTHDC1 and m^{6}A signaling that, over the course of the cellular response to HS, acts directly and indirectly at different genomic locations, different stages of the gene expression process, and at different times. In addition to HSF1 and potentially other transcription factors that induce gene transcription upon heat stress,[6,7] YTHDC1, m^{6}A signaling, and nSBs constitute an elaborate regulatory system that ensures proper orchestration of the heat-induced reprogramming of gene expression. Since YTHDC1 together with RNAPII co-occupy the promoter region of the most downregulated genes in response to HS (Figure 2D), YTHDC1 and m^{6}A may have an even broader role in the stress-dependent gene expression reprogramming by also contributing to the heat-induced repression of genes.[7,60] Taking into consideration the contributions of HSF1, of HSPs, and of the heat stress response, in general, to the development of cancer,[4,61–63] this study, which improves our understanding of the major reprogramming of gene expression induced by heat stress, is susceptible to also provide insights into oncogenic mechanisms.

Limitations of the study

In this study, we show, by using cell fractionation experiments, that the vast majority of YTHDC1 is found in the chromatin-enriched fraction and ChIP-seq experiments further show that YTHDC1 is enriched at thousands of genes. However, these experiments are not sufficient to evaluate to what extent YTHDC1 protein population associates to chromatin only, and not to other cellular elements, such as the nuclear matrix, which co-fractionates with the chromatin fraction. In addition, our MeRIP-qPCR experiments show that HSP transcripts, other protein-coding transcripts subjected to YTHDC1-dependent intron retention, as well as *SATIII* ncRNAs, have their level of m^{6}A modification that significantly increases in response to HS. Yet, they do not provide any information on where the m^{6}A marks accumulate along the RNA. Obtaining such information may shed light on how exactly YTHDC1 regulates the processing and functions of these RNAs. Our findings also strongly support the fact that YTHDC1 acts co-transcriptionally to regulate transcripts and that this co-transcriptional regulation is important for controlling expression of their genes, in response to HS. Nevertheless, the extent to which YTHDC1 may also regulate their expression by acting at a post-transcriptional level remains to be determined. Finally, our data indicate that, later in the HS response, YTHDC1 subsequent and temporary localization to nSBs may mainly have to do with the downregulation of the YTHDC1-dependent activities that take place during HS (i.e., the induction of HSP expression and the temporary repression of the expression of hundreds of other proteins). Yet, an intriguing possibility that our study does not address is that YTHDC1 relocation to nSBs may also have to do with other potential functions of YTHDC1 taking place within these membrane-less structures, such as the processing of the *SATIII* ncRNAs or the re-assembly of the neighboring heterochromatin. Regardless of these limitations, our work identifies YTHDC1 and m^{6}A signaling as key actors of a chromatin-associated reprogramming of expression of hundreds of genes triggered by HS.

STAR★METHODS

Detailed methods are provided in the online version of this paper and include the following:

- KEY RESOURCES TABLE
- RESOURCE AVAILABILITY
  - Lead contact
  - Materials availability
  - Data and code availability
- EXPERIMENTAL MODEL AND SUBJECT DETAILS
  - Cell lines
  - Bacteria
- METHOD DETAILS
  - RNA interference, and plasmid transfections
  - DNA constructs and mutagenesis
  - RNA purification and analysis
  - Western-blot analysis
  - Subcellular fractionation
  - Protein immunopurification
  - Microscopy analyses with immunofluorescence, RNA-FISH and DNA-FISH
  - Chromatin immunoprecipitation (ChIP)
  - RNA immunoprecipitation (RIP)
  - Bioinformatic analysis for chIP-seq data
  - Bioinformatic analysis of RNA-seq data

- Mass spectrometry (MS)-based quantitative proteomic analysis
- QUANTIFICATION AND STATISTICAL ANALYSIS

SUPPLEMENTAL INFORMATION

Supplemental information can be found online at https://doi.org/10.1016/j.celrep.2022.111784.

ACKNOWLEDGMENTS

We thank L. Sistonen for HSF1 KD HeLa cells, J.M. Escudier (Plateforme de synthèse d'Oligonucléotides modifiés de l'Interface Chimie Biologie de l'ITAV-Toulouse, France) for the synthesis of oligonucleotide probes for *in situ* analysis. We thank Valérie Mezger, Ramesh Pillai, and members of the A.V. and R.K. laboratories for their helpful comments and critical reading of the manuscript. We thank Cyril Boyault for his help with GO tools, Virginie Faure for her initial input with ChIP, members of the cell imaging core facility (MicroCell) from IAB for technical support with microscope analyses and the IAB InGeProt (Innovative Genome editing and Protein purification) service. Most of the computations presented in this paper were performed using the GRICAD infrastructure (https://gricad.univ-grenoble-alpes.fr), which is supported by Grenoble research communities, and the bioinformatics core facility of the Bioenvironnement platform at Perpignan. This study was supported by grants from the French Agence National pour la Recherche (ANR) "RNAgerm-Silence" to A.V. and "Heat-EpiRNA" to C.B.-A. and A.V., from MSDAVENIR (ERiCAN, Epigenetic Reprogramming of Cancer Cell Plasticity and Resilience) to A.V. and S.K., from ProFI (ANR-10-INBS-08-01 grant) to Y.C., and from ANRS, MSDAVENIR (Hide, Inflame & Seq) and European Research Council (CoG RNAmedTGS) to R.K. Work conducted at LGDP (Perpignan) was set within the framework of the "Laboratoires d'Excellences (LABEX)" TULIP (ANR-10-LABX-41) and of the "École Universitaire de Recherche (EUR)" TULIP-GS (ANR-18-EURE-0019).

AUTHOR CONTRIBUTIONS

K.T., D.S.-B., and A.V. planned the study and designed the experiments. K.T., M.-C.C., R.M., C.V., C.B.-A., R.K., D.S.-B., and A.V. analyzed the data. K.T., D.S.-B., and A.V. wrote the paper and all authors refined the manuscript. D.S.-B. performed IPs and cell fractionations. S.F. and Y.C. performed the mass spectrometry-based quantitative proteomic analyses. D.S.-B. and M.H. performed the ChIPs. K.T., C.B., M.H., R.K., D.S.-B., and A.V. performed the analyses of the ChIP-seq data. M.-C.C., R.M., C.B.-A., D.S.-B., and A.V. performed the analyses of the RNA-seq data. K.T. with the help of D.S.-B. performed western blots and splicing assays. K.T., D.S.-B., and L.T.-T. designed and performed the RNAi and rescue experiments. K.T., A.G., and D.S.-B. performed RNA analyses. R.M., L.T.-T., D.S.-B., and A.V. performed the RNA IP-qPCR analyses. S.D. performed *SATIII* RNA/DNA-FISH. K.T. and S.D. performed immunofluorescence analyses. K.T., S.D., C.V., D.S.-B., and A.V. planned and designed *in situ* experiments. F.C., S.R., S.K., D.S.-B., and A.V. conducted the intron retention analyses. D.S.-B. performed most of the other experiments with help from K.T.

DECLARATION OF INTERESTS

The authors declare no competing interests.

Received: February 15, 2021
Revised: August 1, 2022
Accepted: November 15, 2022
Published: December 13, 2022

REFERENCES

1. Jolly, C., and Morimoto, R.I. (2000). Role of the heat shock response and molecular chaperones in oncogenesis and cell death. J. Natl. Cancer Inst. *92*, 1564–1572. https://doi.org/10.1093/jnci/92.19.1564.
2. Akerfelt, M., Morimoto, R.I., and Sistonen, L. (2010). Heat shock factors: integrators of cell stress, development and lifespan. Nat. Rev. Mol. Cell Biol. *11*, 545–555. https://doi.org/10.1038/nrm2938.
3. Dai, C. (2018). The heat-shock, or HSF1-mediated proteotoxic stress, response in cancer: from proteomic stability to oncogenesis. Philos. Trans. R. Soc. Lond. B Biol. Sci. *373*, 20160525. https://doi.org/10.1098/rstb.2016.0525.
4. Gomez-Pastor, R., Burchfiel, E.T., and Thiele, D.J. (2018). Regulation of heat shock transcription factors and their roles in physiology and disease. Nat. Rev. Mol. Cell Biol. *19*, 4–19. https://doi.org/10.1038/nrm.2017.73.
5. Richter, K., Haslbeck, M., and Buchner, J. (2010). The heat shock response: life on the verge of death. Mol. Cell *40*, 253–266. https://doi.org/10.1016/j.molcel.2010.10.006.
6. Mahat, D.B., Salamanca, H.H., Duarte, F.M., Danko, C.G., and Lis, J.T. (2016). Mammalian heat shock response and mechanisms underlying its genome-wide transcriptional regulation. Mol. Cell *62*, 63–78. https://doi.org/10.1016/j.molcel.2016.02.025.
7. Vihervaara, A., Mahat, D.B., Guertin, M.J., Chu, T., Danko, C.G., Lis, J.T., and Sistonen, L. (2017). Transcriptional response to stress is pre-wired by promoter and enhancer architecture. Nat. Commun. *8*, 255. https://doi.org/10.1038/s41467-017-00151-0.
8. Vihervaara, A., Duarte, F.M., and Lis, J.T. (2018). Molecular mechanisms driving transcriptional stress responses. Nat. Rev. Genet. *19*, 385–397. https://doi.org/10.1038/s41576-018-0001-6.
9. Hussong, M., Kaehler, C., Kerick, M., Grimm, C., Franz, A., Timmermann, B., Welzel, F., Isensee, J., Hucho, T., Krobitsch, S., and Schweiger, M.R. (2017). The bromodomain protein BRD4 regulates splicing during heat shock. Nucleic Acids Res. *45*, 382–394. https://doi.org/10.1093/nar/gkw729.
10. Shalgi, R., Hurt, J.A., Lindquist, S., and Burge, C.B. (2014). Widespread inhibition of posttranscriptional splicing shapes the cellular transcriptome following heat shock. Cell Rep. *7*, 1362–1370. https://doi.org/10.1016/j.celrep.2014.04.044.
11. Yost, H.J., and Lindquist, S. (1991). Heat shock proteins affect RNA processing during the heat shock response of Saccharomyces cerevisiae. Mol. Cell Biol. *11*, 1062–1068. https://doi.org/10.1128/mcb.11.2.1062-1068.1991.
12. Saavedra, C., Tung, K.S., Amberg, D.C., Hopper, A.K., and Cole, C.N. (1996). Regulation of mRNA export in response to stress in Saccharomyces cerevisiae. Genes Dev. *10*, 1608–1620. https://doi.org/10.1101/gad.10.13.1608.
13. Zander, G., Hackmann, A., Bender, L., Becker, D., Lingner, T., Salinas, G., and Krebber, H. (2016). mRNA quality control is bypassed for immediate export of stress-responsive transcripts. Nature *540*, 593–596. https://doi.org/10.1038/nature20572.
14. Lindquist, S. (1981). Regulation of protein synthesis during heat shock. Nature *293*, 311–314. https://doi.org/10.1038/293311a0.
15. Shalgi, R., Hurt, J.A., Krykbaeva, I., Taipale, M., Lindquist, S., and Burge, C.B. (2013). Widespread regulation of translation by elongation pausing in heat shock. Mol. Cell *49*, 439–452. https://doi.org/10.1016/j.molcel.2012.11.028.
16. Tabuchi, Y., Takasaki, I., Wada, S., Zhao, Q.L., Hori, T., Nomura, T., Ohtsuka, K., and Kondo, T. (2008). Genes and genetic networks responsive to mild hyperthermia in human lymphoma U937 cells. Int. J. Hyperthermia *24*, 613–622. https://doi.org/10.1080/02656730802140777.
17. Trinklein, N.D., Murray, J.I., Hartman, S.J., Botstein, D., and Myers, R.M. (2004). The role of heat shock transcription factor 1 in the genome-wide

regulation of the mammalian heat shock response. Mol. Biol. Cell *15*, 1254–1261. https://doi.org/10.1091/mbc.e03-10-0738.

18. Kampinga, H.H. (2006). Chaperones in preventing protein denaturation in living cells and protecting against cellular stress. Handb. Exp. Pharmacol., 1–42. https://doi.org/10.1007/3-540-29717-0_1.
19. Joutsen, J., and Sistonen, L. (2019). Tailoring of proteostasis networks with heat shock factors. Cold Spring Harb. Perspect. Biol. *11*, a034066. https://doi.org/10.1101/cshperspect.a034066.
20. Morimoto, R.I. (1998). Regulation of the heat shock transcriptional response: cross talk between a family of heat shock factors, molecular chaperones, and negative regulators. Genes Dev. *12*, 3788–3796. https://doi.org/10.1101/gad.12.24.3788.
21. Pirkkala, L., Nykänen, P., and Sistonen, L. (2001). Roles of the heat shock transcription factors in regulation of the heat shock response and beyond. FASEB. J *15*, 1118–1131. https://doi.org/10.1096/fj00-0294rev.
22. Vourc'h, C., Dufour, S., Timcheva, K., Seigneurin-Berny, D., and Verdel, A. (2022). HSF1-Activated non-coding stress response: satellite lncRNAs and beyond, an emerging story with a complex scenario. Genes *13*, 597. https://doi.org/10.3390/genes13040597.
23. Jolly, C., Konecny, L., Grady, D.L., Kutskova, Y.A., Cotto, J.J., Morimoto, R.I., and Vourc'h, C. (2002). In vivo binding of active heat shock transcription factor 1 to human chromosome 9 heterochromatin during stress. J. Cell Biol. *156*, 775–781. https://doi.org/10.1083/jcb.200109018.
24. Col, E., Hoghoughi, N., Dufour, S., Penin, J., Koskas, S., Faure, V., Ouzounova, M., Hernandez-Vargash, H., Reynoird, N., Daujat, S., et al. (2017). Bromodomain factors of BET family are new essential actors of pericentric heterochromatin transcriptional activation in response to heat shock. Sci. Rep. *7*, 5418. https://doi.org/10.1038/s41598-017-05343-8.
25. Lellahi, S.M., Rosenlund, I.A., Hedberg, A., Kiær, L.T., Mikkola, I., Knutsen, E., and Perander, M. (2018). The long noncoding RNA NEAT1 and nuclear paraspeckles are up-regulated by the transcription factor HSF1 in the heat shock response. J. Biol. Chem. *293*, 18965–18976. https://doi.org/10.1074/jbc.RA118.004473.
26. Cotto, J., Fox, S., and Morimoto, R. (1997). HSF1 granules: a novel stress-induced nuclear compartment of human cells. J. Cell Sci. *110*, 2925–2934.
27. Jolly, C., Metz, A., Govin, J., Vigneron, M., Turner, B.M., Khochbin, S., and Vourc'h, C. (2004). Stress-induced transcription of satellite III repeats. J. Cell Biol. *164*, 25–33. https://doi.org/10.1083/jcb.200306104.
28. Rizzi, N., Denegri, M., Chiodi, I., Corioni, M., Valgardsdottir, R., Cobianchi, F., Riva, S., and Biamonti, G. (2004). Transcriptional activation of a constitutive heterochromatic domain of the human genome in response to heat shock. Mol. Biol. Cell *15*, 543–551. https://doi.org/10.1091/mbc.E03-07-0487.
29. Biamonti, G., and Vourc'h, C. (2010). Nuclear stress bodies. Cold Spring Harb. Perspect. Biol. *2*, a000695. https://doi.org/10.1101/cshperspect.a000695.
30. Ninomiya, K., Adachi, S., Natsume, T., Iwakiri, J., Terai, G., Asai, K., and Hirose, T. (2020). LncRNA-dependent nuclear stress bodies promote intron retention through SR protein phosphorylation. EMBO J. *39*, e102729. https://doi.org/10.15252/embj.2019102729.
31. Knuckles, P., Carl, S.H., Musheev, M., Niehrs, C., Wenger, A., and Bühler, M. (2017). RNA fate determination through cotranscriptional adenosine methylation and microprocessor binding. Nat. Struct. Mol. Biol. *24*, 561–569. https://doi.org/10.1038/nsmb.3419.
32. Meyer, K.D., Patil, D.P., Zhou, J., Zinoviev, A., Skabkin, M.A., Elemento, O., Pestova, T.V., Qian, S.B., and Jaffrey, S.R. (2015). 5' UTR m(6)A promotes cap-independent translation. Cell *163*, 999–1010. https://doi.org/10.1016/j.cell.2015.10.012.
33. Zhou, J., Wan, J., Gao, X., Zhang, X., Jaffrey, S.R., and Qian, S.B. (2015). Dynamic m(6)A mRNA methylation directs translational control of heat shock response. Nature *526*, 591–594. https://doi.org/10.1038/nature15377.
34. Zaccara, S., Ries, R.J., and Jaffrey, S.R. (2019). Reading, writing and erasing mRNA methylation. Nat. Rev. Mol. Cell Biol. *20*, 608–624. https://doi.org/10.1038/s41580-019-0168-5.
35. Shi, H., Wei, J., and He, C. (2019). Where, when, and how: context-dependent functions of RNA methylation writers, readers, and erasers. Mol. Cell *74*, 640–650. https://doi.org/10.1016/j.molcel.2019.04.025.
36. Duan, H.C., Wang, Y., and Jia, G. (2019). Dynamic and reversible RNA N(6)-methyladenosine methylation. Wiley Interdiscip. Rev. RNA *10*, e1507. https://doi.org/10.1002/wrna.1507.
37. Huang, H., Weng, H., and Chen, J. (2020). The biogenesis and precise control of RNA m(6)A methylation. Trends Genet. *36*, 44–52. https://doi.org/10.1016/j.tig.2019.10.011.
38. Ke, S., Pandya-Jones, A., Saito, Y., Fak, J.J., Vågbø, C.B., Geula, S., Hanna, J.H., Black, D.L., Darnell, J.E., Jr., and Darnell, R.B. (2017). m(6)A mRNA modifications are deposited in nascent pre-mRNA and are not required for splicing but do specify cytoplasmic turnover. Genes Dev. *31*, 990–1006. https://doi.org/10.1101/gad.301036.117.
39. Slobodin, B., Han, R., Calderone, V., Vrielink, J.A.F.O., Loayza-Puch, F., Elkon, R., and Agami, R. (2017). Transcription impacts the efficiency of mRNA translation via Co-transcriptional N6-adenosine methylation. Cell *169*, 326–337.e12. https://doi.org/10.1016/j.cell.2017.03.031.
40. Yu, J., Li, Y., Wang, T., and Zhong, X. (2018). Modification of N6-methyladenosine RNA methylation on heat shock protein expression. PLoS One *13*, e0198604. https://doi.org/10.1371/journal.pone.0198604.
41. Xiang, Y., Laurent, B., Hsu, C.H., Nachtergaele, S., Lu, Z., Sheng, W., Xu, C., Chen, H., Ouyang, J., Wang, S., et al. (2017). RNA m(6)A methylation regulates the ultraviolet-induced DNA damage response. Nature *543*, 573–576. https://doi.org/10.1038/nature21671.
42. Zhou, J., Wan, J., Shu, X.E., Mao, Y., Liu, X.M., Yuan, X., Zhang, X., Hess, M.E., Brüning, J.C., and Qian, S.B. (2018). N(6)-Methyladenosine guides mRNA alternative translation during integrated stress response. Mol. Cell *69*, 636–647.e7. https://doi.org/10.1016/j.molcel.2018.01.019.
43. Engel, M., Eggert, C., Kaplick, P.M., Eder, M., Röh, S., Tietze, L., Namendorf, C., Arloth, J., Weber, P., Rex-Haffner, M., et al. (2018). The role of m(6)A/m-RNA methylation in stress response regulation. Neuron *99*, 389–403.e9. https://doi.org/10.1016/j.neuron.2018.07.009.
44. Ninomiya, K., Iwakiri, J., Aly, M.K., Sakaguchi, Y., Adachi, S., Natsume, T., Terai, G., Asai, K., Suzuki, T., and Hirose, T. (2021). m(6) A modification of HSATIII lncRNAs regulates temperature-dependent splicing. EMBO J. *40*, e107976. https://doi.org/10.15252/embj.2021107976.
45. Kasowitz, S.D., Ma, J., Anderson, S.J., Leu, N.A., Xu, Y., Gregory, B.D., Schultz, R.M., and Wang, P.J. (2018). Nuclear m6A reader YTHDC1 regulates alternative polyadenylation and splicing during mouse oocyte development. PLoS Genet. *14*, e1007412. https://doi.org/10.1371/journal.pgen.1007412.
46. Lesbirel, S., Viphakone, N., Parker, M., Parker, J., Heath, C., Sudbery, I., and Wilson, S.A. (2018). The m(6)A-methylase complex recruits TREX and regulates mRNA export. Sci. Rep. *8*, 13827. https://doi.org/10.1038/s41598-018-32310-8.
47. Xiao, W., Adhikari, S., Dahal, U., Chen, Y.S., Hao, Y.J., Sun, B.F., Sun, H.Y., Li, A., Ping, X.L., Lai, W.Y., et al. (2016). Nuclear m(6)A reader YTHDC1 regulates mRNA splicing. Mol. Cell *61*, 507–519. https://doi.org/10.1016/j.molcel.2016.01.012.
48. Salifou, K., Burnard, C., Basavarajaiah, P., Helsmoortel, M., Mac, V., Depierre, D., Grasso, G., Franckhauser, C., Beyne, E., Contreras, X., et al. (2020). Chromatin-associated MRN complex protects highly transcribing genes from genomic instability. Preprint at bioRxiv. https://doi.org/10.1101/2020.05.27.118638.
49. Xu, C., Wang, X., Liu, K., Roundtree, I.A., Tempel, W., Li, Y., Lu, Z., He, C., and Min, J. (2014). Structural basis for selective binding of m6A RNA by the YTHDC1 YTH domain. Nat. Chem. Biol. *10*, 927–929. https://doi.org/10.1038/nchembio.1654.

50. Ninomiya, K., Kataoka, N., and Hagiwara, M. (2011). Stress-responsive maturation of Clk1/4 pre-mRNAs promotes phosphorylation of SR splicing factor. J. Cell Biol. *195*, 27–40. https://doi.org/10.1083/jcb.201107093.

51. Uzor, S., Zorzou, P., Bowler, E., Porazinski, S., Wilson, I., and Ladomery, M. (2018). Autoregulation of the human splice factor kinase CLK1 through exon skipping and intron retention. Gene *670*, 46–54. https://doi.org/10.1016/j.gene.2018.05.095.

52. Lee, Y., Choe, J., Park, O.H., and Kim, Y.K. (2020). Molecular mechanisms driving mRNA degradation by m(6)A modification. Trends Genet. *36*, 177–188. https://doi.org/10.1016/j.tig.2019.12.007.

53. Li, Y., Xia, L., Tan, K., Ye, X., Zuo, Z., Li, M., Xiao, R., Wang, Z., Liu, X., Deng, M., et al. (2020). N(6)-Methyladenosine co-transcriptionally directs the demethylation of histone H3K9me2. Nat. Genet. *52*, 870–877. https://doi.org/10.1038/s41588-020-0677-3.

54. Parker, M.T., Knop, K., Sherwood, A.V., Schurch, N.J., Mackinnon, K., Gould, P.D., Hall, A.J., Barton, G.J., and Simpson, G.G. (2020). Nanopore direct RNA sequencing maps the complexity of Arabidopsis mRNA processing and m(6)A modification. Elife *9*, e49658. https://doi.org/10.7554/eLife.49658.

55. Touat-Todeschini, L., Shichino, Y., Dangin, M., Thierry-Mieg, N., Gilquin, B., Hiriart, E., Sachidanandam, R., Lambert, E., Brettschneider, J., Reuter, M., et al. (2017). Selective termination of lncRNA transcription promotes heterochromatin silencing and cell differentiation. EMBO J. *36*, 2626–2641. https://doi.org/10.15252/embj.201796571.

56. Denegri, M., Chiodi, I., Corioni, M., Cobianchi, F., Riva, S., and Biamonti, G. (2001). Stress-induced nuclear bodies are sites of accumulation of pre-mRNA processing factors. Mol. Biol. Cell *12*, 3502–3514. https://doi.org/10.1091/mbc.12.11.3502.

57. Metz, A., Soret, J., Vourc'h, C., Tazi, J., and Jolly, C. (2004). A key role for stress-induced satellite III transcripts in the relocalization of splicing factors into nuclear stress granules. J. Cell Sci. *117*, 4551–4558. https://doi.org/10.1242/jcs.01329.

58. Harigaya, Y., Tanaka, H., Yamanaka, S., Tanaka, K., Watanabe, Y., Tsutsumi, C., Chikashige, Y., Hiraoka, Y., Yamashita, A., and Yamamoto, M. (2006). Selective elimination of messenger RNA prevents an incidence of untimely meiosis. Nature *442*, 45–50. https://doi.org/10.1038/nature04881.

59. Hiriart, E., and Verdel, A. (2013). Long noncoding RNA-based chromatin control of germ cell differentiation: a yeast perspective. Chromosome Res. *21*, 653–663. https://doi.org/10.1007/s10577-013-9393-5.

60. Mahat, D.B., and Lis, J.T. (2017). Use of conditioned media is critical for studies of regulation in response to rapid heat shock. Cell Stress Chaperones *22*, 155–162. https://doi.org/10.1007/s12192-016-0737-x.

61. Lang, B.J., Guerrero-Giménez, M.E., Prince, T.L., Ackerman, A., Bonorino, C., and Calderwood, S.K. (2019). Heat shock proteins are essential components in transformation and tumor progression: cancer cell intrinsic pathways and beyond. Int. J. Mol. Sci. *20*, E4507. https://doi.org/10.3390/ijms20184507.

62. Alasady, M.J., and Mendillo, M.L. (2020). The multifaceted role of HSF1 in tumorigenesis. Adv. Exp. Med. Biol. *1243*, 69–85. https://doi.org/10.1007/978-3-030-40204-4_5.

63. Puustinen, M.C., and Sistonen, L. (2020). Molecular mechanisms of heat shock factors in cancer. Cells *9*. https://doi.org/10.3390/cells9051202.

64. Sandqvist, A., Björk, J.K., Akerfelt, M., Chitikova, Z., Grichine, A., Vourc'h, C., Jolly, C., Salminen, T.A., Nymalm, Y., and Sistonen, L. (2009). Heterotrimerization of heat-shock factors 1 and 2 provides a transcriptional switch in response to distinct stimuli. Mol. Biol. Cell *20*, 1340–1347. https://doi.org/10.1091/mbc.E08-08-0864.

65. Li, H., and Durbin, R. (2009). Fast and accurate short read alignment with Burrows-Wheeler transform. Bioinformatics *25*, 1754–1760. https://doi.org/10.1093/bioinformatics/btp324.

66. Li, H., Handsaker, B., Wysoker, A., Fennell, T., Ruan, J., Homer, N., et al. (2009). The Sequence Alignment/Map format and SAMtools. Bioinformatics *25*, 2078–2079. https://doi.org/10.1093/bioinformatics/btp352.

67. Ramírez, F., Ryan, D.P., Grüning, B., Bhardwaj, V., Kilpert, F., Richter, A.S., Heyne, S., Dündar, F., and Manke, T. (2016). deepTools2: a next generation web server for deep-sequencing data analysis. Nucleic Acids Res. *44*, W160–W165. https://doi.org/10.1093/nar/gkw257.

68. Helmuth, J., Li, N., Arrigoni, L., Gianmoena, K., Cadenas, C., Gasparoni, G., Sinha, A., Rosenstiel, P., Walter, Hengstler, J.G., Manke, T., and Chung, H.R. (2016). normR: Regime enrichment calling for ChIP-seq data. bioRxiv 082263; doi: https://doi.org/10.1101/082263

69. Bolger, A.M., Lohse, M., and Usadel, B. (2014). Trimmomatic: a flexible trimmer for Illumina sequence data. Bioinformatics *30*, 2114–2120. https://doi.org/10.1093/bioinformatics/btu170.

70. Langmead, B., and Salzberg, S.L. (2012). Fast gapped-read alignment with Bowtie 2. Nat. Methods *9*, 357–359. https://doi.org/10.1038/nmeth.1923.

71. Kim, D., Langmead, B., and Salzberg, S.L. (2015). HISAT: a fast spliced aligner with low memory requirements. Nat. Methods *12*, 357–360. https://doi.org/10.1038/nmeth.3317.

72. Anders, S., Pyl, P.T., and Huber, W. (2015). HTSeq–a Python framework to work with high-throughput sequencing data. Bioinformatics *31*, 166–169. https://doi.org/10.1093/bioinformatics/btu638.

73. Love, M.I., Huber, W., and Anders, S. (2014). Moderated estimation of fold change and dispersion for RNA-seq data with DESeq2. Genome Biol. *15*, 550. https://doi.org/10.1186/s13059-014-0550-8.

74. Wickham, H. (2016). ggplot2: Elegant Graphics for Data Analysis (Springer-Verlag).

75. Middleton, R., Gao, D., Thomas, A., Singh, B., Au, A., Wong, J.J.L., Bomane, A., Cosson, B., Eyras, E., Rasko, J.E.J., and Ritchie, W. (2017). IRFinder: assessing the impact of intron retention on mammalian gene expression. Genome Biol. *18*, 51. https://doi.org/10.1186/s13059-017-1184-4.

76. Tyanova, S., Temu, T., and Cox, J. (2016). The MaxQuant computational platform for mass spectrometry-based shotgun proteomics. Nat. Protoc. *11*, 2301–2319. https://doi.org/10.1038/nprot.2016.136.

77. Wieczorek, S., Combes, F., Lazar, C., Giai Gianetto, Q., Gatto, L., Dorffer, A., Hesse, A.M., Couté, Y., Ferro, M., Bruley, C., and Burger, T. (2017). DAPAR & ProStaR: software to perform statistical analyses in quantitative discovery proteomics. Bioinformatics *33*, 135–136. https://doi.org/10.1093/bioinformatics/btw580.

78. Robinson, J.T., Thorvaldsdottir, H., Winckler, W., Guttman, M., Lander, E.S., Getz, G., et al. (2011). Integrative genomics viewer. Nat. Biotechnol. *29*, 24–26. https://doi.org/10.1038/nbt.1754.

79. Schneider, C.A., Rasband, W.S., and Eliceiri, K.W. (2012). NIH Image to ImageJ: 25 years of image analysis. Nat. Methods *9*, 671–675. https://doi.org/10.1038/nmeth.2089.

80. Lawrence, M., Huber, W., Pagès, H., Aboyoun, P., Carlson, M., Gentleman, R., Morgan, M.T., and Carey, V.J. (2013). Software for computing and annotating genomic ranges. PLoS Comput. Biol. *9*, e1003118. https://doi.org/10.1371/journal.pcbi.1003118.

81. Lander, E.S., Linton, L.M., Birren, B., Nusbaum, C., Zody, M.C., Baldwin, J., Devon, K., Dewar, K., Doyle, M., FitzHugh, W., et al. (2001). Initial sequencing and analysis of the human genome. Nature *409*, 860–921. https://doi.org/10.1038/35057062.

82. Anders, S., and Huber, W. (2010). Differential expression analysis for sequence count data. Genome Biol. *11*, R106. https://doi.org/10.1186/gb-2010-11-10-r106.

83. Salvetti, A., Couté, Y., Epstein, A., Arata, L., Kraut, A., Navratil, V., Bouvet, P., and Greco, A. (2016). Nuclear functions of nucleolin through global proteomics and interactomic approaches. J. Proteome Res. *15*, 1659–1669. https://doi.org/10.1021/acs.jproteome.6b00126.

STAR★METHODS

KEY RESOURCES TABLE

REAGENT or RESOURCE	SOURCE	IDENTIFIER
Antibodies		
Rabbit polyclonal anti-YTHDC1	Abcam	Cat# 122340; RRID:AB_11128253
Rabbit polyclonal anti-YTHDC1	Bethyl	Cat# A305-096A; RRID:AB_2631491
Rabbit polyclonal anti-YTHDC1 raised against an N-terminal peptide of YTHDC1	Eurogentec	N/A
Mouse polyclonal anti-HSF1	Santa Cruz Biotechnology	Cat# Sc-17757; RRID:AB_627753
Rabbit polyclonal anti-METTL3	Proteintech	Cat# 15073-1-AP; RRID:AB_2142033
Rat monoclonal anti-RNA polymerase II subunit B1 (phospho CTD Ser-2), clone 3E10	Merck	Cat#04-1571-I
Mouse monoclonal anti-RNA polymerase II, F-12	Santa Cruz Biotechnology	Cat#sc-55492; RRID:AB_630203
Rabbit polyclonal anti-DNAJB1	Bethyl	Cat# A305245AM; RRID:AB_2782499
Rabbit polyclonal anti-HSP70	Stressgen	Cat# SPA-812; RRID:AB_10013742
Rabbit polyclonal anti-HA	Abcam	Cat# ab9110; RRID:AB_307019
Mouse monoclonal anti-Tubulinb	Sigma	Cat# T5168; RRID:AB_477579
Rabbit polyclonal anti-Histone H3	Abcam	Cat#ab1791; RRID:AB_302613
Mouse monoclonal anti-CLK1	Cliniscience	Cat#sc-515307; RRID:AB_2924406
Rabbit polyclonal anti m6a	Synaptic system	Cat#202003; RRID:AB_2279214
Mouse monoclonal anti-SRSF6	MERCK	Cat#MABE152; RRID:AB_10807837
Mouse monoclonal anti-SRSF1	Santa Cruz Biotechnology	Cat#sc33652; RRID:AB_628248
Goat polyclonal anti-rabbit igg Dylight 549	Vector	Cat# DI-1549; RRID:AB_2336407
Goat polyclonal anti-mouse igg Alexa Fluor 488	Invitrogen	Cat# A-11029; RRID:AB_2534088
HRP-conjugated goat anti-rabbit IgG	Dako	Cat# P0448; RRID:AB_2617138
HRP-conjugated goat anti-mouse IgG	Dako	Cat# P0447; RRID:AB_2617137
Rabbit polyclonal IgG (irrelevant IgG)	Diagenode	Cat#C15410206; RRID:AB_2722554
IgG from human serum (irrelevant IgG)	Sigma	Cat#I4506; RRID:AB_1163606
Bacterial and virus strains		
E coli TOP10	Thermofischer	Cat#C404010
Chemicals, peptides, and recombinant proteins		
Trizol Reagent	Thermo Scientific	Cat#15596026
DNaseI RNase free	Sigma	Cat#4716728001
RNase inhibitor	Thermo Scientific	Cat#EO0381
Transcriptor reverse transcriptase	Roche	Cat# 03531287001
Phusion High-Fidelity DNA Polymerase	NEB	Cat# M0530S
Kanamycin sulfate	Sigma	Cat# 60615-5G
Ampicillin	Sigma	Cat# A0166-5G
DAPI	Euromedex	Cat#1050A
DTT	Invitrogen	Cat# 772590
Random Primer	Invitrogen	Cat# P/N 58875
SuperscriptIV reverse transcriptase	Thermo Scientific	Cat#18090050
MESA BLUE qPCR MasterMix Plus	Eurogentec	Cat# 10-SY2X-03
Benzonase	Merck	Cat# 70664-3
RNase A	Merck	Cat#10109142001
Formamide	Euromedex	Cat#1117

(*Continued on next page*)

Continued

REAGENT or RESOURCE	SOURCE	IDENTIFIER
Paraformaldehyde	Merck	Cat#1003403932
N6-methyladenosine 5′ monophosphate sodium salt	Merck	Cat#M2780-10MG
Proteinase K	Roche	Cat#3115887001
DMEM	Thermo Scientific	Cat#21969035
Fetal bovine serum	Gibco	Cat#10270-106
OptiMEM	Thermo Scientific	Cat#31985-047
Chloroform	Carlo Erba	Cat#438601
Isopropanol	Prolabo	Cat#20542298
Acid phenol:chloroform	Thermo Scientific	Cat#AM9722
Ammonium acetate	Prolabo	Cat#33602-264
Triton X-100	Sigma	Cat#T9284
Tris	Euromedex	Cat#EU1018-A
B-mercaptoethanol	Sigma	Cat#63689
SDS 20%	Euromedex	Cat#EU0660B
Glycerol	Euromedex	Cat#EU3550
Bromophenol blue	Sigma	Cat#B5525
Tween 20	Euromedex	Cat#2001
PMSF	Sigma	Cat#78830
Sucrose	Sigma	Cat#S7903
NP-40/Igepal	Sigma	Cat#I8896
Na-deoxycholate	Sigma	Cat#D6750
Saponine	Sigma	Cat#S7900
Glycine	Euromedex	Cat#26-128-6405-C
Hepes	Sigma	Cat#H3375
EDTA	Euromedex	Cat#EU0007
Glycogen	Roche	Cat#10901393001
BSA	Sigma	Cat#B6917
Geneticine	Gibco	Cat#10131-035
Sequencing Grade Modified Trypsin	Promega	Cat#V5111
Critical commercial assays		
Biomixtm Red	Bioline	Cat# BIO-25006
Lipofectamine rnaimax Transfection Reagent	Thermo Scientific	Cat# 13778150
JetPEI	Polyplus transfection	Cat# 101-10N
Q5® Site-Directed Mutagenesis Kit	Biolabs	Cat# E0554S
Next Gen DNA library kit	Active motif	Cat# 53216
Chip-IT High Sensitivity®	Active motif	Cat# 53040
Dynabeads Protein A	Thermo Fisher	Cat# 10001D
nProteinA Sepharose 4 Fast Flow	GE Health Care	Cat# 17-5280-01
Dynabeads mRNA Direct Kit	Thermo Fisher	Cat#61006
Protein-G Dynabeads	Thermo Fisher	Cat#10003D
Clarity Western ECL kit	Biorad	Cat#1705060
Deposited data		
YTHDC1 ChIPseq data	This paper	GEO: GSE166456
RNAPII ChIPseq data	This paper	GEO:GSE143591
RNAseq data	This paper	NCBI Bioproject: PRJNA773186
Raw data (gel, western blots, microscopy images) are deposited at Mendeley Data	This paper	Mendeley data https://doi.org/10.17632/gttn89vbpn.1

(*Continued on next page*)

Continued

REAGENT or RESOURCE	SOURCE	IDENTIFIER
MS data	This paper	Proteomexchange: PXD037414
Experimental models: Cell lines		
Human HeLa cells	ATCC	Cat#CCL-2
Human HT1080	ATCC	Cat#CCL-121
Human HFF2-TERT	Decottignies's Lab	N/A
Human HeLa cells KD-HSF1	Sandqvist et al., 2009[64]	N/A
Oligonucleotides		
For oligonucleotides and siRNA, see Table S4	N/A	N/A
Recombinant DNA		
peGFP-N3 Mammalian expression vector	Addgene	Cat#6080-1
pCI-neo Mammalian Expression Vector	Addgene	Cat#E1841
pGFP-HSF1-DBD-Trim	Jolly et al., 2002[23]	N/A
peGFP_YTHDC1	This paper	N/A
peGFP_YTHDC2	This paper	N/A
peGFP_YTHDF1	This paper	N/A
peGFP_YTHDF2	This paper	N/A
peGFP_YTHDF3	This paper	N/A
pCI-neo-HA-YTHDC1imm	This paper	N/A
pCI-neohythdc1immw428a	This paper	N/A
pCI-neo-HA-YTHDC1	This paper	N/A
Software and algorithms		
FastQC	N/A	https://www.bioinformatics.babraham.ac.uk/projects/fastqc/
Burrows-Wheeler Aligner	Li H. And Durbin R, 2009[65]	http://bio-bwa.sourceforge.net
SAM tools	Li et al., 2009[66]	http://www.htslib.org
DeepTools	Ramirez et al., 2016[67]	https://pubmed.ncbi.nlm.nih.gov/27079975/
NormR	Helmuth et al., 2016[68]	https://www.biorxiv.org/content/10.1101/082263v3
Plotrix package	N/A	https://www.rdocumentation.org/packages/plotrix/versions/3.7-7
Trimmomatic v0.39	Bolger et al., 2014[69]	https://pubmed.ncbi.nlm.nih.gov/24695404/
Bowtie2 v2.3.5	Langmead and Salzberg, 2012[70]	https://www.nature.com/articles/nmeth.1923
Hisat2 v2.1.0	Kim et al., 2015[71]	https://www.nature.com/articles/nmeth.3317
Htseq-count v0.12.4	Anders et al., 2015[72]	https://doi.org/10.1093/bioinformatics/btu638
Bioconductor R v4.1.2 package deseq2	Love et al., 2014[73]	https://genomebiology-biomedcentral-com.insb.bib.cnrs.fr/articles/10.1186/s13059-014-0550-8
Bedtools coverage v2.30.0	Kim et al., 2015[71]	https://bedtools.readthedocs.io/en/latest/content/tools/coverage.html
ggplots2/tidyverse	Wickham, 2016[74]	https://ggplot2.tidyverse.org/authors.html#citation
IRFinder 1.3.0	Middleton et al., 2017[75]	https://github.com/williamritchie/irfinder
MaxQuantversion 1.5.3.30	Tyanova et al., 2016[76]	https://pubmed.ncbi.nlm.nih.gov/27809316/
Uniprot database	N/A	https://www.uniprot.org/
ProStaR	Wieczorek et al., 2017[77]	https://pubmed.ncbi.nlm.nih.gov/27605098/

(*Continued on next page*)

Continued

REAGENT or RESOURCE	SOURCE	IDENTIFIER
IGV	Robinson et al., 2011[78]	https://www-nature-com.insb.bib.cnrs.fr/articles/nbt.1754
ImageJ	Schneider et al., 2012[79]	https://imagej-nih-gov.insb.bib.cnrs.fr/ij/
Seqplots	N/A	https://bioc.ism.ac.jp/packages/3.7/bioc/html/seqplots.html
R	N/A	https://www.r-project.org/
ImageLab	Biorad	N/A
Fusion-Capt	Vilber Lourmat	N/A
DAVID	N/A	https://david-d.ncifcrf.gov/
Genomic Ranges	Lawrence et al., 2013[80]	https://pubmed.ncbi.nlm.nih.gov/23950696/

RESOURCE AVAILABILITY

Lead contact

Further information and requests for resources and reagents should be directed to and will be fulfilled by the lead contact, André Verdel (andre.verdel@univ-grenoble-alpes.fr).

Materials availability

Reagents (including plasmids) generated in this study are available from the lead contact.

Data and code availability

- Datasets for YTHDC1 ChIP-seq and RNAPII ChIP-seq have been deposited at GEO under the accession numbers GSE166456 and GSE143591. RNA-seq data have been deposited at NCBI Bioproject under the accession number PRJNA773186. All the unprocessed gel images, western blot images and microscopy images have been deposited in Mendeley data (https://doi.org/10.17632/gttn89vbpn.1).
- This paper does not report original code.
- Any additional information required to reanalyze the data reported in this paper is available from the lead contact upon request.

EXPERIMENTAL MODEL AND SUBJECT DETAILS

Cell lines

Human HeLa cell line (cervix adenocarcinoma from American Type Culture Collection, ATCC, VA, USA), HT1080 cell line (human fibrosarcoma from American Type Culture Collection, VA, USA) and HFF2-TERT (Human foreskin fibroblasts immortalized from Decottignies's Lab) were grown in Dulbecco's modified Eagle's medium (DMEM) supplemented with 10% fetal bovine serum and 2% glutamine, medium named "DMEM complete", under stable physicochemical conditions (37°C, 5% CO_2, 95% humidity). Heat-stress experiments were performed by immersion of the culture flasks or culture plates in a warm water bath for 1h at 43°C. Cells were then either harvested directly or returned to 37°C for recovery for the indicated time. All the cell lines have been authenticated by ATCC or Decottignies's Lab, and tested as free of mycoplasma contamination.

Stable HSF1 Knock Down (KD HSF1) HeLa cells (kindly provided by Lea Sistonen[64] were grown in HeLa medium supplemented with Geneticine antibiotic at 0.4%final concentration.

Bacteria

Bacterial transformations were performed with competent *E. Coli* strain (Top10). All the plasmids were verified by DNA sequencing. Bacteria were grown in Luria-Bertani (LB) Broth medium, at 37°C under constant agitation (200 rpm).

METHOD DETAILS

RNA interference, and plasmid transfections

RNA interference experiments were performed using Lipofectamine RNAiMAX (Thermo Fisher Scientific) according to the reverse transfection protocol provided by the manufacturer. For each well of a 6 well-culture plate, 75 pmol of RNAi duplex were diluted in 500 μl of OptiMEM (Opti-MEM I Medium without serum), and then 5 μl of Lipofectamine RNAiMAX were added. After mixing the solution and an incubation of 15 min at RT, 240,000 cells diluted in 2 ml of DMEM complete medium were added to each well. The final siRNA concentration was 40 nM in each well (the same siRNA final concentration was used for transfection of cells

grown in 10 cm or 15 cm dishes). Cells were then incubated for 72 h. Knockdowns were verified by western blot and IF analyses. All siRNAs were purchased from Eurogentec. The sequences are shown in Table S4.

For transfection of plasmids coupled to RNA interference experiments, cells were first transfected using jetPEI (Polyplus transfection) following the manufacturer's batch transfection protocol. For each well in a 6-well plate 1 μl of jetPEI diluted in 100 μl 150 mM NaCl (supplied with the jetPEI reagent) were added to 1 μg of plasmid DNA diluted in 100 μl of 150 mM NaCl. After incubation for 15 min at RT, the mix jetPEI/DNA was added to 600,000 cells. After 24h, cells were diluted four times in DMEM complete medium transfected with siRNA using Lipofectamine RNAiMAX and grown for 72h.

Transfection of plasmids coding for YTH-domain proteins fused to GFP was carried out using jetPEI following the manufacturer's forward transfection protocol. For each well in a 6-well plate 2 μl of jetPEI were diluted in 100 μl 150 mM NaCl and 1 μg of plasmid DNA was diluted in 100 μl 150 mM NaCl. Solutions were mixed, vortexed briefly, incubated 15 min at RT and the mix jetPEI/DNA was added to the cells at 50% confluence.

Transfection of plasmid coding for protein HSF1-*dbdtrim* domains fused to GFP[23] was carried out using jetPEI following the manufacturer's forward transfection protocol. For each well in a 24-well plate 0.5 μl of jetPEI were diluted in 25 μl 150 mM NaCl and 100 ng of plasmid DNA was diluted in 25 μl 150 mM NaCl. Solutions were mixed, vortexed briefly, incubated 15 min at RT and the mix jetPEI/DNA was added to the cells at 50% confluence. The HSF1-DBD-Trim-GFP construct retains both the DNA binding and trimerization domains and is deleted of the *C*-terminal part of HSF1. This construct forms granules in all cells, both at 37°C and 42°C without production of *SATIII* transcripts. This mutant acts as a dominant negative, by preventing the endogenous HSF1 from accumulating into the granules upon heat stress (described in[27]).

DNA constructs and mutagenesis

Coding sequence for full-length human YTHDC1 (hYTHDC1; 727 aa; Accession number NP_001026902) cDNA was amplified from a HEK cells cDNA library by reverse transcription-PCR. The PCR product was then cloned into a mammalian modified pCI-neo plasmid allowing the production of HA tagged proteins. Primers used are listed in the Table S4.

Plasmid coding for an ectopically expressed form of YTHDC1, which cannot be recognized by the siRNAs used for the transient knockdown of the endogenous protein were obtained by site-directed mutagenesis (Q5 Site-Directed Mutagenesis Kit, biolabs) using the following primers (Table S4): siC1_1immF and siC1_1immR; siC1_3immF and siC1_3immR (the mutated DNA sequence does not modify the amino acid sequence). From this plasmid (called pci-neo-HA-YTHDC1imm), we established by PCR-based mutagenesis YTHDC1 point mutants that lost its capacity to recognize m^6A. The point mutation concerns the tryptophan 428 located in the hydrophobic cage of the YTH domain that recognizes m^6A that was substituted by alanine (A) using the primers W428A_F and W428A_R (Table S4) to produce a point-mutant form of YTHDC1 named pCI-neohYTHDC1imm*W428A*.

The mammalian expression vector pEGFP-N3 (Addgene # 6080-1) was used to express the human YTH-domain proteins in fusion with GFP. Coding sequences for human YTHDC2 (hYTHDC2; 1430 aa; Accession number NP_073739), YTHDF1 (hYTHDF1; 559 aa; Accession number NP_060268), YTHDF2 (hYTHDF2; 579aa; Accession number NP_001166599) and YTHDF3 (hYTHDF3; 585 aa; Accession number NP_689971) cdnas were amplified from a HEK cells cDNA library by reverse transcription-PCR using the following primers: YTHDC1_Xho and YTHDC1_Xma; YTHDC2-Xho and YTHDC-2Bam; YTHDF1-Xho and YTHDF1-Bam; YTHDF2-Xho and YTHDF2-Bam; YTHDF3-Xho and YTHDF3-Bam (Table S4). The PCR products were digested by the restriction enzymes *XhoI-BamHI* (for hYTHDF1-2-3 and hYTHDC2 cdnas) or *Xho*I-*Xma*I for hYTHDC1 cDNA. The fragments obtained were then inserted into the *XhoI-BamHI* or *Xho*I-*Xma*I digested pEGFP-N3 vector.

RNA purification and analysis

Total RNA was extracted from cells using the TRIzol Reagent (Invitrogen) following the manufacturer's instructions. Cells from 6-well plates or 10 cm dishes were collected by trypsinization and centrifuged 5 min at 600 g. For 10^5-10^7 cells, 1 ml of TRIzol reagent was added and the mix was thoroughly vortexed (at this step occasionally samples were frozen and stored at −80°C). After 5 min incubation, 0.2 ml of chloroform were added, the mix was vortexed and then incubated for another 2–3 min at RT. Following centrifugation at 12,000 g for 15 min at 4°C, the aqueous phase (containing RNA) was carefully transferred to a new tube. Isopropanol (0.5 ml) was added, the mix was vortexed and centrifuged for 10 min at 12,000 g, 4°C. The pellet was then washed in 75% (v/v) EtOH and centrifuged at 7500g for 5 min, 4°C. The RNA pellet was then air-dried, dissolved in 20–50 μl RNAse-free water, incubated at 60°C for 10 min and stored at −20°C. RNA concentration and A260/280 ratio were determined using NanoDrop ND-1000 UV spectrophotometer. RNA integrity was evaluated by electrophoresis on 1% (w/v) agarose gel using the gelgreen Nucleic Acid Stain (Biotium) dye following the manufacturer's instructions.

Reverse transcriptase PCR was performed on 2 μg of RNA using Transcriptor Reverse Transcriptase (Roche). RNA was first subjected to DNAse (Roche) treatment in the presence of 5X DNAse buffer (100 mM Tris pH 8, 10 mM $MgCl_2$), 100 mM DTT (Invitrogen) and RNAse inhibitor (Thermo Scientific) for 20 min at 37°C. Next 0.7 μl of 50 mM EDTA were added to the RNA-DNAse mixture and incubated 10 min at 70°C. RNA was then hybridized with a mix of specific primers at 2 μM in the presence of 50 mM $MgCl_2$ for 10 min at 65°C. cDNA synthesis was performed by adding 10 mM dNTP (Thermo Scientific), RNAse Inhibitor (Thermo Scientific), RT buffer (Roche) and Reverse Transcriptase (Roche) and subsequent incubation for 10 min at 25°C, 40 min at 55°C and 5 min at 85°C.

For RNA-seq analysis, RNA was subjected to DNAse as described above and then purified by phenol/chloroform extraction. One volume of acid phenol:chloroform (5:1, pH 4.7) was added to RNA and the mix was thoroughly vortexed 5 sec. Following

centrifugation at 12,000 g for 5 min at 4°C, the aqueous phase (containing RNA) was carefully transferred to a new tube. One volume of chloroform was added, the mix was vortexed and centrifuged at 12,000 g for 5 min at 4°C. The aqueous phase was recovered in a new tube. 1/10 volume of 3 M ammonium acetate was added and then 2 volumes of 100% ethanol. After mixing, RNA was precipitated by incubation 30 min at −80°C. After centrifugation 15 min at 12,000 g, 4°C, the pellet was washed in cold 70% (v/v) ethanol and centrifuged at 12,000 g for 5 min, 4°C. The RNA pellet was then air-dried, dissolved in 20–50 μl RNAse-free water. RNA concentration and A260/280 ratio were determined using nanodrop ND-1000 UV spectrophotometer. RNA-seq libraries were made after depleting the total RNA population of ribosomal RNAs and by using multiplexing. Construction of the libraries and high throughput sequencing (nextseq 2000, Illumina) were performed at EMBL Genecore facility.

Western-blot analysis

Cells were washed with PBS and collected by centrifugation 5 min at 600 g. Proteins were extracted using lysis buffer (50 mM Tris, pH 7.5, 150 mM NaCl, 5 mM $MgCl_2$, 1% (w/v) Triton X-100, 0.5% (w/v) sodium deoxycholate) supplemented with protease inhibitor (Roche) and benzonase (Merck Milipore, 1/100). After 15 min on ice, total protein extracts were quantified using a Pierce BCA Protein Assay Kit or a Bradford assay. Protein samples (10 μg) were then incubated at 95°C for 5 min in Laemmli sample buffer (50 mM Tris-HCl, pH 6.8, 10% (v/v) β-mercaptoethanol, 1% (v/v) SDS, 10% (v/v) glycerol and 0.1% (w/v) bromophenol blue), separated by SDS-PAGE, transferred to nitrocellulose membranes and analyzed using appropriate primary and secondary antibodies (listed in Table S5). Antibodies were diluted in TBS- 0.1% (v/v) Tween20- 1% (w/v) fat dry milk, and membranes were washed in TBS- 0.1% (v/v) Tween 20.

Enhanced chemiluminescence (ECL) detection was performed using reagents from Bio-Rad (Clarity Western ECL kit) and revealed using ChemiDocMPSystem (BioRad) or the Fusion FX (Vilber) camera. Signals were quantified with the corresponding software, the ImageLab software (Bio-Rad) or the Fusion-Capt software (Vilber Lourmat).

Subcellular fractionation

Fractionation was performed to obtain cytosolic and nuclear fractions from WT, YTHDC1 KD and METTL3 KD cells. HeLa cells were seeded in 10 cm dishes and transfected transiently with control siRNA or siRNA against YTHDC1. 72 h after transfection, cells were submitted or not to heat stress treatment followed or not by a recovery period. Cells together with the dead floating cells were manually collected using a scraper, centrifuged for 5 min at 400 g and washed in cold 1x PBS (phosphate-buffered saline). On ice 150 μl of lysis buffer (10 mM Tris pH 7.5, 60 mM KCl, 15 mM NaCl, 0.34 M sucrose, 650 μM spermidine, 2 mM EDTA, 0.5 mM EGTA, 1 mM DTT, 0.5 mM PMSF, 0.05% (w/v) Triton X-100 + 1 μl RNasin) were added gently to the cell pellet (obtained from one 10 cm dish) and incubated for 10 min. After a 5 min centrifugation at 400 g, the supernatant (cytosolic fraction) was collected and stored on ice. 200 μl of washing buffer (10 mM Hepes pH 7.5, 10 mM KCl, 0.3 M sucrose, 1.5 mM $MgCl_2$, 1 mM DTT, 0.5 mM PMSF, + 1μl RNasin) were added carefully to the pellet and the suspension was centrifuged 5 min at 400 g to obtain a final pellet containing the washed nuclei.

For purification of sub-nuclear fractions, the pellet containing the washed nuclei was resuspended into 75 μl of nucleus lysis buffer (50 mM Tris pH 7.5, 140 mM NaCl, 1.5 mM $MgCl_2$, 0.5% (w/v) NP-40), incubated 20 min on ice, and centrifuged 10 min at 20,000 g (4°C). The supernatant (nucleoplasm) was collected and stored on ice. The remaining pellet was resuspended into 75 μl of 10 mM Tris pH 7.5, 700 mM NaCl, incubated 20 min on ice and then centrifuged for 5 min at 20,000 g at 4C and the supernatant containing the chromatin associated fraction was recovered. For SDS-PAGE and western blot analyses, one volume of cytosolic fraction and two volumes of nuclear fractions (nucleoplasm and chromatin associated) were loaded on gels. For RNA extraction, 1 ml of TRIzol Reagent was added to each fraction, and the purification of RNA was performed as described above (RNA purification and analysis).

Protein immunopurification

Cells from 4 T75 flasks, at 90% of confluence were trypsinized, washed in 1X PBS and lysed 10 min on ice in 2 ml of lysis buffer (50 mM Tris pH 8.0, 150 mM NaCl, 5 mM $MgCl_2$, 0.5% (w/v) Na-deoxycholate, 1% (w/v) Triton X-100, 10% (w/v) glycerol, 1 mM PMSF and 1 mM DTT). The soluble total extract was recovered after centrifugation at 20,000 g for 10 min at 4°C and nucleases (benzonase, Merck Millipore) were added to this extract to degrade nucleic acids. Magnetic beads coupled to protein A (Dynabeads Protein A, Thermo Fisher) were used for immunoprecipitation of YTHDC1 and the associated proteins. 7 μl of beads per IP were washed in 1X PBS, 0.02% (w/v) Tween 20 and incubated with 10 μl of the purified polyclonal rabbit antibody raised against the *N*-terminal part of YTHDC1 (homemade antibody) or with 5 μl of rabbit polyclonal IgG (control experiment, diagenode C15410206) for 20 min at RT under agitation. The Dynabeads/antibody complexes were next equilibrated in the lysis buffer and then incubated with 1 ml of the soluble proteins extract per IP. After incubation for 6 h at 4°C on a rotating shaker, the Dynabeads/antibody/antigen complexes were washed four time in 25 mM Tris pH 8.0, 1 mM $MgCl_2$, 150 mM NaCl, 0.01% (w/v) NP40 washing buffer and the antibody-antigen complexes were eluted by addition of 40 μl 2X Laemmli loading buffer (60 mM Tris-HCl, pH 6.8, 2% (v/v) SDS, 10% (w/v) glycerol, 10% (v/v) β-mercaptoethanol, 0.01% (w/v) bromophenol blue) and incubated 10 min at 70°C. 10 μl were loaded on SDS-PAGE followed by silver staining and 25 μl were used for MS/MS analysis. For Co-IP analysis, the same protocol was used except that we used a commercial antibody (Anti-YTHDC1 A305-096A, Bethyl laboratories). 10 μl of the eluate and 5 μl of a 1/25 dilution of the soluble extract were loaded on SDS-PAGE for the western blot analysis.

Microscopy analyses with immunofluorescence, RNA-FISH and DNA-FISH

For immunofluorescence, HeLa cells grown on coverslips were fixed in 4% paraformaldehyde in phosphate-buffered saline (PBS) for 10 min at RT, washed three times 5 min in PBS 1X and permeabilized with PBS, 0.5% (v/v) Triton X-100, 0.5% (w/v) Saponin for 15 min at RT, and washed again three times 5 min in PBS 1X. Unspecific sites were blocked 30 min at 37°C in PBS, 10% (v/v) FBS, 0.3% (v/v) Triton X-100. Following this, cells were incubated 1 h at 37°C with appropriate primary antibody (listed in Table S5) diluted in PBS 1X, 1% (v/v) FBS. Cells were then washed three times 5 min in PBS 1X, 0.3% (v/v) Triton X-100 and incubated 30 min at 37°C with a secondary goat anti-rabbit IgG Dylight 549 antibody (Vector; 1:1000) or goat anti-mouse IgG Alexa Fluor 488 antibody (Invitrogen; 1:500). DNA was counterstained with 250 ng/ml DAPI. To have comparative analysis between cell samples submitted to different conditions, images were acquired with the same exposure time with an Apotome microscope using the 63x, oil immersion objective. Images were analyzed using Fiji software and a minimum of 100 cells were analyzed for each experimental condition.

For RNA and DNA FISH to detect *SATIII* ncRNA and DNA, respectively, the cells were fixed and permeabilized as described in the protocol used for immunofluorescence. Cells were then dehydrated by successive incubation for 3 min in 70% (v/v) ethanol, 90% (v/v) ethanol, 100% ethanol. Coverslips were air-dried and DNA was denatured 10 min at 80°C in PBS 50% formamide (for DNA FISH only). Then 5–10 μl and precipitated probe were deposited on each coverslip. The cells were incubated overnight at 37°C. Next, cells were washed three times for 5 min in 50% (v/v) formamide, 2X SSC solution warmed to 45°C and three times for 5 min in 2X SSC at RT under agitation -for DNA FISH- or washed three times for 5 min in 15% (v/v) formamide, 2X SSC solution and three times for 5min in 2X SSC at RT-for RNA FISH. For studies combining RNA or DNA FISH and protein immunostaining after the final washing steps of the FISH protocol, the cells were fixed again in PFA 4% (w/v), washed in 1X PBS and then incubated with the blocking solution for IF and the IF protocol was applied as usual. A minimum of 100 cells were analyzed for each experimental condition.

For RNase treatment, HeLa cells grown on coverslips were briefly washed with sterile CSK buffer (20 mM Tris-HCl, 3 mM $MgCl_2$, 300 mM sucrose), then permeabilized 5 min at 4°C in CSK/0.5% (v/v) Triton X-100 solution, and briefly washed in PBS 1X. Cells were incubated 10 min at room temperature with a 1 mg/ml RNase A solution (Merck 10109142001), washed with PBS 1X, and fixed in 4% paraformaldehyde in phosphate-buffered saline (PBS) for 10 min at RT, and finally washed three times 5 min in PBS 1X. RNA FISH or IF was performed as described above.

Chromatin immunoprecipitation (ChIP)

ChIP experiments were performed mainly as described previously (Motamedi et al., 2004) with the following modifications. HeLa cells (from two 15 cm dishes at 70–80% confluency, around 2×10^7 cells) were cross-linked with 1% (v/v) formaldehyde (Sigma) at room temperature for 15 min. The reaction was quenched with glycine (Sigma) at a final concentration of 125 mM for 5 min at room temperature. Cells were collected, centrifuged for 3 min at 1250 g, and the pellets washed twice in cold PBS. Cell pellets were resuspended in 7 ml of cell lysis buffer (50 mM HEPES pH 7.5, 10 mM KCl, 0.1% (w/v) NP40, and protease inhibitors) and transferred to a chilled Dounce homogenizer on ice and homogenized for 36 strokes. The suspension was then centrifuged for 3 min at 1250 g at 4°C, and resuspended in 1 ml of nuclear lysis buffer (50 mM HEPES-KOH at pH 7.5, 500 mM NaCl, 1 mM EDTA at pH 8.0, 1% (v/v) Triton X-100, 0.1% (v/v) sodium deoxycholate, 0.1% (v/v) SDS, and protease inhibitors). Lysates were sonicated for 10 min (30″on, 30″off) at 30% amplitude in a water bath sonicator (Active motif), centrifuged at 18,000 g for 10 min and the supernatant stored at −80°C. To obtain input DNA, 25 μl of clarified lysate was used.

Each immunoprecipitation reaction was performed from 30 μg of sheared chromatin incubated overnight at 4°C on a wheel with 2 μg of specific antibody (Anti-RNA polymerase II subunit B1 (phospho CTD Ser-2) Antibody, clone 3E10, Millipore; Anti-YTHDC1 A305-096A, Bethyl laboratories) or irrelevant IgG (Rabbit polyclonal igG, Diagenode C15410206). Forty microliters of a 50% slurry of prewashed prota-Sepharose beads (nproteina Sepharose 4 Fast Flow, GE Health Care) were incubated with each lysate at 4°C for 1 h. Beads were washed two times in nuclear lysis buffer, once with 10 mM Tris-HCl (pH 8.0), 0.25 M LiCl, 0.5% (v/v) NP-40, 0.5% (v/v) sodium deoxycholate, and 1 mM EDTA, and once with TE (10 mM Tris-HCl ph 8.0, 1 mM EDTA) at room temperature. Immunopurified material was eluted by incubating with 100 μl of 50 mM Tris-HCl (pH 8.0), 10 mM EDTA, and 1% (v/v) SDS at 65°C for 20 min. Eluate was transferred to a fresh tube and pooled with a final bead wash of 150 μl of TE with 0.67% (v/v) SDS. For input DNA, 200 μl of TE with 1% (v/v) SDS was added to 25 μl of lysate. All samples were incubated at 65°C overnight before addition of 200 μl of TE and 100 μg of Proteinase K (Roche), then incubated at 37°C for a further 2 h. After addition of 55 μl of 4 M LiCl, DNA samples were extracted once with phenol:chloroform:isoamyl alcohol and once with chloroform and then precipitated (1 ml 100% (v/v) ethanol and 2 μl glycogen (20 mg/ml) were added to the recovered upper phase, incubated at −80°C for 20 min, centrifuged at 4°C for 20 min and washed once with 70% (v/v) ethanol). Precipitated and washed DNA was resuspended in 50 μl 10 μg/ml RNase A (for the input) or 0.5 μg/ml RNase A (for IP) and incubated at 37°C for 1 h.

Quantitative PCR was conducted with 2 μl of a 1/2 dilution of the IP DNA. Relative enrichment was calculated as the ratio of signal of interest to signal of control IP. Primers used are listed in Table S4.

Chromatin immunoprecipitation for whole-genome analysis was performed from HeLa cells using the "ChIP-IT High Sensitivity" kit from Active Motif following the manufacturer's instructions. Sheared chromatin was obtained using a probe sonicator (Active Motif) by 10 cycles, 30 s ON, 30 s OFF at 63 W. ChIP were performed using 25 μg chromatin and 4 μg of antibody detecting YTHDC1 (Table S5). ChIP-seq libraries were constructed using the Next Gen DNA Library Kit (Active Motif 53216 and 53264). Library quality was assessed using Agilent 2100 Bioanalyzer and Agilent High Sensitivity DNA assay. High throughput sequencing was performed by Sequence-By-Synthesis technique using a nextseq 500 (Illumina) at Genom'ic facility, Institut Cochin, Paris.

RNA immunoprecipitation (RIP)

YTHDC1 RNA-IP experiments were performed on WT and METTL3 KD cells. Briefly, cells were seeded in 15 cm dishes were cross-linked with 1% (v/v) formaldehyde (Sigma) at room temperature for 15 min. The reaction was quenched with glycine (Sigma) at a final concentration of 125 mM for 5 min at room temperature. Cells were collected, centrifuged for 3 min at 1250 g, and the pellets washed twice in cold PBS. Cell pellets were resuspended in 400 μl of lysis buffer (50 mM HEPES-KOH at ph 7.5, 150 mM NaCl, 1 mM EDTA at pH 8.0, 1% (v/v) Triton X-100, 0.1% (v/v) sodium deoxycholate, 5 mM DTT, 1 mM PMSF, and 100 U/ml ribolock (Thermofisher)) and incubated 10 min on ice. The lysed cells were sonicated in a water bath sonicator (Active motif), for 10 min (30″on, 30″off) at 30% amplitude centrifuged at 1000 g for 5 min and the supernatant is collected in new tubes. The pellet was resuspended in 400 μl of lysis buffer and the sonication, centrifugation and supernatant collection were repeated twice to obtain a final volume of 1.2 ml of cell lysate. The clarified lysate (1.2 ml) was DNase treated 1 h at 30°C by the addition of 133 μl of 10x DNase buffer and 700 Units of DNase I (RNase free, from Sigma). The DNase reaction was stopped by the addition of 80 μl EDTA 0.5 M, then the samples were centrifugated 5 min at 15,000 g and the supernatants were transferred to new tubes. The lysates were incubated at 4°C for 1 h with either with 10 μg of anti-YTHDC1 (A305-096A, Bethyl Laboratories) or 10 μg of irrelevant igG (Sigma I4506). 40 μl of a 50% slurry of prewashed protein A-Sepharose beads (N-protein A Sepharose 4 Fast Flow, GE Health Care) were added to the lysates and incubated at 4°C for another 1 h. Beads were washed five times with, first, two washes with the lysis buffer, then one with the lysis buffer containing 500 mM of NaCl and 10 U/ml RiboLock, one with the wash buffer (10 mM Tris-HCl ph 8.0, 1 mM EDTA, 0.25 M LiCl, 0.5% (v/v) NP-40, 0.5% (v/v) sodium deoxycholate, and 5 mM DTT and 10 U/ml RiboLock), and finally one with TE-DTT (10 mM Tris-HCl pH 8.0, 1 mM EDTA, 5 mM DTT and 10 U/ml RiboLock) at room temperature. Immunopurified material was eluted by incubating with 100 μl of 50 mM Tris-HCl (pH 8.0), 10 mM EDTA, 1% (v/v) SDS, 5 mM DTT and 10 U/ml RiboLock at 65°C for 20 min. The eluate was transferred to a fresh tube and pooled with a final bead wash of 150 μl of TE with 0.67% (v/v) SDS, 5 mM DTT and 10 U/ml RiboLock. All samples were reverse crosslinked at 65°C overnight prior to their treatment for 30 min with 100 μg of Proteinase K (Roche). After addition of 55 μl of 3 M NaOAc pH 5,2, RNA samples were extracted once with Acid-Phenol:Chloroform pH 4,5 (25:24:1, Thermofisher), once with chloroform. Nucleic acids from the recovered upper phase were precipitated in 1 ml 100% (v/v) ethanol and 2 μl glycogen (20 mg/ml), incubated at −80°C for 20 min, centrifuged at 4°C for 20 min and washed once with 70% (v/v) ethanol. Precipitated and washed rnas were resuspended in 20 μl of TE with 5 mM DTT and 10 U/ml ribolock. The purified rnas were subjected to analysis by qRT-PCR.

For the MeRIP-qPCR analysis mRNAs were purified using Dynabeads mRNA Direct Kit (Fisher Scientific) according to manufacturer's instructions. 5 μg of mRNAs were fragmented 10 min at 96°C by alkaline hydrolysis (100 mM bicarbonate buffer pH 9.2). For immunoprecipitation, 100 μl of Protein-G Dynabeads were blocked with 1 ml of blocking solution (1mg/ml BSA, 1X PBS). After two washes, beads were resuspended in 990 μl of blocking solution. 10 μl of m6A primary antibody (Synaptic Systems, 10 μg/μl) was added to the beads. The mixture was incubated overnight at 4°C under constant agitation. Beads were then washed 3 times with 1 ml of cold blocking solution. After the final wash, beads were resuspended in 25 μl of blocking solution. Fragmented mRNAs were then diluted in 975 μl of immunoprecipitation buffer (10 mM Tris-HCl, 150 mM NaCl, 0.05% v/v IGEPAL, 40U RNase inhibitor) and added to beads. The mixture was then incubated overnight at 4°C under constant agitation. Beads were washed 2 times with 2 ml of immunoprecipitation buffer, 2 times with 2 ml of low salt washing buffer (10 mM Tris-HCl, 50 mM NaCl, 0.1% v/v IGEPAL, 0.1% v/v SDS) and 2 times with 2 ml of high salt washing buffer (10 mM Tris-HCl, 500 mM NaCl, 0.1% v/v IGEPAL, 0.1% v/v SDS) for a total of 6 washes. Elution was performed 3 times by adding each time 100 μl of elution buffer (10 mM Tris-HCl, 150 mM NaCl, 0.05% v/v IGEPAL, 40U RNase inhibitor, 6.7 mM N6-methyladenosine 5′ monophosphate sodium salt). Each time, the mixture was incubated 1 h at 4°C under constant agitation. Eluted fractions were then combined and precipitated overnight. After centrifugation, pellets were resuspended in rnase/dnase free water in a final volume of 15 μl.

Bioinformatic analysis for chIP-seq data

For analysis of ChIP-seq data, sequencing reads were first filtered, using fastq_illumina_filter, and quality control of filtered reads was performed using FastQC (http://www.bioinformatics.babraham.ac.uk/projects/fastqc/). Filtered reads were then aligned to GRCh38[81] using the Burrows-Wheeler Aligner (BWA, http://bio-bwa.sourceforge.net/) with default parameters. The sorted BAM files generated by SAM tools (http://www.htslib.org), keeping only reads with a mapping quality at least 30, were then normalized by DeepTools[67] bamCoverage function, with a bin size of 10 bp. RPGC normalization was applied, with an effective genome size of 2913022398, according to DeepTools' user manual instructions. Files were then further normalized by subtracting an RPGC normalized input data file, using bigwigCompare. From these normalized data files, peak calling was performed using NormR's (https://doi.org/10.1101/082263) enrichR function, searching for enrichment of each BAM file of ChIP-seq reads against the input BAM file, using a False Discovery Rate (FDR) correction. Genomic Ranges[80] was then used to determine overlap between the peak range and genomic features of interest, such as genes with a transcription start site (TSS) and transcript end site (TES) from GRCh38. Profile matrices were extracted from the normalized data files using DeepTools' computeMatrix, using a bin size of 10 bp. Profiles were generated from -5kb of tsss up to 5 kb after tess. Further quantification of the normalized ChIP-seq reads was calculated from the start to end positions of gene bodies +/− 500 bp. Genomic elements and protein coding genes were obtained from Ensembl.

Protein binding variation between conditions was calculated using Z-scores, which were calculated as follows: *Z*-score = (HS – NHS)/sqrt((HS + NHS)/2) (*i.e.*, difference weighted by mean signal), which transforms the distribution of variations into a normal

distribution, allowing for better statistical interpretation of the variations. Average binding profiles of proteins across genomic features of interest were generated using seqplots' (https://doi.org/10.18129/B9.bioc.seqplots) plotAverage function.

Decile matrices were created using color2D matplot from the plotrix package (https://www.rdocumentation.org/packages/plotrix/versions/3.7-7). Decile matrices were generated by ranking genes by *Z*-score of variation of RNAPII or YTHDC1 binding in HS versus NHS condition, followed by distribution by deciles. The number of genes in each decile, for both RNAPII and YTHDC1 variation, was used to generate a matrix (10 × 10). The number of genes in each intersection was tested for significance (number of genes found compared to expected) by hypergeometric test, generating a 10 × 10 matrix of p values.

Bioinformatic analysis of RNA-seq data

Raw reads were trimmed using Trimmomatic v0.39.[69] Trimmed reads were filtered out read corresponding to mitochondrial sequences using bowtie2 v2.3.5[70] in 'sensitive-local' mode. Reads mapping against GRCh38 genome without gtf file was performed using Hisat2 v2.1.0.[71] Read count was performed using htseq-count v0.12.4[72] in 'union' mode and normalized by total of mapped reads (reads per millions, rpm). Differential analysis was performed using Bioconductor R v4.1.2 package deseq2[73] with a false discovery rate of 0.05. P values were corrected for multiple tests by the Benjamini-Hochberg rule (adjusted P value).

Readthrough analysis. Counting of reads in the gene region or the 3 prime region (15 kb after the end of the gene) was performed by bedtools coverage v2.30.0.[71] Normalization was applied by dividing by the total mapped reads and the gene length (RPKM). To optimize the difference between region and condition, for each gene the difference was calculated between the Log2 of the mean count region and the mean of all Log2 counts in the 9 conditions. This difference was divided by the standard deviation of the Log2 counts in the 9 conditions. The ratio of the RNA-seq reads of the 15 kb downstream the 3′UTR (Downstream) over the gene body (GB) was then calculated as follow $[[Log_2(Reads\ Downstream_n)\text{-}mean(Log_2ReadsDownstream_{n1\text{-}9})]/sd(Log_2ReadsDownstream_{n1\text{-}9})] - [[Log_2(Reads\ gb_n)\text{-}mean(Log_2ReadsGB_{n1\text{-}9})]/sd(Log_2ReadsGB_{n1\text{-}9})]$, where "n" corresponds to a given condition in which the reads over the corresponding regions are counted and "n1-9" corresponds to all 9 conditions taken together for the same gene. This value corresponds to normcount. The heatmap was made by the geom_tile function in the ggplots2/tidyverse package.[74]

Detecting intron retention from RNA-Seq experiments. Intron retention study were performed using IRFinder 1.3.0.[75] The raw counts files were produced from fastq files using IRFinder binary with option -r REF/Human-grch38-release100 where REF/Human-grch38-release100 is the genome reference index provided by irfinder authors (https://github.com/williamritchie/irfinder). Delta_IR HS/NHS (resp. Delta_IR R/NHS) for a given condition (WT, YTHDC1 KD or METTL3 KD) is the result of the statistical analysis HS vs. NHS (ref.) (resp. R vs. NHS (ref.)) Performed by DESeq2[73,82] and R (R Core Team. R: A language and environment for statistical computing. Vienna, Austria: R Foundation for Statistical Computing, 2017) script provided by IRFinder authors (https://github.com/williamritchie/irfinder) in this condition. Only IR presenting variations between conditions in WT were kept, IR presenting variations meaning introns with $-Log_{10}(padj) > (-10 * IR.changes + 6)$, or $-Log_{10}(padj) > (10 * IR.changes + 4)$ for HS vs. NHS (ref.) Model, or $-Log10(padj) > (-10 * IR.changes + 4)$, or $-Log_{10}(padj) > (10 * IR.changes + 2)$ for R vs. NHS (ref.) Model, padj meaning 5% FDR adjusted p values according to Benjamini-Hochberg procedure.

Mass spectrometry (MS)-based quantitative proteomic analysis

Eluted proteins were separated by SDS-PAGE (4–12% nupage, Life Technologies) and stained with Coomassie blue R-250 (Bio-Rad) before in-gel digestion using modified trypsin (Promega, sequencing grade) as previously described.[83] For each sample, bands corresponding to light and heavy chains of immunoglobulins were processed separately from the rest. Resulting peptides were analyzed by online nanoliquid chromatography coupled to tandem MS (Ultimate 3000 and LTQ-Orbitrap Velos Pro, Thermo Scientific). Peptides were sampled on a 300 μm × 5 mm PepMap C18 precolumn and separated on a 75 μm × 250 mm C18 column (PepMap, Thermo Scientific) using a 25-min gradient for immunoglobulin-containing bands and a 120-min gradient for the rest of the eluates. MS and MS/MS data were acquired using Xcalibur (Thermo Scientific).

Peptides and proteins were identified and quantified using MaxQuant (version 1.5.3.30, (Tyanova et al., 2016) using the Uniprot database (Homo sapiens taxonomy, April 2017 version) and the frequently observed contaminant database embedded in maxquant. Trypsin was chosen as the enzyme and 2 missed cleavages were allowed. Peptide modifications allowed during the search were: carbamidomethylation (C, fixed), acetyl (Protein N-ter, variable) and oxidation (M, variable). Minimum peptide length was set to 7 amino acids. Minimum number of peptides and razor + unique peptides were set to 1. Maximum false discovery rates - calculated by employing a reverse database strategy - were set to 0.01 at peptide and protein levels.

Statistical analyses were performed using ProSstar.[77] Proteins identified in the reverse and contaminant databases, proteins only identified by site, immunoglobulin chains, and proteins exhibiting less than 3 intensity values in one condition were discarded from the list. After log2 transformation, intensity values were normalized by median centering before missing value imputation (slsa algorithm for partially observed values in the condition and DetQuantile algorithm for totally absent values in the condition); statistical testing was conducted using Limma test. Differentially-expressed proteins were sorted out using a log2 (fold change) cut-off of 2 and a p value cut-off of 0.01, allowing to reach an FDR inferior to 2% according to the Benjamini-Hochberg procedure. For the volcano plot of YTHDC1 interactome showed in Figure 1, only proteins identified with at least one unique peptide in three independent purifications and with more than four-fold enrichment relative to the control purifications were considered.

QUANTIFICATION AND STATISTICAL ANALYSIS

Western blot signals were quantified with the ImageLab software (Bio-Rad) or the Fusion-Capt software (Vilber Lourmat). All the data were expressed as the mean ± standard error of the mean (SEM) except for the data in Figures S6 and S7 expressed as the mean ± standard deviation (SD). The number of replicates (n) is described in the Figure legends. Data from Figures 3F, 6G, S6A, S6B and S7A were statistically analyzed with Student's t test. Significance level achieved as indicated in figures is ***: $p < 0.001$, **: $p < 0.01$, *: $p < 0.05$.

Cell Reports, Volume *41*

Supplemental information

Chromatin-associated YTHDC1 coordinates heat-induced reprogramming of gene expression

Kalina Timcheva, Solenne Dufour, Leila Touat-Todeschini, Callum Burnard, Marie-Christine Carpentier, Florent Chuffart, Rémy Merret, Marion Helsmoortel, Sabrina Ferré, Aude Grézy, Yohann Couté, Sophie Rousseaux, Saadi Khochbin, Claire Vourc'h, Cécile Bousquet-Antonelli, Rosemary Kiernan, Daphné Seigneurin-Berny, and André Verdel

Figure S1

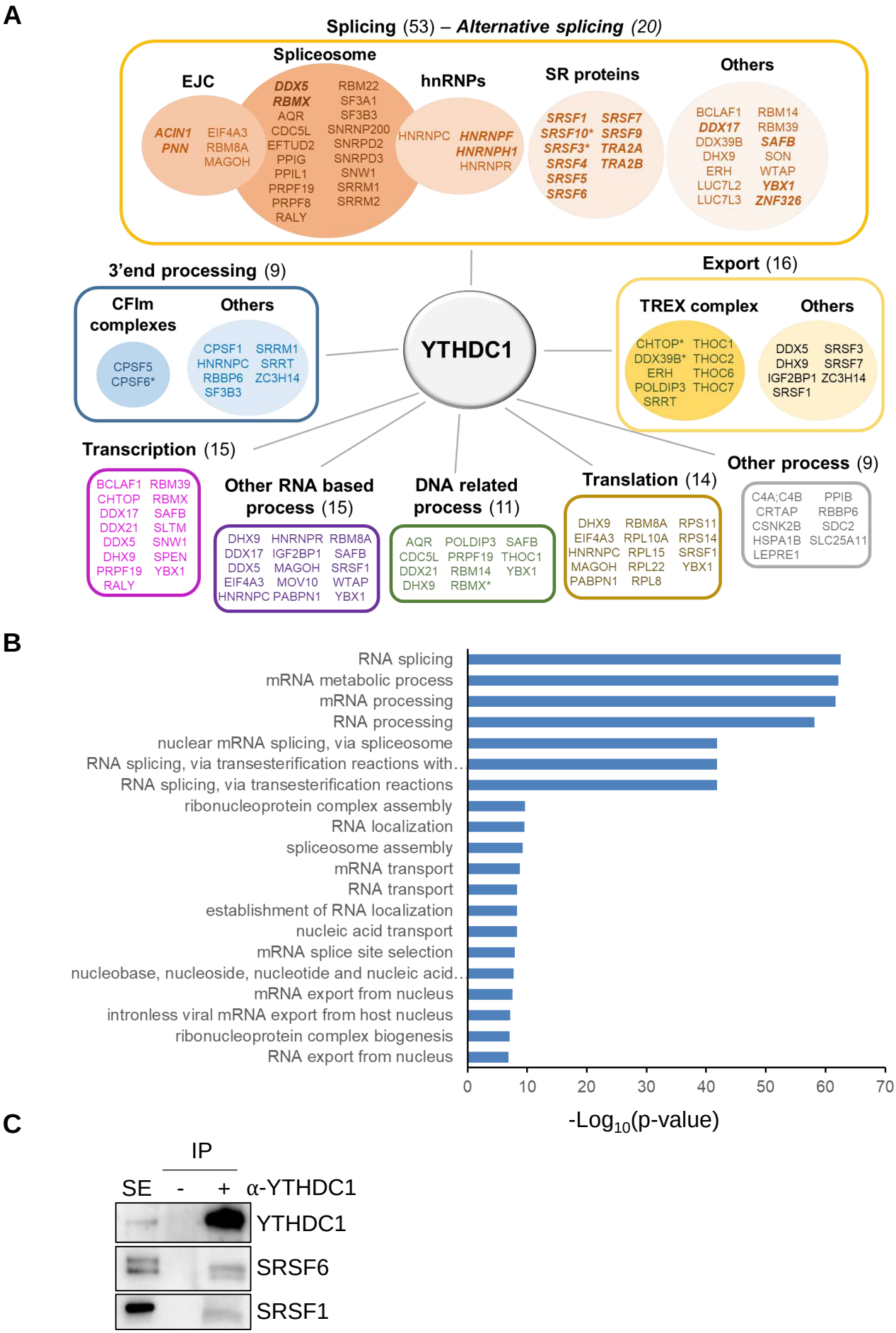
A
Splicing (53) – Alternative splicing (20)
Spliceosome
EJC
ACIN1 PNN EIF4A3 RBM8A MAGOH
DDX5 RBMX AQR CDC5L EFTUD2 PPIG PPIL1 PRPF19 PRPF8 RALY
RBM22 SF3A1 SF3B3 SNRNP200 SNRPD2 SNRPD3 SNW1 SRRM1 SRRM2
hnRNPs
HNRNPC HNRNPF HNRNPH1 HNRNPR
SR proteins
SRSF1 SRSF10* SRSF3* SRSF4 SRSF5 SRSF6 SRSF7 SRSF9 TRA2A TRA2B
Others
BCLAF1 DDX17 DDX39B DHX9 ERH LUC7L2 LUC7L3 RBM14 RBM39 SAFB SON WTAP YBX1 ZNF326
3'end processing (9)
CFIm complexes
CPSF5 CPSF6*
Others
CPSF1 HNRNPC RBBP6 SF3B3 SRRM1 SRRT ZC3H14
YTHDC1
Export (16)
TREX complex
CHTOP* DDX39B* ERH POLDIP3 SRRT THOC1 THOC2 THOC6 THOC7
Others
DDX5 DHX9 IGF2BP1 SRSF1 SRSF3 SRSF7 ZC3H14
Transcription (15)
BCLAF1 CHTOP DDX17 DDX21 DDX5 DHX9 PRPF19 RALY RBM39 RBMX SAFB SLTM SNW1 SPEN YBX1
Other RNA based process (15)
DHX9 DDX17 DDX5 EIF4A3 HNRNPC HNRNPR IGF2BP1 MAGOH MOV10 PABPN1 RBM8A SAFB SRSF1 WTAP YBX1
DNA related process (11)
AQR CDC5L DDX21 DHX9 POLDIP3 PRPF19 RBM14 RBMX* SAFB THOC1 YBX1
Translation (14)
DHX9 EIF4A3 HNRNPC MAGOH PABPN1 RBM8A RPL10A RPL15 RPL22 RPL8 RPS11 RPS14 SRSF1 YBX1
Other process (9)
C4A;C4B CRTAP CSNK2B HSPA1B LEPRE1 PPIB RBBP6 SDC2 SLC25A11
B
RNA splicing
mRNA metabolic process
mRNA processing
RNA processing
nuclear mRNA splicing, via spliceosome
RNA splicing, via transesterification reactions with…
RNA splicing, via transesterification reactions
ribonucleoprotein complex assembly
RNA localization
spliceosome assembly
mRNA transport
RNA transport
establishment of RNA localization
nucleic acid transport
mRNA splice site selection
nucleobase, nucleoside, nucleotide and nucleic acid…
mRNA export from nucleus
intronless viral mRNA export from host nucleus
ribonucleoprotein complex biogenesis
RNA export from nucleus
0 10 20 30 40 50 60 70
-Log10(p-value)
C
IP
SE - + α-YTHDC1
YTHDC1
SRSF6
SRSF1

Figure S1. YTHDC1 protein interactome (related to Figure 1).
(A) Schematic representation of YTHDC1 protein interactome. The 86 proteins from YTHDC1 protein interactome are grouped according to their molecular function and protein complexes in which they have been identified, as described in PubMed and UniProt databases. Proteins implicated in alternative splicing are highlighted in bold and italic. Protein can be found in different complexes and have several functions. The number of proteins associated with each function is given in brackets.
(B) GO analysis performed on YTHDC1 protein interactome. The analysis was done using DAVID Bioinformatics Resources. Biological processes identified with a $-Log_{10}$(p-value) > 5 are shown.
(C) Co-IP analysis of YTHDC1 with SRSF1 and SRSF6 by western blot. YTHDC1 immunoprecipitation eluates were obtained using an irrelevant antibody (-) or a specific antibody against YTHDC1 (+). SE: 0.5% of soluble extract input.

Figure S2

A

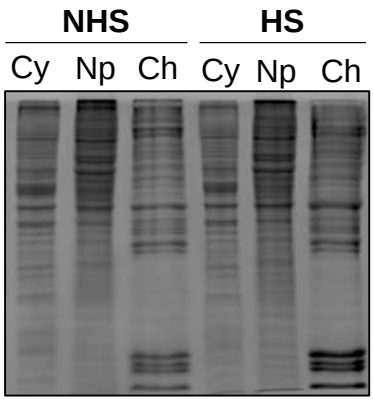

B

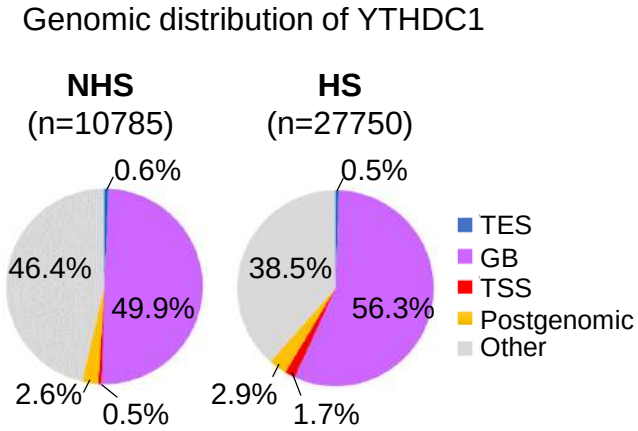

C

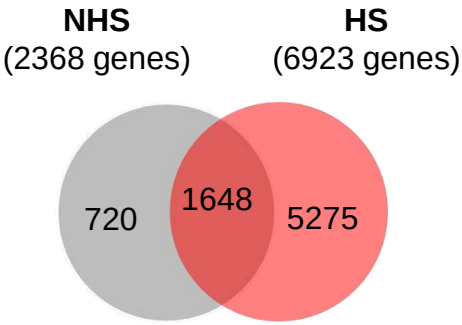

D

		-Log_{10}(p-value)
NHS	Translation	12-10
	Cell cycle	4
HS	Protein folding	13-9
	Translation	7
	Apoptosis	7
	Cell Cycle	6
	RNA processing	4
	Chromatin organization	4

E

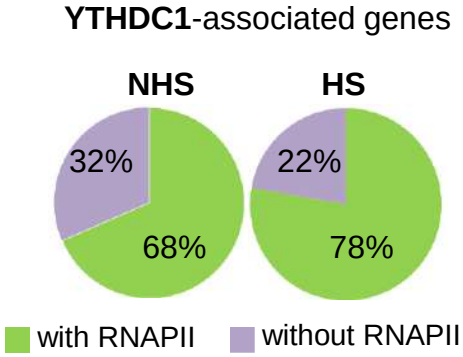

F

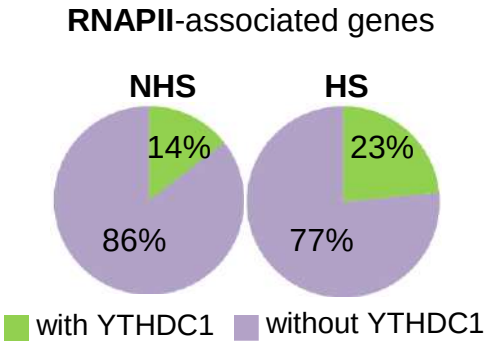

G

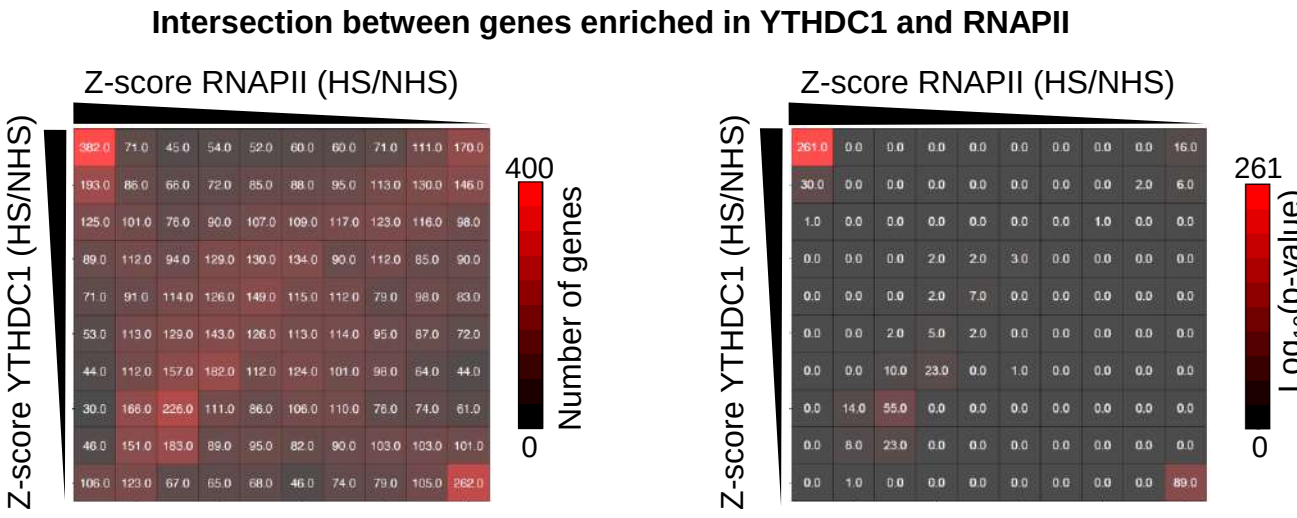

Figure S2. YTHDC1 associates with chromatin and heat stress reshapes YTHDC1 genomic localization (related to Figure 2).

(A) Coomassie-stained gel after SDS-PAGE of the proteins present in the cytoplasmic (Cy), nucleoplasmic (Np) or chromatin-associated (Ch) fractions of cells grown in no heat stress condition (NHS) or after one hour of heat stress (HS).

(B) Distribution of YTHDC1 ChIP peaks, expressed as percentage of the total peaks, and mapping at transcription start site (TSS), gene body (GB), transcript end site (TES), beyond TES (Postgenomic) or other regions (Others). Total numbers of peaks in NHS and HS conditions are indicated in brackets.

(C) Venn diagram of genes enriched in YTHDC1 in NHS and HS conditions and identified by peak-calling analysis.

(D) GO enrichment (Biological Process using DAVID Bioinformatics Resources) conducted on the top 30% of the genes ranked by their normalized YTHDC1 ChIP-seq reads of YTHDC1 targeted over gene bodies, in NHS and HS conditions. Common biological processes identified in response to heat stress (Mahat and Lis, 2017; Vihervaara et al., 2017) are indicated.

(E) Pie charts showing the percentage of YTHDC1-associated genes that are occupied or not occupied by RNAPII, in NHS or HS conditions.

(F) Pie charts showing the percentage of RNAPII-associated genes that are occupied or not occupied by YTHDC1, in NHS or HS conditions.

(G) Analysis of the co-variation of RNAPII and YTHDC1 gene occupancy in heat-stressed cells relative to unstressed cells. Left panel, decile matrix showing the change in RNAPII or YTHDC1 binding as Z-scores at gene bodies in HS compared to NHS condition, ranked by deciles from the most up-regulated to the most down-regulated. The numbers in each box indicate the number of common genes in each decile. Right panel, decile matrix showing the Log10 p-value for the intersection of the number of common genes determined for each decile compared to expected. Lowest intersection is black while the highest is red (0 to 261, Hypergeometric test).

Figure S3

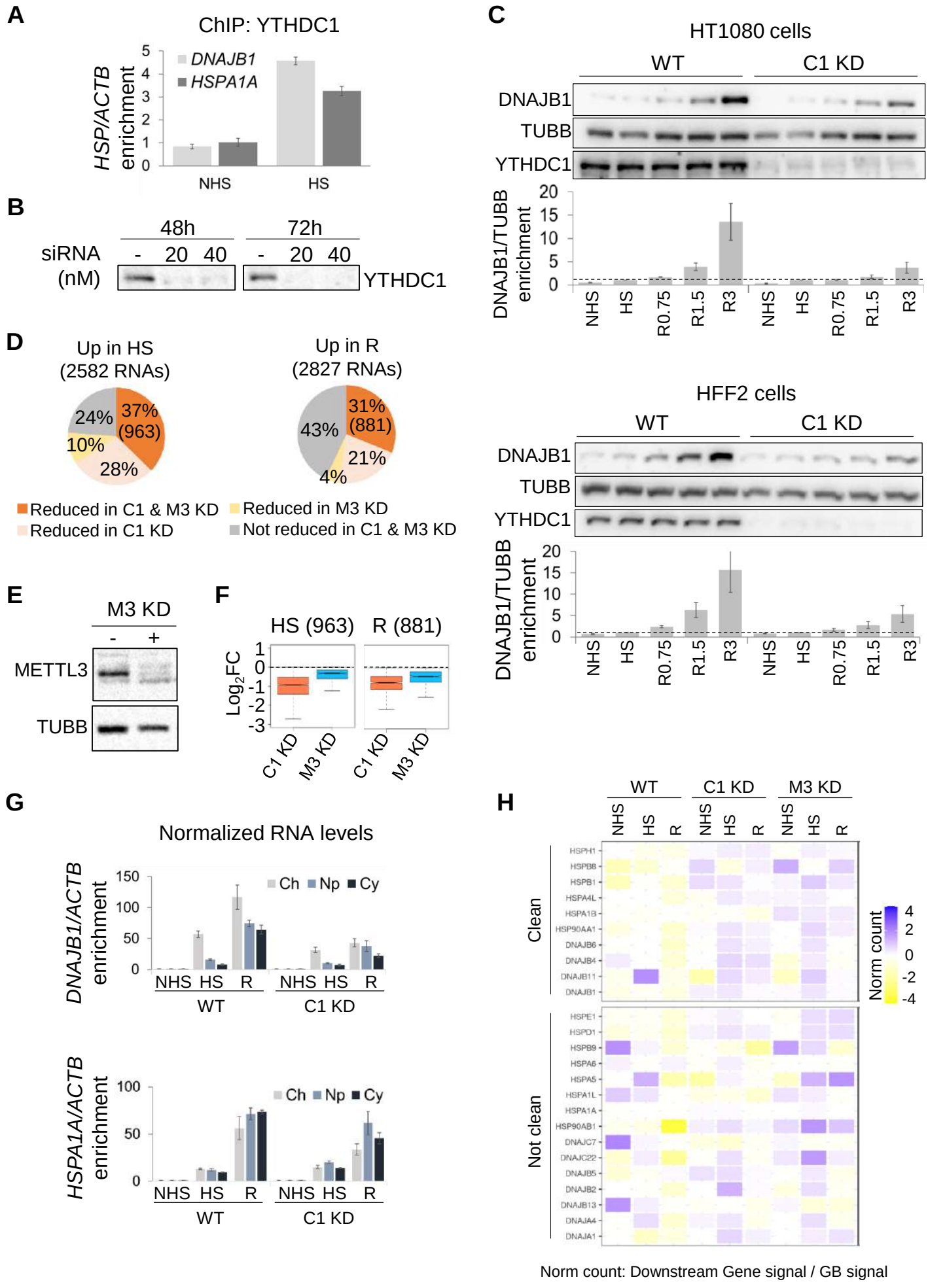

Norm count: Downstream Gene signal / GB signal

Figure S3. YTHDC1 binding to m6A promotes heat-induced expression of HSPs in cis (related to Figure 3).

(A) ChIP-qPCR showing the enrichment of YTHDC1 at the 3' end of *HSP70* (*HSPA1A*) and *DNAJB1* genes in cells in non-heat-stressed (NHS) or heat-stressed (HS) cells. Data show the fold enrichment normalized to control IP (done with irrelevant IgG) and *ACTB* gene used to monitor the background. Values are mean ± standard error of three independent biological replicates.

(B) Western blots showing the efficiency of YTHDC1 knockdown 48 and 72 hours post transfection with 20 or 40 nM of YTHDC1-specific siRNAs.

(C) Western blots showing the levels of DNAJB1 protein in wild-type (WT) or YTHDC1 knocked down (YTHDC1 KD) in HT1080 cells (top panels) or HFF2 cells (bottom panels) in NHS, HS or recovery (R). Tubulinß (TUBB) was used as loading control. Quantification of the western blot signals with protein levels expressed as fold-change relative to the protein levels in HS condition (highlighted by the horizontal dotted line) are shown below the western blots. Error bars represent standard error from three independent biological replicates.

(D) Pie charts showing the distribution of the RNAs with their level increased in HS (Up in HS) or in R (Up in R) according to the variation of their RNA level in YTHDC1 KD, METTL3 KD or both KD cells, in HS or R condition.

(E) Western blots validating METTL3 knockdown. Expression of METTL3 protein was analyzed 72h after transfection with 40 nM of specific METTL3 siRNAs. TUBB was used as loading control.

(F) Box plots showing the Log2Fold Change (FC) for the RNAs having their level Up in WT cells and that are deregulated in YTHDC1 and METTL3 KD cells, in HS vs NHS (963 RNAs) or after 3 hours of recovery vs NHS (881 RNAs).

(G) RT-qPCR showing the level of *DNAJB1* and *HSP70* (*HSPA1A*) RNA levels in the chromatin-associated (Ch), nucleoplasmic (Np), cytoplasmic (Cy) fractions in wild-type (WT) or YTHDC1 KD cells, in NHS, HS or 3 hours of recovery (R) after heat stress. Variation of RNA levels is expressed in fold-change relative to the NHS condition and normalized to *ACTB*. Graphs show the mean and SEM of three independent experiments.

(H) Heatmap showing for individual heat-induced HSP genes the normalized ratio of the RNA reads mapping their 15 kb genomic region downstream the gene over the RNA reads within their gene body, in WT, YTHDC1 KD or METTL3 KD cells subjected to NHS, HS or 3 hours of recovery (R) after heat stress. The genes were grouped as "Clean" when no other gene was identified in the 15 kb genomic window downstream its 3'UTR and as “Not clean” in the converse case. The HSP genes analyzed (25) have their RNAs that accumulate in HS or R, compared to the NHS condition, and that accumulate less in HS or R condition in both YTHDC1 KD and METTL3 KD cells.

Figure S4

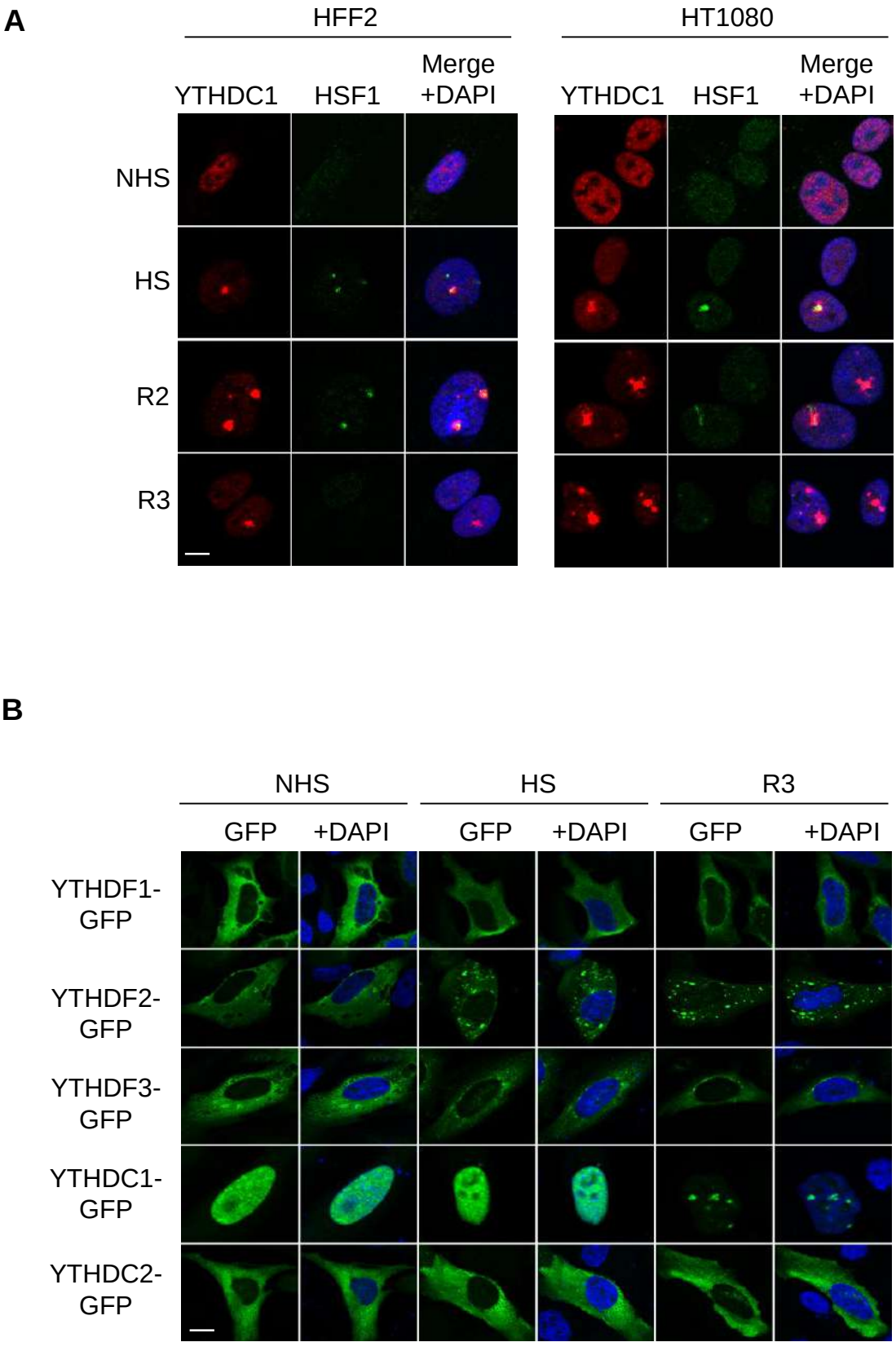
A
HFF2
HT1080
YTHDC1
HSF1
Merge +DAPI
YTHDC1
HSF1
Merge +DAPI
NHS
HS
R2
R3
B
NHS
HS
R3
GFP
+DAPI
GFP
+DAPI
GFP
+DAPI
YTHDF1-GFP
YTHDF2-GFP
YTHDF3-GFP
YTHDC1-GFP
YTHDC2-GFP

Figure S4. Human YTH proteins localization upon heat stress (related to Figure 4).

(A) Microscopy images of YTHDC1 (red) and HSF1 (green) fluorescent immunostainings showing their subcellular localization in HFF2 cells (left panel) and HT1080 cells (right panel) in non-heat-stressed (NHS), heat-stressed (HS) or heat-stressed followed by 2 or 3 hours of recovery (R2 or R3) conditions. Nuclear DNA was stained with DAPI (blue). Scale bar, 10 µm.

(B) Microscopy images of YTHDF1, 2 and 3, and YTHDC1 and 2 fused to GFP showing their subcellular localization in NHS, HS or R3 conditions, after being transfected with plasmids expressing the YTH proteins. The GFP signal was used to detect the localization of the ectopic expressed proteins. DAPI was used for staining the nucleus. Scale Bar, 10 µm.

Figure S5

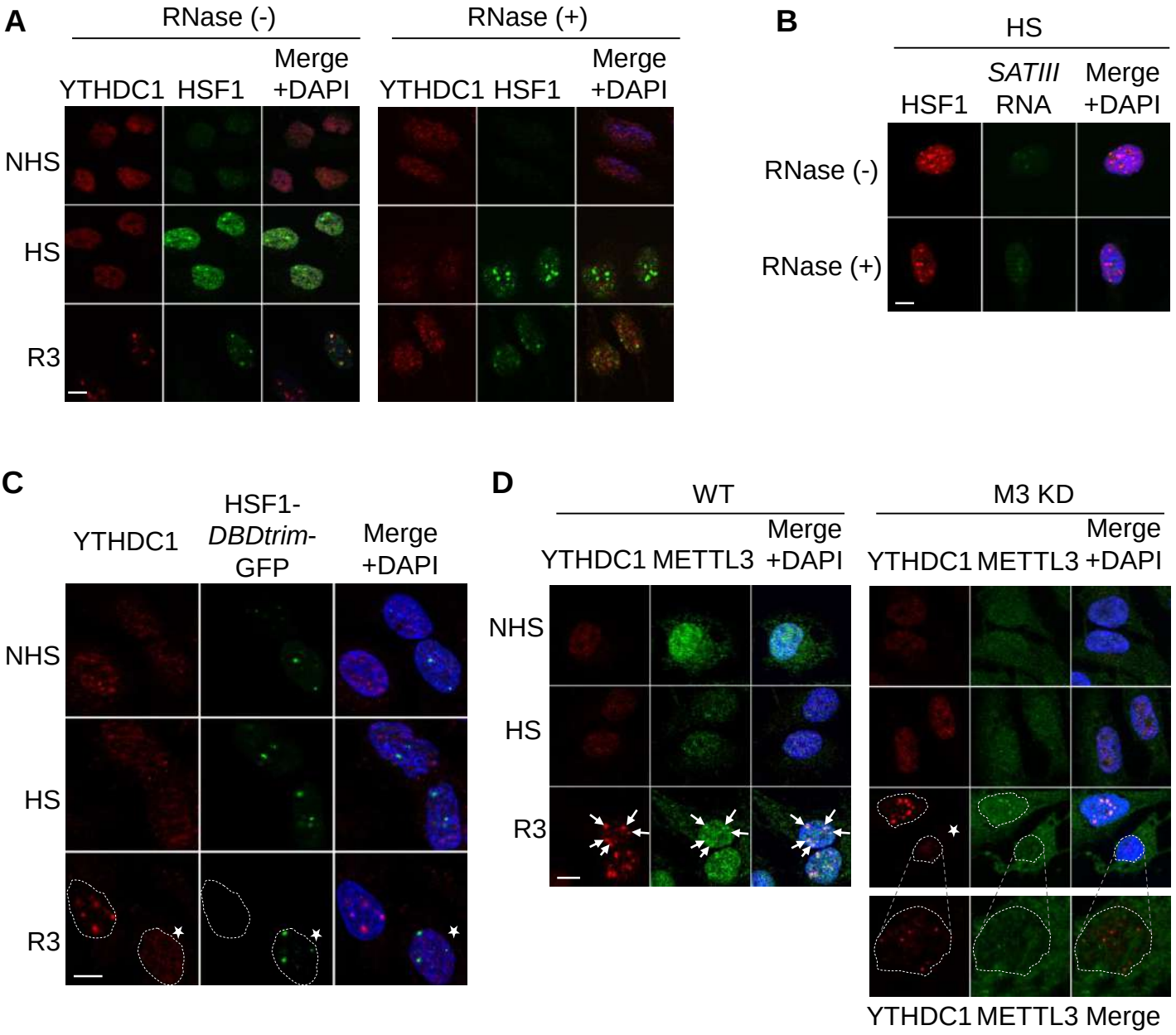
A
RNase (-)
RNase (+)
YTHDC1
HSF1
Merge +DAPI
NHS
HS
R3
B
HS
HSF1
SATIII RNA
Merge +DAPI
RNase (-)
RNase (+)
C
YTHDC1
HSF1-DBDtrim-GFP
Merge +DAPI
NHS
HS
R3
D
WT
M3 KD
YTHDC1
METTL3
Merge +DAPI
NHS
HS
R3
E
HA-YTHDC1
HA-YTHDC1-W428A
HA
HSF1
Merge + DAPI
NHS
HS
R3
F
YTHDC1
Merge + DAPI
WT
C1 KD

Figure S5. YTHDC1 relocates to nSBs and associates with *SATIII* ncRNAs (related to Figure 4).

(A) Microscopy images showing that the relocation of YTHDC1 to nSBs is strongly reduced in cells treated with RNaseA. YTHDC1 (red) and HSF1 (green) were detected by immunofluorescence in cells subjected to heat stress (HS) only or allowed to recover for 3 hours after the HS. Nuclear DNA stained with DAPI. Scale bar: 10 µm.

(B) Microscopy images of RNA FISH experiments showing that the RNaseA treatment strongly reduces *SATIII* RNA signal under HS. Scale bar: 10 µm.

(C) Microscopy images of YTHDC1 (red) and HSF1-DBDtrim-GFP mutant (green) fluorescent immunostainings showing the loss of YTHDC1 foci in cells expressing HSF1-DBDtrim-GFP. The white star highlights a cell that expresses the HSF1-DBDtrim-GFP mutant, during the recovery period (R3), while the other visible on the same image does not express the HSF1-DBDtrim-GFP dominant negative mutant. Immunostainings were conducted on non-heat-stressed (NHS), heat-stressed (HS) or heat-stressed followed by 3 hours of recovery (R3) conditions. The arrows point to YTHDC1 and METTL3 foci. Nuclear DNA was stained with DAPI. Scale bar, 10 µm.

(D) Microscopy images showing the nuclear localization of METTL3 (green) and YTHDC1 (red), analyzed by immunodetection, in WT (left panel) and METTL3 KD (right panel) cells in NHS, HS or R3 condition. The star highlights a cell knocked-down for METTL3. Note that while YTHDC1 signal still relocates to nSBs the signal is much weaker compared to the neighboring cell which expresses METTL3 at a higher level and which concentrates within the nSBs in R3. Nuclear DNA stained with DAPI. Scale bar: 10 µm.

(E) Microscopy images showing the relocation of ectopic HA-YTHDC1 or HA-YTHDC1-W428A fusion proteins to nSBs in cells subjected to HS (HS) or HS followed by for 3 hours of recovery (R). The expressed ectopic YTHDC1 proteins (green) and HSF1 (red) were detected by immunofluorescence. Nuclear DNA was counterstained with DAPI. Scale bar: 10 µm.

(F) Microscopy images validating the loss of YTHDC1 signal in YTHDC1 KD cells. WT and YTHDC1 KD cells were fixed 72h after transfection and analyzed by immunofluorescence using specific antibody against YTHDC1 (red). Nuclear DNA stained with DAPI. Scale bar: 10 µm.

Figure S6

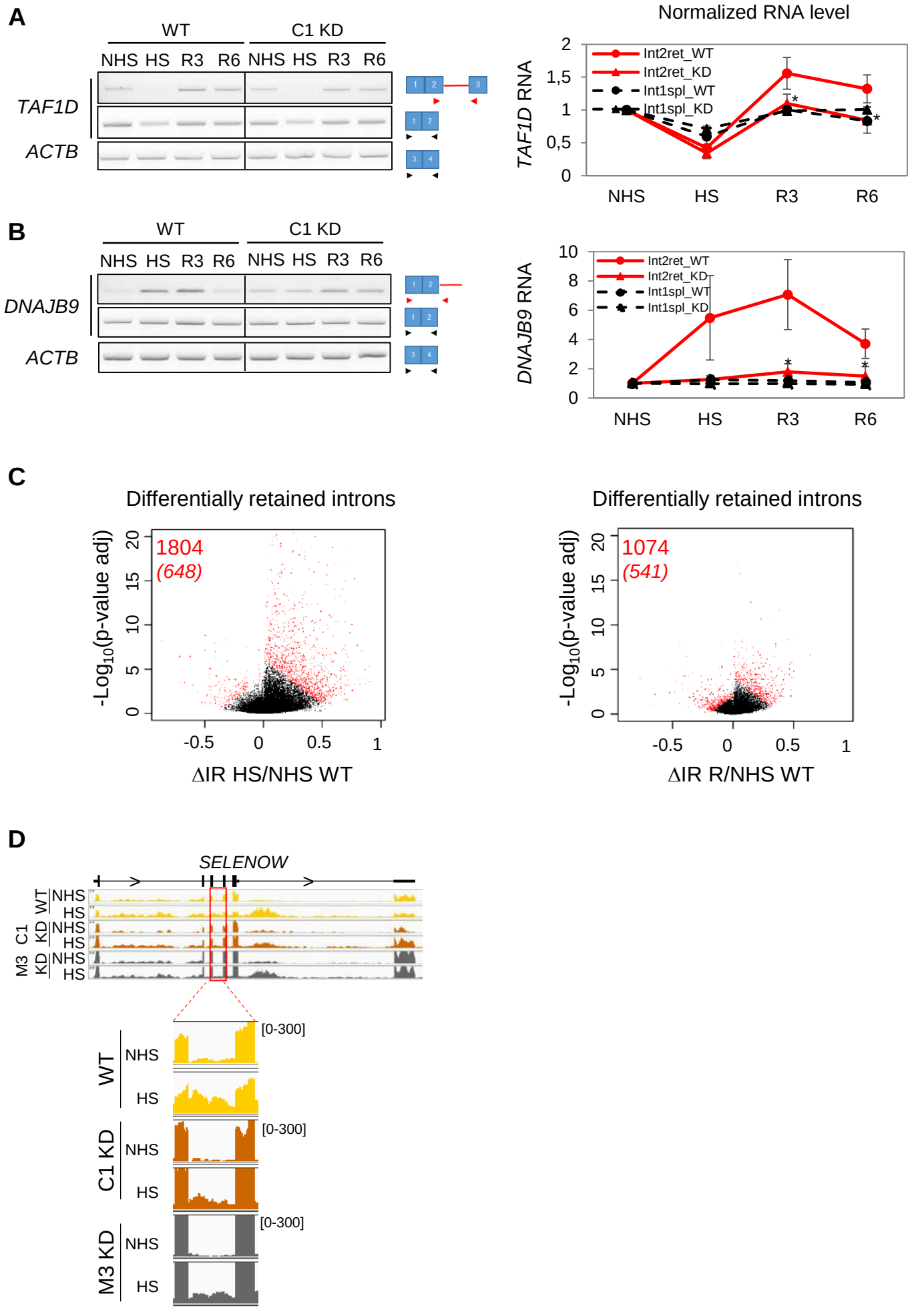
A
WT
C1 KD
NHS HS R3 R6 NHS HS R3 R6
TAF1D
ACTB
Normalized RNA level
TAF1D RNA
Int2ret_WT
Int2ret_KD
Int1spl_WT
Int1spl_KD
NHS HS R3 R6
B
DNAJB9
ACTB
DNAJB9 RNA
C
Differentially retained introns
1804
(648)
-Log10(p-value adj)
ΔIR HS/NHS WT
1074
(541)
ΔIR R/NHS WT
D
SELENOW
M3 C1 KD WT
M3 C1 KD KD
[0-300]
WT
C1 KD
M3 KD

Figure S6. YTHDC1 controls heat-induced intron retention both during and after HS (related to Figure 5).

(A-B). Analysis of *TAF1D* and *DNAJB9* pre-mRNAs splicing. Left panels, pictures of agarose/TAE gels showing products of RT-PCR from WT and YTHDC1 KD cells, in no heat stress (NHS), heat stress (HS) or heat stress followed by 3 or 6 hours of recovery (R3 or R6) conditions. Red arrows indicate positions of the PCR primers used to detect, respectively, intron 2 retention of *TAF1D* and intron 2 retention of *DNAJB9* pre-mRNAs. Black arrows indicate positions of the PCR primers used to detect constitutive spliced intron on the three transcripts. ActinB pre-mRNA was used as a control of constitutive splicing. Right panels, quantification of the signals shown in the left panels using Fusion-Capt software (Vilber Lourmat). Int2ret: intron 2 retention; Int1spl: intron 1 splicing. Error bars represent standard deviation from three independent biological replicates. P-value was calculated using a two-tailed Student's t-test. *: $p<0.05$; ***: $p<0.001$. Only significant p-values are indicated and are for *TAF1D*: 0.048 (R3) and 0.0325 (R6) and for *DNAJB9*: 0.0204 (R3), 0.0325 (R6).

(C) Volcano plots of retained introns in HS or R compared to NHS. Red dots are introns that are differentially retained in WT cells subjected to HS (left panel) or after 3 hours of recovery (R) after the HS (right panel), compared to non-heat stress condition (NHS). The number of differentially retained introns is indicated in red. The average Intron Retention (IR) change (ΔIR HS/NHS or ΔIR R/NHS) from 3 independent experiments was plotted along the X-axis, and adjusted p-values [-Log10(p-value adj)] along the Y-axis.

(D) Browser shots of RNA-seq reads at SELENOW gene shown as an example of the intron retention deregulation ongoing in YTHDC1 KD or METTL3 KD vs WT cells in HS vs NHS condition.

Figure S7

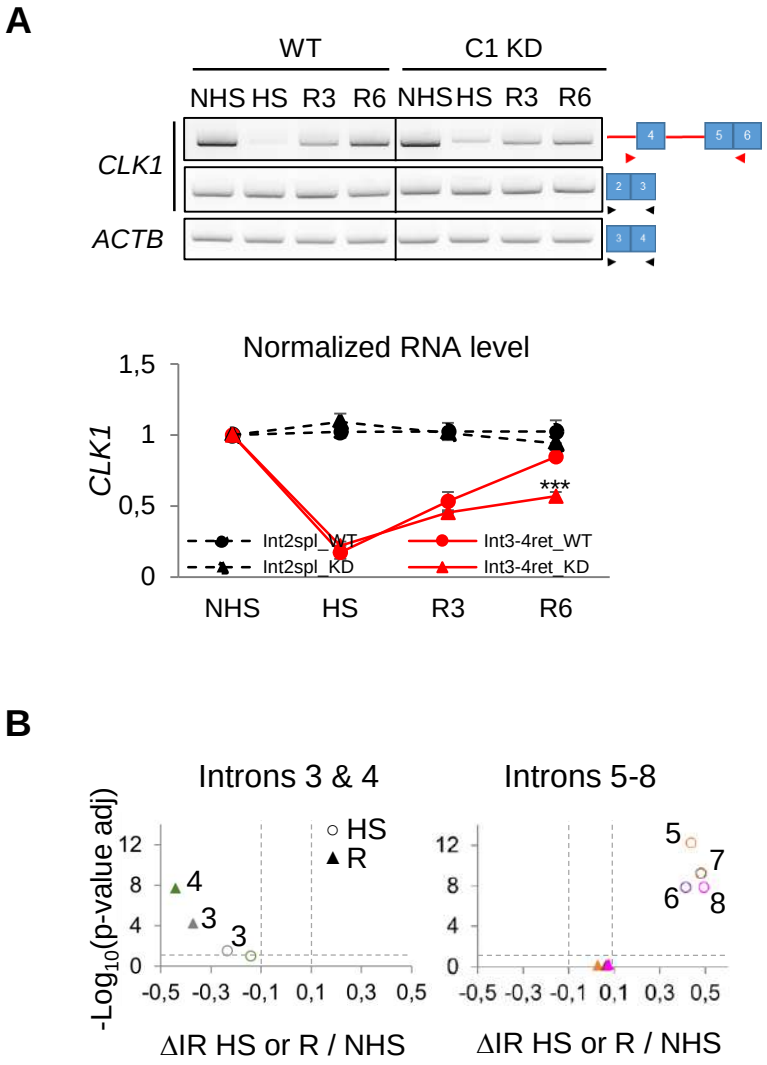
A
WT
C1 KD
NHS HS R3 R6 NHS HS R3 R6
CLK1
ACTB
4
5 6
2 3
3 4
Normalized RNA level
CLK1
1,5
1
0,5
0
***
Int2spl_WT
Int2spl_KD
Int3-4ret_WT
Int3-4ret_KD
NHS
HS
R3
R6
B
Introns 3 & 4
Introns 5-8
-Log10(p-value adj)
HS
R
12
8
4
0
4
3
3
5
7
6
8
-0,5 -0,3 -0,1 0,1 0,3 0,5
ΔIR HS or R / NHS

Figure S7. YTHDC1 promotes the splicing of *CLK1* introns retained during HS (related to Figure 6).

(A) Analysis of *CLK1* introns 3 and 4 splicing in response to HS. Upper panel, pictures of products of RT-PCR from WT and YTHDC1 KD cells, in non-heat-stressed (NHS), heat-stressed (HS) or heat-stressed followed by 3 or 6 hours of recovery (R3 or R6) conditions, analyzed on agarose/TAE gels. Red arrows indicate positions of the PCR primers used to detect introns 3-4 retention of *CLK1* pre-mRNAs. Black arrows indicate positions of the PCR primers used to detect constitutive spliced intron on the three transcripts. *ACTB* pre-mRNA was used as a control of constitutive splicing. Lower panel, quantification of the signals shown in the panels using Fusion-Capt software (Vilber Lourmat). Int3-4ret: intron 3 and 4 retention; Int2spl: intron 2 splicing. Error bars represent standard deviation from three independent biological replicates. P-value was calculated using a two-tailed Student's t-test. *: $p<0.05$; ***: $p<0.001$. Only significant p-values are indicated and are for *CLK1*: 0.00029 (R6).

(B) Volcano plots of *CLK1* introns 3-4 and 5-8 retention in HS versus NHS (circles) and R3 versus NHS (triangles) in WT cells. The average intron retention (IR) change from 3 independent experiments conducted on WT cells in HS vs NHS (circles) and R3 vs NHS (triangles) conditions is plotted along the X-axis and p-values [-Log10(p-value adjusted)] along the Y-axis.

Figure S8

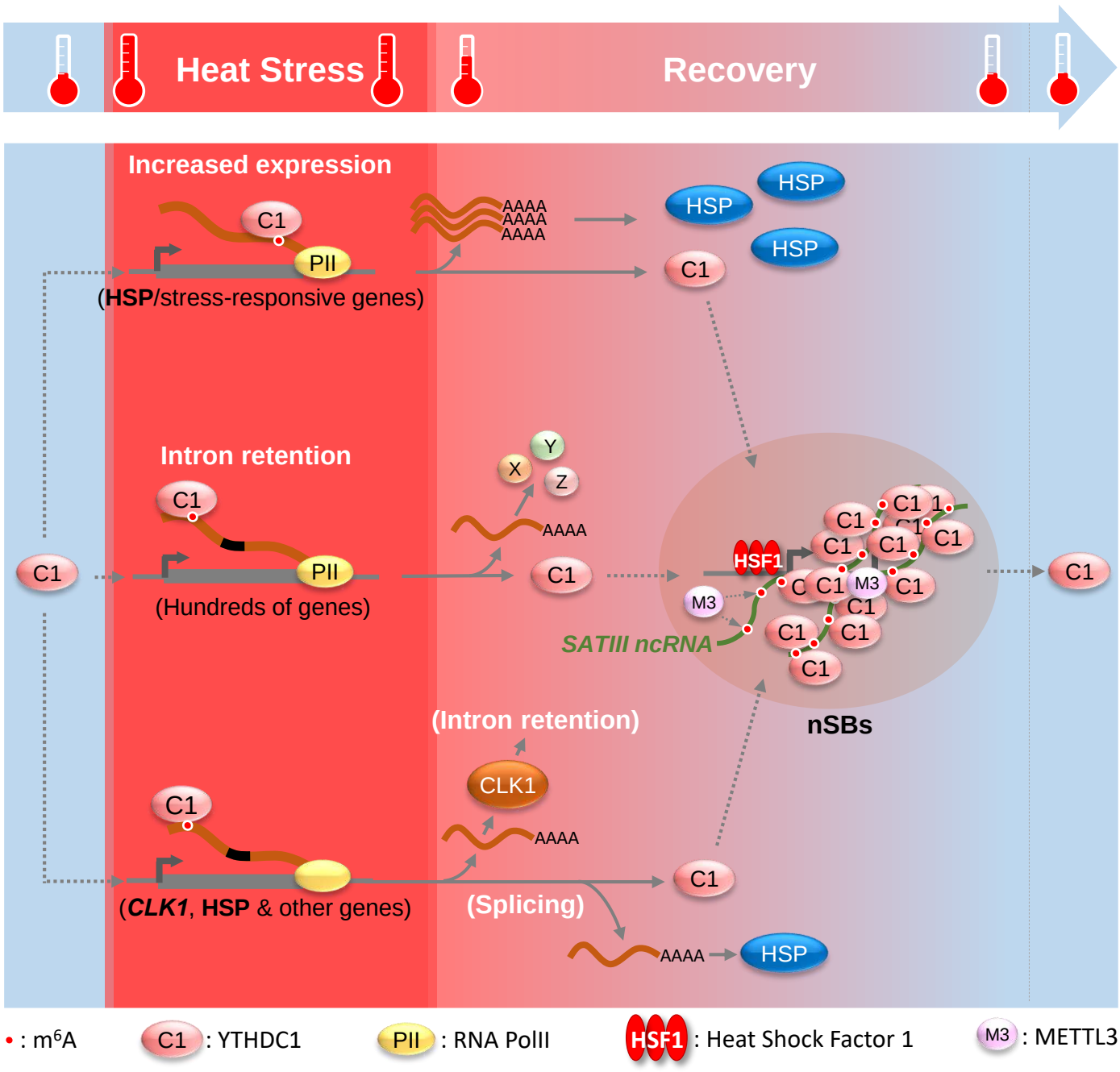
Heat Stress
Recovery
Increased expression
C1
PII
(HSP/stress-responsive genes)
AAAA
AAAA
AAAA
HSP
HSP
HSP
C1
Intron retention
C1
PII
(Hundreds of genes)
Y
X
Z
AAAA
C1
C1
HSF1
M3
C1
C1
C1
C1
C1
C1
C1
C1
C1
C1
C1
C1
C1
C1
SATIII ncRNA
nSBs
(Intron retention)
CLK1
AAAA
C1
(CLK1, HSP & other genes)
(Splicing)
C1
AAAA
HSP
• : m6A
C1 : YTHDC1
PII : RNA PolII
HSF1 : Heat Shock Factor 1
M3 : METTL3

Figure S8. Model of YTHDC1 and m6A functions in coordinating heat-induced gene expression reprograming during both HS and recovery periods, and of their regulation by sequestration of YTHDC1 within nSBs.
We propose that YTHDC1 and m6A are part of a cellular system that orchestrates diverse changes in gene expression over the course of the heat stress (HS) response, by acting in the close environment of chromatin. First, HS triggers YTHDC1 relocation to stress-induced genes, in particular HSP genes. There, YTHDC1 co-transcriptionally promotes HSPs expression in a m6A-dependent fashion. Second, HS triggers YTHDC1 relocation to hundreds other genes where it promotes co-transcriptional m6A-dependent intron retention. Third, HS may also trigger an YTHDC1-dependent imprinting on dozens of transcripts, including *CLK1* and HSP transcripts, for their splicing later during the recovery period, while YTHDC1 no more binds these transcripts. In parallel, in response to HS, the m6A methyltransferase METTL3 starts depositing m6A methylation marks on the non-coding and cis-acting *SATIII* RNAs, produced in a HSF1- and RNA polymerase II-dependent fashion. As the level of m6A on *SATIII* RNAs increase, YTHDC1 further concentrates within these bodies. As more YTHDC1 concentrates within nSBs, YTHDC1-dependent upregulation of HSPs and intron retention are gradually tuned down. During the recovery period, YTHDC1 continues to regulate intron retention, but in an indirect manner, notably by controlling the expression of CLK1, a key regulator of intron retention during this period.
YTHDC1 (C1), METTL3 (M3), m6A (red dots), RNA polymerase II (PII).

Table S3. Plasmids generated in this study.
Related to Star Methods and Figures 3, S4 and S5

Name	Description	Vector	Insert or treatment
pCI-neo_HA-YTHDC1	hYTHDC1 cDNA fused to HA tag (in 5') under control of a CMV promoter used for over-expression in mammalian cells	pCI-neo cut with EcoRI and NotI	YTHDC1 coding cDNA amplified from an HEK cells cDNA library with the C1-pCI-neo For and C1-pCI-neo Rev primers (Table S3) and cut with EcoRI and NotI
pCI-neo-HA-YTHDC1 imm	pCI-neo-HA-YTHDC1 mutagenized to obtain a hYTHDC1 cDNA non degradable by siRNAs targeted to YTHDC1	pCI-neo-HA-YTHDC1	Mutagenized using Q5 Site-Directed Mutagenesis Kit (BioLabs) with siC1_1immF/siC1_1immR and siC1_3immF/siC1_3immR primers (Table S3)
pCI-neo-HA-YTHDC1immW428A	pCI-neo-HA-YTHDC1imm mutagenized to substitute the tryptophan 248 into an alanin	pCI-neo-HA-YTHDC1 imm	Mutagenized using Q5 Site-Directed Mutagenesis Kit (BioLabs) with W428A_F /W428A_R primers (Table S3)
peGFP-YTHDC1	hYTHDC1 cDNA fused in 3' to GFP cDNA under control of a CMV promoter used for over-expression in mammalian cells	peGFP-N3 vector cut with XhoI and XmaI	YTHDC1 coding cDNA amplified from an HEK cells cDNA library with the YTHDC1_Xho/YTHDC1_Xma primers (Table S3) and cut with XhoI and XmaI
peGFP-YTHDC2	hYTHDC2 cDNA fused in 3' to GFP cDNA under control of a CMV promoter used for over-expression in mammalian cells	peGFP-N3 vector cut with XhoI and BamHI	YTHDC2 coding cDNA amplified from an HEK cells cDNA library with the YTHDC2_Xho/YTHDC2_Bam primers (Table S3) and cut with XhoI and BamHI
peGFP-YTHDF1	hYTHDF1 cDNA fused in 3' to GFP cDNA under control of a CMV promoter used for over-expression in mammalian cells	peGFP-N3 vector cut with XhoI and BamHI	YTHDF1 coding cDNA amplified from an HEK cells cDNA library with the YTHDF1_Xho/YTHDF1_Bam primers (Table S3) and cut with XhoI and BamHI
peGFP-YTHDF2	hYTHDF2 cDNA fused in 3' to GFP cDNA under control of a CMV promoter used for over-expression in mammalian cells	peGFP-N3 vector cut with XhoI and BamHI	YTHDF2 coding cDNA amplified from an HEK cells cDNA library with the YTHDF2_Xho/YTHDF2_Bam primers (Table S3) and cut with XhoI and BamHI
peGFP-YTHDF3	hYTHDF3 cDNA fused in 3' to GFP cDNA under control of a CMV promoter used for over-expression in mammalian cells	peGFP-N3 vector cut with XhoI and BamHI	YTHDF3 coding cDNA amplified from an HEK cells cDNA library with the YTHDF3_Xho/YTHDF3_Bam primers (Table S3) and cut with XhoI and BamHI

Table S5. Antibodies used in this study.
Related to Star Methods and Figures 1, 2, 3 , 4 , 6, S1, S3, S4, S5.

			WB dilution	IF dilution	
Rabbit polyclonal anti-YTHDC1	Abcam	Cat# 122340	1/1000	1/250	used for WB and IF
Rabbit polyclonal anti-YTHDC1 raised against an N-terminal peptide of YTHDC1	Eurogentec	N/A	1/250		used for YTHDC1 IP
Rabbit polyclonal anti-YTHDC1	Bethyl	Cat# A305-096A	1/1000		used for ChIP, RIP and Co-IP
Mouse polyclonal anti-HSF1	Santa Cruz Biotechnology	Cat# Sc-17757	1/1000	1/100	
Rabbit polyclonal anti-HSF1	Cell Signaling Technology	Cat# 4356	1/1000	1/200	
Rabbit polyclonal anti-YTHDF2	Proteintech	Cat# 24744-1-AP	1/1000		
Rabbit polyclonal anti-METTL3	Proteintech	Cat# 15073-1-AP	1/1000	1/500	
Rat monoclonal anti-RNA polymerase II subunit B1 (phospho CTD Ser-2), clone 3E10	Merck	Cat#04-1571-I			used for ChIP-qPCR
Mouse monoclonal anti-RNA polymerase II, F-12	Santa Cruz Biotechnology	Cat#sc-55492			used for ChIPseq analysis (Salifou et al, 2020)
Rabbit polyclonal anti-HSP70	Stressgen	Cat# SPA-812	1/1000		
Rabbit polyclonal anti-DNAJB1	Bethyl	Cat# A305245AM	1/1000		
Rabbit polyclonal anti-GAPDH	Proteintech	Cat# 10494-1-AP	1/1000		
Mouse monoclonal anti-Tubulinβ	Sigma	Cat# T5168	1/5000		
Rabbit polyclonal anti-HA	Abcam	Cat# ab9110	1/1000	1/1000	
Rabbit polyclonal anti-Histone H3	Abcam	Cat#ab1791	1/5000		
Mouse monoclonal anti-CLK1	cliniscience	Cat#sc-515307	1/200		
Rabbit polyclonal anti m6A	synaptic system	Cat#202003			used for RIP
Mouse monoclonal anti-SRSF6	MERCK	Cat#MABE152	1/1000		
Mouse monoclonal anti-SRSF1	Santa Cruz Biotechnology	Cat#sc33652	1/1000		
Goat polyclonal anti-rabbit IgG Dylight 549	Vector	Cat# DI-1549		1/1000	
Goat polyclonal anti-mouse IgG Alexa Fluor 488	Invitrogen	Cat# A-11029		1/500	
HRP-conjugated goat anti-rabbit IgG	Dako	Cat# P0448	1/5000		
HRP-conjugated goat anti-mouse IgG	Dako	Cat# P0447	1/5000		
Rabbit polyclonal IgG (irrelevant IgG)	Diagenode	Cat#C15410206			used for YTHDC1 IP and ChIP negative control
IgG from human serum (irrelevant IgG)	Sigma	Cat#I4506			used for RIP negative control